

NATIONAL ADVISORY COMMITTEE
FOR AERONAUTICS

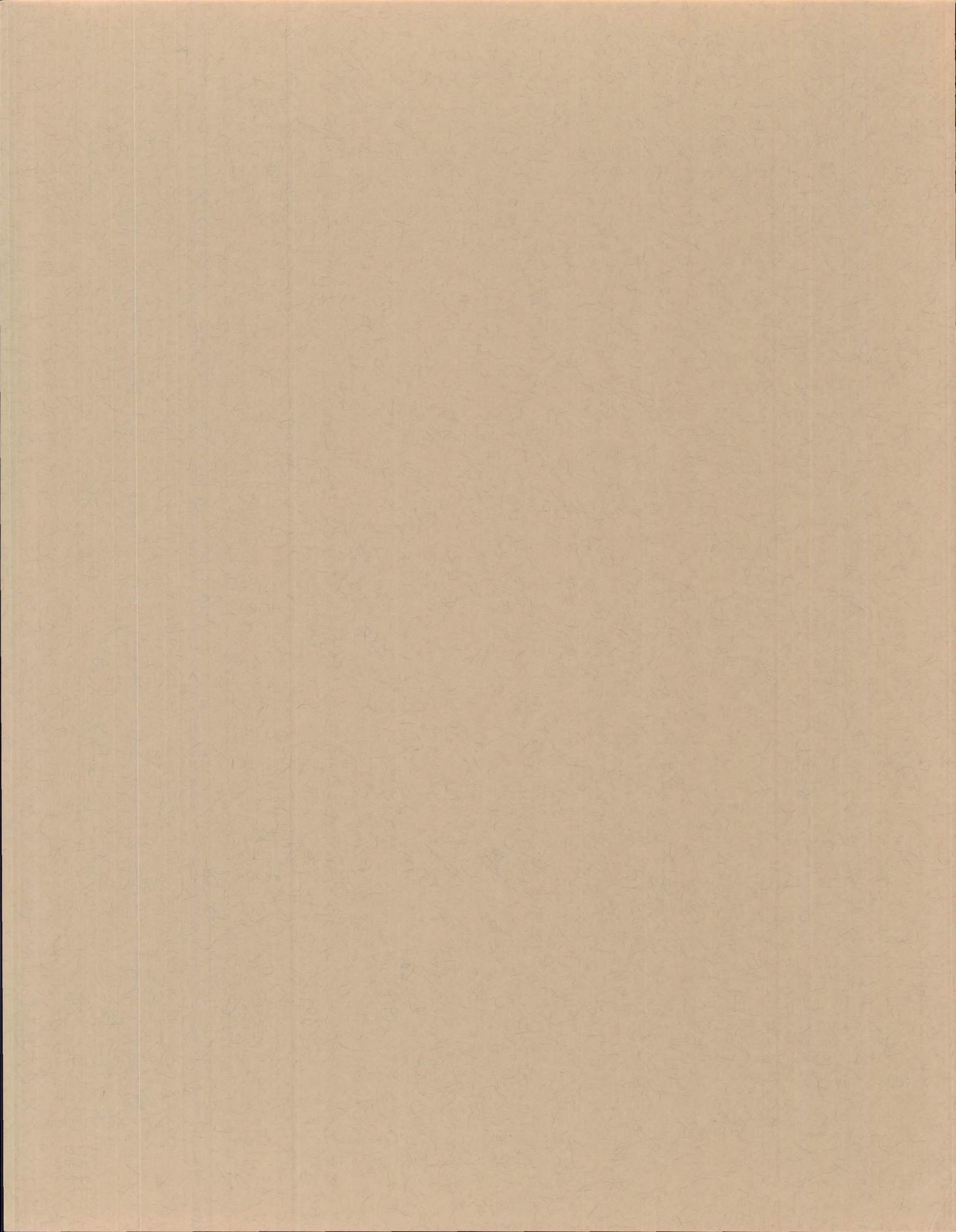
REPORT 1355

A THEORETICAL AND EXPERIMENTAL STUDY OF
PLANING SURFACES INCLUDING EFFECTS OF
CROSS SECTION AND PLAN FORM

By CHARLES L. SHUFORD, Jr.



1958



REPORT 1355

A THEORETICAL AND EXPERIMENTAL STUDY OF PLANING SURFACES INCLUDING EFFECTS OF CROSS SECTION AND PLAN FORM

By CHARLES L. SHUFORD, Jr.

Langley Aeronautical Laboratory
Langley Field, Va.

National Advisory Committee for Aeronautics

Headquarters, 1512 H Street NW., Washington 25, D. C.

Created by Act of Congress approved March 3, 1915, for the supervision and direction of the scientific study of the problems of flight (U. S. Code, title 50, sec. 151). Its membership was increased from 12 to 15 by act approved March 2, 1929, and to 17 by act approved May 25, 1948. The members are appointed by the President and serve as such without compensation.

JAMES H. DOOLITTLE, Sc. D., Vice President, Shell Oil Company, *Chairman*

LEONARD CARMICHAEL, Ph. D., Secretary, Smithsonian Institution, *Vice Chairman*

ALLEN V. ASTIN, Ph. D., Director, National Bureau of Standards.
PRESTON R. BASSETT, D. Sc.

DETLEV W. BRONK, Ph. D., President, Rockefeller Institute for Medical Research.

FREDERICK C. CRAWFORD, Sc. D., Chairman of the Board, Thompson Products, Inc.

WILLIAM V. DAVIS, JR., Vice Admiral, United States Navy, Deputy Chief of Naval Operations (Air).

PAUL D. FOOTE, Ph. D., Assistant Secretary of Defense, Research and Engineering.

WELLINGTON T. HINES, Rear Admiral, United States Navy, Assistant Chief for Procurement, Bureau of Aeronautics.

JEROME C. HUNSAKER, Sc. D., Massachusetts Institute of Technology.

CHARLES J. McCARTHY, S. B., Chairman of the Board, Chance Vought Aircraft, Inc.

DONALD L. PUTT, Lieutenant General, United States Air Force, Deputy Chief of Staff, Development.

JAMES T. PYLE, A. B., Administrator of Civil Aeronautics.

FRANCIS W. REICHELDERFER, Sc. D., Chief, United States Weather Bureau.

EDWARD V. RICKENBACKER, Sc. D., Chairman of the Board, Eastern Air Lines, Inc.

LOUIS S. ROTHSCHILD, Ph. B., Under Secretary of Commerce for Transportation.

THOMAS D. WHITE, General, United States Air Force, Chief of Staff.

HUGH L. DRYDEN, PH. D., *Director*

JOHN F. VICTORY, LL. D., *Executive Secretary*

JOHN W. CROWLEY, JR., B. S., *Associate Director for Research*

EDWARD H. CHAMBERLIN, *Executive Officer*

HENRY J. E. REID, D. Eng., Director, Langley Aeronautical Laboratory, Langley Field, Va.

SMITH J. DEFRENCE, D. Eng., Director, Ames Aeronautical Laboratory, Moffett Field, Calif.

EDWARD R. SHARP, Sc. D., Director, Lewis Flight Propulsion Laboratory, Cleveland, Ohio

WALTER C. WILLIAMS, B. S., Chief, High-Speed Flight Station, Edwards, Calif.

REPORT 1355

A THEORETICAL AND EXPERIMENTAL STUDY OF PLANING SURFACES INCLUDING EFFECTS OF CROSS SECTION AND PLAN FORM¹

By CHARLES L. SHUFORD, Jr.

SUMMARY

A summary is given of the background and present status of the pure-planing theory for rectangular flat plates and V-bottom surfaces. The equations reviewed are compared with experiment. In order to extend the range of available planing data, the principal planing characteristics for models having sharp chines have been obtained for a rectangular flat and two V-bottom surfaces having constant angles of dead rise of 20° and 40°. Planing data were also obtained for flat-plate surfaces with very slightly rounded chines for which decreased lift and drag coefficients are obtained.

A revision of the theory presented in NACA Technical Note 3233 is presented for the rectangular flat plate. The revised theory bases the aerodynamic suction effects on the total lift rather than solely on the linear component. Also a crossflow drag coefficient which is dependent on the shape of the chines was found from experiment to be constant for a given immersed cross section; however, for surfaces, such as those having horizontal chine flare or vertical chine strips, the crossflow drag coefficient is constant only for the chine-immersed condition. The theory is extended to include triangular flat plates planing with base forward and V-shaped prismatic surfaces having a constant angle of dead rise, horizontal chine flare, or vertical chine strips. A method is also presented for estimating the center of pressure for surfaces having either rectangular or triangular plan form. The results calculated by the proposed theory have been correlated only with the data considered to be pure planing; however, for conditions not considered pure planing, a method is given for estimating the effects of buoyancy. The agreement between the results calculated by the proposed theory and the experimental data is, in general, good for calculations of pure-planing lift and center-of-pressure location for flat plate, V-bottom, and related planing surfaces.

INTRODUCTION

Recent developments in water-based aircraft have resulted in configurations utilizing planing surfaces operating at angles of trim, length-beam ratio, and Froude number beyond those for which most of the available planing theories were correlated with experimental data. In reference 1 a preliminary review of these theories for a pure-planing rectangular flat plate was made to determine whether available planing theories were adequate in estimating the

planing lift in these extended ranges. In addition to this review, a modification and addition to existing theory which is useful in predicting the lift and center of pressure for pure-planing rectangular flat plates was presented.

The review in reference 1 indicated there were no data available in the extended ranges of combined high trim and high length-beam ratios; consequently, the principal planing characteristics for models having sharp chines have been obtained in these extended ranges for a rectangular flat and two V-bottom surfaces. It was also noted in reference 1 that there was a difference in the lift coefficients obtained from various experimental investigations; therefore, data have been obtained for rectangular flat-plate surfaces having very slightly rounded chines to determine the influence of slight differences in construction at the point of flow separation on the lift coefficient.

The review of existing theories and data has been extended to include those applicable to V-bottom surfaces. The theory presented in reference 1 for estimating the lift and center-of-pressure location of a pure-planing rectangular flat plate has been revised and extended to include triangular flat plates planing with base forward and V-shaped prismatic surfaces having a constant angle of dead rise, horizontal chine flare, or vertical chine strips. Since water-based aircraft operate at low Froude numbers as well as high Froude numbers, an approximate method has also been presented for estimating the effect of buoyancy on lift coefficient.

SYMBOLS

A	aspect ratio, $\frac{b}{l_m}$
A_t	ratio of maximum beam to overall length (see fig. 40)
b	beam of planing surface, ft
$C_{D,b}$	drag coefficient based on square of beam, $\frac{D}{qb^2}$
$C_{D,c}$	crossflow drag coefficient
$(C_{D,c})_{\beta=0}$	crossflow drag coefficient for a cross section having an effective angle of dead rise of 0°
$C_{D,s}$	drag coefficient based on principal wetted area, $\frac{D}{qS}$
$C_{D,i}$	induced drag coefficient, $C_{L,S} \tan \tau$
C_f	skin-friction coefficient, $C_{D,S} - C_{L,S} \tan \tau$

¹ Supersedes NACA Technical Note 3939 by Charles L. Shuford, Jr., 1957.

C_L	lift coefficient
$C_{L,B}$	lift coefficient due to buoyancy, $\frac{L_B}{qS}$ (see eq. (31))
$C_{L,b}$	lift coefficient based on square of beam, $\frac{L}{qb^2}$
$C_{L,s}$	lift coefficient based on principal wetted area, $\frac{L}{qS}$
$C_{L,vol}$	lift coefficient due to buoyancy based on total wedge-shaped volumetric displacement of the planing surface, $\frac{L_{vol}}{qS}$ (see eqs. (28) to (30))
C_V	speed coefficient or Froude number, $\frac{V}{\sqrt{gb}}$
D	drag of planing surface, lb
$G(\beta_e)$	dead-rise function (applied only to crossflow term, see fig. 2)
g	acceleration due to gravity, 32.2 ft/sec ²
$K(\beta_e)$	dead-rise function (applied only to linear term, see fig. 1)
L	lift of planing surface, lb
L_B	lift due to buoyancy, lb
L_{vol}	lift due to buoyancy based on total wedge- shaped volumetric displacement of the plan- ing surface, lb
l	length of planing surface, ft
l_c	chine wetted length, ft
l_k	keel wetted length, ft
l_m	mean wetted length (distance from aft end of planing surface to the mean of the heavy spray line), ft
l_{cp}	center-of-pressure location (measured forward of trailing edge), ft
\bar{l}_m	nondimensional center-of-pressure location
N	normal force, lb
q	free-stream dynamic pressure, $\frac{1}{2}\rho V^2$, lb/sq ft
R	Reynolds number, $\frac{Vl_m}{\nu}$
S	principal wetted area (bounded by trailing edge, chines, and heavy spray line), sq ft
V	horizontal velocity, ft/sec
β	angle of dead rise, radians unless otherwise stated
β_e	effective angle of dead rise (angle between a straight line drawn from keel to the chines and the horizontal), radians unless otherwise stated
β_{basic}	basic angle of dead rise (angle between V- shaped portion of model and a horizontal line perpendicular to keel), radians unless other- wise stated
ρ	mass density of water, slugs/cu ft
τ	trim (angle between planing bottom and hori- zontal), radians unless otherwise stated
ν	kinematic viscosity, sq ft/sec
Subscript:	
1,2,3,...	9 used to indicate various terms in equations for lift coefficient

REVIEW OF EXISTING PLANING-LIFT THEORY

In reference 1 the pure-planing lift equations for rectangular flat plates presented in references 2 to 11 were reviewed and compared with experiment. In addition to lift theories for rectangular flat plates, the present review considers V-shaped surfaces having a constant angle of dead rise and V-shaped surfaces having horizontal chine flare.

Since publication of reference 1, Farshing (ref. 12) presented a cubic equation for the lift on rectangular flat plates derived from a consideration of deflected mass and based on an effective angle of attack. The equation has the form

$$C_L^3 + [(2.292 - 1.571A)\tau - 2.379 - A]C_L^2 + [2A + 4 + (6.283A - 4.584)\tau]C_L - 6.283A\tau = 0 \quad (1)$$

However, the lift coefficient obtained from equation (1) was multiplied by an empirical factor to get better agreement with experimental data; thus,

$$C_{L,s} = C_L \xi \quad (2)$$

where

$$\xi = 1.359 - t \operatorname{nh} \left(\frac{1+A}{8A} \right) \quad (2^\circ \leq \tau \leq 18^\circ) \quad (3)$$

$$\xi = 1.359 - \operatorname{tanh} \left(\frac{1+A}{8A} \right) + \left(\frac{\tau - 18^\circ}{90.53} \right) \tanh \frac{1}{A^2} \quad (18^\circ \leq \tau \leq 30^\circ) \quad (4)$$

and τ is measured in degrees.

P. R. Crewe of Sanders-Roe Ltd. (British) in correspondence with the Langley Laboratory proposed an equation for rectangular flat plates and a V-shaped surface having a basic angle of dead rise of 20° and horizontal chine flare that had a linear term with a form analogous to airfoil lifting-surface theory. This equation, based on the data of Kapryan and Weinstein (ref. 13), is

$$C_{L,s} = \sin \tau \cos \tau \left[\frac{8}{\pi} \frac{1}{1 + \sqrt{1 + \left(\frac{2}{A} \right)^2}} \left(1 - \frac{\beta_{basic}}{\pi} \right) + 2 \sin \tau - B \sin^2 \tau \right] \quad (5)$$

where

$$B = 2.67 \quad (A < 2.0)$$

$$B = 3.0 \quad (A > 2.0)$$

and β_{basic} is the basic angle of dead rise in radians for a model having horizontal chine flare.

In reference 14, Korvin-Kroukovsky, Savitsky, and Lehman proposed an equation for rectangular flat plates and V-shaped surfaces having a constant angle of dead rise that was derived primarily on the basis of the data of Sottorf (ref. 15) and Sambraus (ref. 16). This formula can be written as

$$C_{L,s} = 0.012(57.3\tau)^{1.1}A^{0.5} - 0.0065(57.3\beta)A \left[\frac{0.012(57.3\tau)^{1.1}}{A^{0.5}} \right]^{0.6} \quad (6)$$

Locke (ref. 17) proposed that the lift characteristics of rectangular flat plates and V-shaped surfaces having a constant angle of dead rise can be presented by a power function of the form

$$C_{L,S} = 0.5 \left(1 - \frac{2\beta}{\pi}\right) K \tau^\eta \quad (7)$$

where K and η depend only on aspect ratio and are obtained from curves given in reference 17.

Schnitzer (ref. 18) presented an equation for rectangular flat plates and V-shaped surfaces which was derived from a consideration of two-dimensional deflected mass and was modified for three-dimensional flow by Pabst's empirical aspect-ratio correction factor (ref. 19) and Bobyleff's flow coefficients presented in reference 20. The equation can be written in the form:

$$C_{L,S} = A \phi \cos^2 \tau \sin \tau \left\{ \frac{\pi}{4} \left[\left(\frac{\pi}{2\beta} - 1 \right) \tan \beta \right]^2 + B \left(\frac{l_k}{b} \tan \tau - \frac{\tan \beta}{2} \right) \right\} \quad (8)$$

The term ϕ , which is dependent on aspect ratio, and the term B , which is dependent on angle of dead rise, are given in references 19 and 20, respectively. For the case of a flat-plate planing surface, equation (8) reduces to

$$C_{L,S} = \phi \left(\frac{\pi^3 A}{16} \sin \tau \cos^2 \tau + 0.88 \sin^2 \tau \cos \tau \right) \quad (9)$$

In reference 21, Brown presented empirical equations based on deflected-mass considerations for rectangular flat plates and V-shaped surfaces having a constant angle of dead rise. The equations for a flat plate can be written in the form:

$$C_{L,S} = \frac{2\pi}{\cot \frac{\tau}{2} + \pi + \left(2 \cot \frac{\tau}{2} - \pi \right) \frac{l_m}{b}} \quad (l_m \leq b) \quad (10)$$

and

$$C_{L,S} = (1.67 \sin \tau + 0.09) \sin \tau \cos \tau \left(1 - \frac{b}{l_m} \right) + \frac{2\pi}{3 \cot \frac{\tau}{2} \frac{b}{l_m}} \quad (l_m \geq b) \quad (11)$$

For a surface having a constant angle of dead rise,

$$C_{L,S} = 3.6 \frac{l_k}{b} \cot^2 \beta \sin^3 \tau (1 - \sin \tau) \cos \tau \quad (l_k \leq l_{k,cr}) \quad (12)$$

and

$$C_{L,S} = \left[1.67 \left(1 - \frac{2\beta}{\pi} \right) \sin \tau + 0.09 \right] \sin \tau \cos \tau \left(1 - \frac{l_{k,cr}}{l_k} \right) + 0.9 \frac{b}{l_k} \sin \tau (1 - \sin \tau) \cos^3 \tau \quad (l_k \geq l_{k,cr}) \quad (13)$$

where

$$l_{k,cr} = \frac{b}{2} \cot \tau \tan \beta \quad (14)$$

which is defined as the critical keel wetted length. For surfaces having a constant angle of dead rise and a transverse step, the critical keel wetted length is defined as the keel wetted length at which the stillwater line passes through the rearmost point of the chine. For the flat plate the value of the critical keel wetted length was assumed, after analysis of experimental data, to be equal to the beam.

PROPOSED THEORY

LIFT

In reference 1 an equation for the lift on a rectangular flat plate was developed from a consideration of linear and nonlinear components of lift (an approach generally used in low-aspect-ratio and slender-body airfoil theory). In the present report this equation is revised and extended to include V-bottom surfaces. The equation is divided into three parts: (1) a reasonably accurate approximation to the linear components of lift is made; (2) a method for calculating the crossflow effects is presented; and (3) an estimation of the aerodynamic leading-edge suction is made.

Linear term.—The linear term is determined in reference 1 from a consideration of the lifting-line theory and is given by

$$C_{L,1} = \frac{0.5\pi A \tau}{1+A} \quad (15)$$

This relation gives the linear component of lift on a pure-planing flat plate.

In references 3 and 18, a dead-rise function was determined from a consideration of an iterative solution made by Wagner (ref. 2) for the impact force on a V-bottom surface immersing with a constant vertical velocity. The dead-rise function can be written

$$K(\beta) = \left(1 - \frac{2\beta}{\pi} \right)^2 \left(\frac{\tan \beta}{\beta} \right)^2$$

This dead-rise function (developed for application to equations derived from virtual mass concepts) does not correlate well with experiment when applied to equation (15) for angles of dead rise above approximately 25° . Therefore, another dead-rise function $1 - \sin \beta_e$ which correlates well with experiment up to angles of dead rise of 50° is used; thus,

$$C_{L,2} = \frac{0.5\pi A \tau}{1+A} (1 - \sin \beta_e) \quad (16)$$

This expression is for the linear component of lift on rectangular flat and V-bottom planing surfaces. A comparison of the dead-rise function $1 - \sin \beta_e$ with the dead-rise function based on Wagner's solution is given in figure 1.

Crossflow effects.—For a simple theoretical consideration of the crossflow effects, the velocity component perpendicular to the surface of a flat plate is assumed to be of the magnitude $V \sin \tau$. The flow is projected into components

perpendicular to and parallel to the planing surface, and the drag force associated with the flow perpendicular to the planing surface is calculated. The normal force on a flat plate, therefore, is

$$N = C_{D,c} \frac{\rho}{2} S (V \sin \tau)^2$$

Then

$$C_{L,3} = C_{D,c} \sin^2 \tau \cos \tau \quad (17)$$

is a lift coefficient due to crossflow effects, and is proportional to $\sin^2 \tau$. This relation is the concept presented for airfoils by Betz in reference 22. The crossflow drag coefficient $C_{D,c}$ used in this elementary derivation of the crossflow term was assumed in reference 1 to be one-half the value $C_{D,c}=2$ generally used for aerodynamic surfaces. The value of $C_{D,c}$ is known to vary with the shape of the cross section and to be sensitive to local shape at the edges. Since the theoretical determination of these effects is very difficult and the simple cases which have been solved have not correlated with experiment, the analysis of suitable experiments will generally provide the easiest and most accurate method of determining $C_{D,c}$.

For the case of the V-bottom the theoretical effect of dead rise is given by Bobyleff in reference 20 for a bent lamina, the section of which consists of two equal straight lines forming an angle. Bobyleff's flow coefficient, which can be approximated by $\cos \beta_e$ (see fig. 2), represents the ratio of the resultant pressure on a V-bottom to that experienced by a flat plate of the same beam in normal flow; thus,

$$C_{L,4} = (C_{D,c})_{\beta_e=0} \sin^2 \tau \cos \tau \cos \beta_e \quad (18)$$

which is the crossflow component of lift.

Suction component of lift.—An airfoil has a suction component of lift due to the large negative pressures produced by the flow around the leading edge of the airfoil; however, for a planing surface where there is no flow around the leading edge, this suction does not appear. In the strictest sense the suction component of lift should be based only on the linear term (see ref. 1); however, comparison of experiment with theory indicates that better agreement is obtained if the suction component of lift is based on $C_{L,2} + C_{L,4}$. Therefore, the lift is less than that predicted by equations (16) and (18) by an amount

$$C_{L,5} = (C_{L,2} + C_{L,4}) \sin^2 \tau \quad (19)$$

Total lift.—The total lift on pure-planing surfaces can be obtained from the sum of the linear component of lift (eq. (16)) and the crossflow effects (eq. (18)) minus the suction component of lift (eq. (19)); thus, by combining terms

$$\left. \begin{aligned} C_{L,S} &= \left[\frac{0.5\pi A \tau}{1+A} \cos^2 \tau (1 - \sin \beta_e) \right] + \\ &\quad [(C_{D,c})_{\beta_e=0} \cos^3 \tau \sin^2 \tau \cos \beta_e] \\ C_{L,S} &= C_{L,6} + C_{L,7} \end{aligned} \right\} \quad (20)$$

where

$$C_{L,6} = \frac{0.5\pi A \tau}{1+A} \cos^2 \tau (1 - \sin \beta_e) \quad (21)$$

and

$$C_{L,7} = (C_{D,c})_{\beta_e=0} \cos^3 \tau \sin^2 \tau \cos \beta_e \quad (22)$$

For equation (20) to predict adequately the lift on triangular surfaces planing with base forward, it has been necessary to define the aspect ratio as the ratio of maximum beam to overall length; that is, $A_t = b/l$.

APPLICATION OF LIFT THEORY

In order to use equation (20) to predict the lift of planing surfaces, only the determination of the proper value of $C_{D,c}$ is required. Values of $C_{D,c}$ for various chine configurations for which experimental data are available are presented in figure 3. For a given model $C_{D,c}$ did not vary with trim or length-beam ratio. Also it can be seen that, as long as the angle of dead rise was constant for the entire beam, $C_{D,c}$ did not vary with the angle of dead rise.

Rectangular flat and V-bottom surfaces having a constant angle of dead rise.—The crossflow drag coefficient for the sharp-chine models was determined from tests (from ref. 23 and data presented in the present report) to be 4/3. This value is two-thirds the value given for a two-dimensional flat-plate airfoil; thus, from equation (20)

$$C_{L,S} = \frac{0.5\pi A \tau}{1+A} \cos^2 \tau (1 - \sin \beta_e) + \frac{4}{3} \sin^2 \tau \cos^3 \tau \cos \beta_e \quad (23)$$

The relative magnitudes of the total lift (eq. (23)), the total lift before removal of lift due to leading-edge suction (eq. (16) plus eq. (18) with $C_{D,c} = \frac{4}{3}$), and the crossflow term (eq. (22) with $C_{D,c} = \frac{4}{3}$) is shown in figure 4 for surfaces having angles of dead rise of 0°, 20°, and 40°.

Horizontal chine flare.—The total lift on a pure-planing V-shaped prismatic surface with horizontal chine flare similar to the models shown in figure 5 can be determined from equation (20). The crossflow drag coefficients $C_{D,c}$ determined from data presented in references 13, 24, and 25 are given in figure 3.

Vertical chine strips.—The total lift on a pure-planing V-shaped prismatic surface with vertical chine strips similar to the models shown in figure 6 can be determined from equation (20). The crossflow drag coefficients determined from the data presented in references 25 and 26 are given in figure 3.

Triangular flat plate.—The total lift on a pure-planing triangular flat plate planing with base forward can be estimated from equation (23) if the aspect ratio is defined as the ratio of the maximum beam to the overall length or $A_t = b/l$; thus,

$$C_{L,S} = \frac{0.5\pi A_t \tau}{1+A_t} \cos^2 \tau + \frac{4}{3} \cos^3 \tau \sin^2 \tau \quad (24)$$

CENTER OF PRESSURE

The center of pressure on a planing surface may be determined from the lift coefficients given by equations (21) and (22) and by estimating the location of the center of pressure of these two components of the total lift coefficient for a given planing-surface plan form.

Rectangular plan form.—The center of pressure of the component of lift given by equation (21) is assumed to be located at seven-eighths of the mean wetted length from the trailing edge of the planing surface. This location is between the three-quarter-chord position generally assumed in lifting-line theory and the position obtained from the prediction of no lift behind the section maximum width for low-aspect-ratio airfoils (ref. 27).

The center of pressure for the lift due to crossflow effects is generally assumed to be located at the center of the area in airfoil theory. Therefore, the center of pressure for the component of lift given by equation (22) is assumed to be located at the center of the mean wetted length; thus,

$$\left(\frac{l_{cp}}{l_m}\right)_{calc} = \frac{\frac{7}{8}C_{L,6} + \frac{1}{2}C_{L,7}}{C_{L,S}} \quad (25)$$

where $C_{L,6}$ is given by equation (21), $C_{L,7}$ is given by equation (22), and $C_{L,S}$ is given by equation (20).

Triangular plan form.—The center of pressure of the component of lift given by the first term on the right-hand side of equation (24) is assumed to be located at the mean of the heavy spray line which is approximately the section of maximum wetted width.

The center of pressure for the component of lift given by the second term on the right-hand side of equation (24) (that is, the crossflow term) is assumed to be at approximately the center of the wetted area; thus,

$$\left(\frac{l_{cp}}{l_m}\right)_{calc} = \frac{C_{L,S} + \frac{2}{3}C_{L,9}}{C_{L,S}} \quad (26)$$

and is the center-of-pressure location for triangular flat plates planing with base forward. The value of $C_{L,S}$ is determined from equation (24) where $C_{L,8}$ and $C_{L,9}$ are given by the first and second terms on the right-hand side of equation (24), respectively.

COMPARISON OF PROPOSED AND PREVIOUS PLANING FORMULAS

A comparison of the values of lift coefficient (plotted against trim for constant length-beam ratio) calculated from the proposed theory (eq. (20)) and from previous summarized planing formulas is given in figures 7 to 10 and an index to the comparison is given in the following table:

Configuration	Equation (20)* compared with planing formulas presented in—		Lift coefficient values presented in figure—
	Reference	Equation	
Rectangular flat plate	4, 5, 6, and 7 8, 9, and 10	-----	7(a) 7(b)
	-----	(7), (9), (10), and (11) (2), (5), and (6)	7(c) 7(d)
	1 11	-----	7(e) **
V-shaped surface having a constant angle of dead rise of 20°	-----	(6) and (7) (8), (12), and (13)	8(a) 8(b)
V-shaped surface having a constant angle of dead rise of 40°	-----	(6) and (7) (8), (12), and (13)	9(a) 9(b)
V-shaped surface having an angle of dead rise of 20° and horizontal chine flare ($\beta_s=16^\circ$)	-----	(5)***	10

*Value of $C_{D,e}$ of $\frac{4}{3}$ (see eq. (23)) used unless otherwise noted.

**Lift coefficients were not plotted since the results depended on the airfoil data used.

***Value of $C_{D,e}$ of 1.59 used in equation (20).

In figure 11 the values of lift coefficient (plotted against mean-wetted-length-beam ratio for constant trim) calculated from the proposed theory (eq. (23)) and planing formulas as presented in references 14, 17, 18, and 21 are compared with the data of the present report (see tables I(a), II, and III) and references 23 and 28 for models having angles of dead rise of 0° (fig. 11(a)), 20° (fig. 11(b)), and 40° (fig. 11(c)). Only the theories that apply to both flat-plate and V-shaped surfaces have been compared in figure 11.

It can be seen from figures 11 (a) to 11(c) that none of the planing formulas presented in references 14, 17, 18, and 21 are adequate for estimating the lift coefficients for either flat-plate or V-bottom planing surfaces, whereas the lift coefficients calculated from the equation proposed in the present report (eq. (23)) agree very well with experiment. The equation presented in reference 12 (eq. (2)), however, gives a good approximation of the lift coefficient for a flat plate. (See fig. 7(d).)

EXPERIMENTAL INVESTIGATION

DESCRIPTION OF MODELS

The models used for this investigation had a beam of 4 inches and a length of 36 inches. The models shown in figure 12 for a flat plate and surfaces having angles of dead rise of 20° and 40° were constructed of brass and are the same models investigated in references 23 and 28. Additional flat-plate models that had sharp chines, $\frac{1}{64}$ -inch-radius chines, and $\frac{1}{16}$ -inch-radius chines were constructed of plastic. (See fig. 13.) The model with the $\frac{1}{64}$ -inch-radius chines was made by rounding the chines on the sharp-chine model after the tests with the sharp-chine model had been completed. The plastic models were backed with a $\frac{1}{2}$ -inch reinforcing steel plate.

APPARATUS AND PROCEDURES

The experimental investigation was made with the main towing carriage in Langley tank no. 2 and existing strain-gage balances which independently measured the lift, drag, and moment. The lift and drag were measured with the balances capable of measuring: (1) 600 pounds of lift and 250 pounds of drag, and (2) 1,000 pounds of lift and 600 pounds of drag. The moment was measured about an arbitrary point above the model. The tests were made with the wind and spray shield installed, as shown in figure 14, unless otherwise indicated.

The wetted areas were determined from underwater photographs made with a 70-millimeter camera mounted in a waterproof box located at the bottom of the tank. The camera and high-speed flash lamps were set off by the action of the carriage interrupting a photoelectric beam. The wetted length was obtained from markings on the bottom of the models. In order to assure a very smooth bottom, the markings on the brass models were erased except in the region of the heavy spray line. (See fig. 15.) The plastic models had markings each $\frac{1}{2}$ inch for the full length of the models.

The force measurements were made at constant speeds for fixed angles of trim. The change in trim due to structural deflection caused by the lift and drag forces on the model was obtained during the calibration of the balances and the trim of the model was adjusted accordingly before each run. Slight adjustments to lift and resistance to correct the data

to the desired trim were made after completion of tests for the cases where the forces or center-of-pressure location were different from the values used to estimate the trim due to structural deflection. The change in trim due to structural deflection did not exceed 0.2° for most conditions although in a few cases changes up to 0.6° occurred.

The aerodynamic forces on the model and towing gear were found to be negligible when the wind screen was used. The aerodynamic tares were subtracted from the data when the wind screen was not used.

The accuracy of the quantities measured are believed to be within the following limits:

Lift, lb	± 5.0
Resistance, lb	± 3.0
Trimming moment, ft-lb	± 3.0
Wetted length, ft	± 0.01
Trim, deg	± 0.15
Speed, ft/sec	± 0.20

The forces were converted to coefficient form by using a measured value of density of 1.942 slugs/cu ft. The kinematic viscosity measured during the tests varied from 1.53×10^{-5} sq ft/sec to 1.80×10^{-5} sq ft/sec.

RESULTS AND DISCUSSION

GENERAL

The lift coefficient, resistance coefficient, ratio of wetted length to beam, ratio of center-of-pressure location to mean wetted length, speed coefficient, and kinematic viscosity are presented at given trims in tables I to III for all models. The lift and drag coefficients are expressed both in terms of the square of the beam and in terms of principal wetted area.

Sharp chines.—The lift coefficients and center-of-pressure location for the sharp-chine models are considered in the section "Comparison of Theory and Experiment for Lift."

The resistance data for the sharp-chine brass models having constant angles of dead rise of 0° , 20° , and 40° are presented in figure 16 as plots of the variation of drag coefficient $C_{D,S}$ and induced drag coefficient $C_{D,i}$ (which is equal to $C_{L,S} \tan \tau$) with mean-wetted-length—beam ratios for given trims. The difference between the solid and dashed lines represents the friction drag. (Since the data were obtained for speeds above the critical speed of wave propagation for the 6-foot-deep tank, there is no wave drag due to transverse waves included; however, there may be some drag due to spray or other causes included in this difference.) At high trims and low length-beam ratios the induced drag exceeds the total drag and indicates an apparent negative friction force. (This result was previously reported in ref. 23.) The volume of forward spray is large at high trims and appears to have a high forward velocity with respect to the model. The relative velocity of the model in the region of forward spray therefore is effectively reversed (see fig. 17) so that the friction drag due to this spray acts in a direction opposite to that of the drag in the principal wetted area and thereby reduces the total drag. Therefore, at low length-beam ratios where the friction drag is small, this negative friction drag due to forward spray may cause a negative friction force at high trims.

The variation of $\frac{l_k - l_c}{b}$ with trim for the models having

sharp chines and constant angles of dead rise of 0° , 20° , and 40° is given in figure 18. At a trim of 12° , the value of $\frac{l_k - l_c}{b}$ is approximately constant for all length-beam ratios for the models having constant angles of dead rise of 0° , 20° , or 40° . At high trims, however, the values of $\frac{l_k - l_c}{b}$ for the flat-plate model increase with increase in length-beam ratio, are approximately constant for a given trim for a model having a constant angle of dead rise of 20° , and decrease with an increase in length-beam ratio for a model having a constant angle of dead rise of 40° . The value of $\frac{l_k - l_c}{b}$ for the flat-plate model decreases with increase in trim at low length-beam ratios and increases with increase in trim at high length-beam ratios; however, the value of $\frac{l_k - l_c}{b}$ decreases with increase in trim for all length-beam ratios for the models having constant angles of dead rise of 20° and 40° .

Wind screen and spray shield.—The lift coefficient for the flat-plate model with wind screen and spray shield removed (aerodynamic tares subtracted) was approximately the same as the lift coefficient obtained when the wind screen and spray shield were used. (See fig. 19.) At a trim of 12° the drag coefficient for the flat-plate model with the wind screen removed was approximately the same as the drag coefficient obtained with the wind screen installed (see fig. 20); however, for a trim of 18° the drag coefficient of the flat plate with the wind screen removed was less than that obtained when the wind screen was used even before the aerodynamic tares were subtracted. The value of the difference is in the wrong direction to be explained by the aerodynamic tares. (The aerodynamic tares subtracted were less than the difference in fig. 20.) The variation of the center-of-pressure location with mean length-beam ratio on the flat-plate model was approximately the same for data taken with and without the wind screen and spray shield installed. (See fig. 21.)

Speed.—The effect of speed at high trims (24°) is shown in figures 22 to 24. The variation of lift coefficient, drag coefficient, and center-of-pressure location is approximately the same for speeds of 30 and 60 feet per second for 4-inch-beam prismatic models having constant angles of dead rise of 0° , 20° , and 40° ; therefore, there was apparently no speed effect for this range of speeds.

Rounded chines.—The effect of $\frac{1}{4}$ -inch-radius and $\frac{1}{16}$ -inch-radius chines on the lift coefficient, drag coefficient, center-of-pressure location, skin-friction coefficient, and lift-drag ratio of a 4-inch-beam rectangular flat plate is shown in figures 25 to 29. Rounding the sharp chines of the flat-plate model to radii of $\frac{1}{4}$ inch and $\frac{1}{16}$ inch resulted in a decrease in lift and drag coefficients; however, the center-of-pressure location, skin-friction coefficients, and lift-drag ratios remained approximately the same. A decrease in lift of approximately 5 and 9 percent resulted from rounding the sharp chines to a radii of $\frac{1}{4}$ inch and $\frac{1}{16}$ inch, respectively. (See fig. 25.) A decrease in lift for a small rounding of the chines was also observed by Perry (ref. 29).

The variation of skin-friction coefficient with Reynolds

number for a trim of 8° is presented in figure 28 for a flat-plate model having sharp chines and $\frac{1}{16}$ -inch-radius chines. The agreement between the data and the Schoenherr turbulent-flow line indicates that, at low trims and high Reynolds numbers, the drag can be calculated with reasonable accuracy from

$$C_{D,S} = C_f + C_{L,S} \tan \tau \quad (27)$$

where C_f is determined from the Schoenherr turbulent flow line. (See ref. 30.) The lift-drag ratios at high trims are influenced little by the chine condition; however, at low trims (8°) the lift-drag ratios for the sharp-chine models are slightly higher than those for models having rounded chines. (See fig. 29.)

Pure planing.—The experimental data were considered as pure planing if the lift coefficient due to buoyancy based on the total wedge-shaped volumetric displacement of the planing surface $C_{L,vol}$ did not exceed a given value. The lift coefficient due to buoyancy was calculated from the wedge-shaped volumetric displacement of the planing surface below the level water surface given by

$$C_{L,vol} = \frac{l_m}{b} \frac{1}{2C_V^2} \sin 2\tau \quad (28)$$

for rectangular flat plates and

$$C_{L,vol} = \frac{1}{(l_k + l_c) C_V^2} \left[\frac{l_c^2}{b} \sin 2\tau + \frac{1}{3} (2l_c + l_k) \tan \beta \right] \quad (29)$$

for rectangular surfaces having dead rise and

$$C_{L,vol} = \frac{l}{b} \frac{1}{3C_V^2} \sin 2\tau \quad (30)$$

for triangular flat plates with straight leading edge and pointed trailing edge.

The allowable lift coefficient due to buoyancy $C_{L,vol}$, as determined from equations (28) to (30), was arbitrarily selected as 0.01 at a trim of 16° . The maximum allowable lift coefficient due to buoyancy $C_{L,vol}$ for other trims was determined by drawing a straight line from zero trim (and zero lift coefficient due to buoyancy $C_{L,vol}$) through the value 0.01 at a trim of 16° on a curve of the variation of lift coefficient with trim. For the flat-plate data the maximum allowable lift coefficient due to buoyancy $C_{L,vol}$ selected by this method at a trim of 2° varied from 16 percent of the predicted lift coefficient at a length-beam ratio of 8 to 3.3 percent of predicted lift coefficient (eq. (23)) at a length-beam ratio of $\frac{1}{2}$. These values decreased with increasing trim so that at 30° they would vary from 6.6 percent at a length-beam ratio of 8 to 3.0 percent at a length-beam ratio of $\frac{1}{2}$. The permissible lift coefficient for surfaces having dead rise is, in general, a slightly greater percentage of the predicted lift coefficient than the values given for the rectangular flat plate.

Buoyancy.—The experimental lift coefficients given in reference 31 less the lift coefficients calculated from equation (20) with $C_{D,c}=1.15$ plotted against the lift coefficient due to buoyancy $C_{L,vol}$ calculated from equation (28) are plotted in figure 30. Since equation (20) with $C_{D,c}=1.15$ is approximately the pure-planing lift for the model investigated in reference 31 (see fig. 32 (c)), the subtraction of this value from the experimental lift coefficients should indicate the amount of lift due to buoyancy present in the data. Only values of the difference between the experimental lift coefficient and the calculated lift coefficient greater than 0.01 are considered since, for small differences between experimental and calculated values, this method is not considered to be sufficiently accurate to determine the lift coefficient due to buoyancy present in the experimental data; however, this method should give reasonably accurate indications of the lift coefficient due to buoyancy present in the experimental data for the cases where the lift coefficient due to buoyancy is large. Figure 30 shows that the magnitude of the lift coefficient due to buoyancy for different speeds is approximately one-half the lift due to buoyancy based on the total wedge-shaped volumetric displacement computed by equation (28); therefore, a rough empirical approximation of the increase in lift coefficient due to buoyancy can be calculated with reasonable accuracy from

$$C_{L,B} \approx \frac{1}{2} C_{L,vol} \quad (\tau \geq 8^\circ; C_V \geq 3) \quad (31)$$

where $C_{L,vol}$ is given in equations (28) to (30). For low trims (4°) a lift coefficient due to buoyancy greater than that given by equation (31) is required to account for the additional lift coefficient due to buoyancy as indicated by the flagged symbols in figure 30.

COMPARISON OF THEORY AND EXPERIMENT

Lift.—Only the experimental data indicated as pure planing by the method discussed in the preceding section are considered for the comparison with theory. Also, the data considered are only for the chine-immersed condition. The theory is applicable to the non-chine-immersed condition; however, for surfaces having other than a constant angle of dead rise such as those having horizontal chine flare or vertical chine strips, the shape of the cross section varies, and, therefore, the crossflow drag coefficient would not be the same value as that determined for the chine-immersed condition. The values were calculated from the proposed theory as if there were no non-chine-immersed conditions. For the non-chine-immersed condition, the lift coefficient for a surface having a constant angle of dead rise is approximately the value determined at the instant of chine immersion and is a constant for a given trim and angle of dead rise. (The length-beam ratio is approximately a constant value for all non-chine-immersed conditions for a given trim and angle of dead rise.)

In order to simplify the comparison, the data are summarized in the following table:

Configuration	Description of model used	Data to be compared—		Data presented in figure—	Remarks
		Equation of present paper—	Experimental data of reference—		
Rectangular flat plate	4-inch-beam brass model Sharp chine plastic model 4-inch-beam brass model Various models	(23)	{ ----- 23 12, 32, 31, 33, 34, 16, 15, and 25 Present paper	31 (a) 31 (b) 31 (c) 31 (d) to 31 (k) 32 (a) and 32 (b)	{ Agreement good except at trims above approximately 30° at large length-beam ratios Agreement good Agreement good; some differences with wooden models $C_{D,c}$ reduced to 1.15 and 1.20
	4-inch-beam plastic model with $\frac{1}{16}$ -inch-radius chines and $\frac{1}{64}$ -inch-radius chines		(20)	31, 32, and 35	Models used in reference data had either slightly rounded or roughened chines and reduced values of $C_{D,c}$ resulted. In case of reference 35 the chines had greater chine radius or roughness as a result of wear in use; further reduction in $C_{D,c}$ resulted.
	Wooden model (same model used in both ref. 31 and 35)			32 (c) to 32 (e)	
Basic V-surface	With angle of dead rise of 20° With angle of dead rise of 40°	(23)	{ 28 and 25 28 and 25	33 34	{ Agreement good except for trims above approximately 30° Agreement good for length-beam ratios above 3.0; below this value the experimental data failed to show the usual increase in C_L as l_m/b decreased. Similar effect slightly evident in fig. 34 (b) for $\beta=40^\circ$.
	With angle of dead rise of 50°		{ 36	35	
V-surface with horizontal chine flare	With an effective angle of dead rise of 16° With an effective angle of dead rise of 32°47'	(20) ($C_{D,c}$ value from fig. 3)	{ 13 and 25 24 and 25	36 37	{ Agreement good Agreement good
V-surface with vertical chine strip	With an effective angle of dead rise of 15°33' With an effective angle of dead rise of 31°59'	(20) ($C_{D,c}$ value from fig. 3)	{ 26 26	38 39	{ Agreement good Agreement good
Triangular flat plate (base forward)	Wooden surfaces (see fig. 40)	(24)	31 and unpublished tank no. 2 data	41	Agreement good up to trims of 16°. Values lower than those at trim of 20°; chines may be slightly rounded since they are made of wood.

Some of the experimental data that were obtained with wooden models (for example, see ref. 31) were lower than the values predicted by the proposed theory; this difference is thought to be due to the influence of the local shape at the edges (slightly rounded or roughened chines).

The effects of Reynolds number, scale, and nonuniform chine radii on $C_{D,c}$ have not been determined because of the limited data available.

The lift on various pure-planing surfaces with rectangular or triangular plan forms similar to those considered can be estimated by changing the value of the crossflow drag coefficient $C_{D,c}$ for a given configuration. Values of the crossflow drag coefficient should be determined from tests; however, reasonably accurate approximations that are satisfactory for engineering calculations can probably be made (see fig. 3) that will approximate the pure-planing lift for surfaces similar to those considered herein.

For planing surfaces that vary considerably from those considered herein, only data for a given angle of trim and

aspect ratio (for a given effective angle of dead rise) are required to determine the value of $C_{D,c}$ from equation (20). (The experimental values of lift coefficient, trim, aspect ratio, and effective angle of dead rise are substituted into equation (20), which is then solved for the value of $C_{D,c}$.) Since the value of $C_{D,c}$ is a constant for a given planing-surface cross section, the lift coefficient for wide ranges of trim and aspect ratio can then be estimated. If values of $C_{D,c}$ are obtained for two or more effective angles of dead rise for a given type of planing surface, the value of $C_{D,c}$ for similar surfaces having a different effective angle of dead rise can be estimated by interpolation. Therefore, in order to calculate the lift coefficient from equation (20) for wide ranges of trim, length-beam ratio, and effective angle of dead rise for a given family of planing surfaces, only a very few test points are required.

Center-of-pressure location.—A comparison of theory and experiment for the center of pressure is given in the following table:

Configuration	Description of model used	Data to be compared—		Data presented in figure—	Remarks
		Equation of present paper (a)	Experimental data of reference—		
Rectangular flat plate	4-inch-beam brass model	(25)	23, 31, and 25	42	Good agreement
Basic V-surface	With angle of dead rise of 20° With angle of dead rise of 40° With angle of dead rise of 50°	(25) (25) (25)	{ 25 and 28 25 and 28 36	43 44 45	{ Good agreement Good agreement Good agreement
V-surface with horizontal chine flare	With an effective angle of dead rise of 16° With an effective angle of dead rise of 32°47'	(25) (25)	{ 13 and 25 24 and 25	46 47	{ Good agreement Good agreement
V-surface with vertical chine strips	With an effective angle of dead rise of 15°33' With an effective angle of dead rise of 31°59'	(25) (25)	{ 26 26	48 49	{ Good agreement Good agreement
Triangular plan form	Wooden surfaces (see fig. 40)	(26)	31 and unpublished tank no. 2 data	50	Good agreement

^a The values of $C_{D,c}$ for equation (25) were determined from figure 3.

CONCLUDING REMARKS

The principal planing characteristics for models have been obtained in extended ranges of trim and length-beam ratio for a rectangular flat plate and two V-bottom surfaces; therefore, force approximations for water-based aircraft can be made in these extended ranges with more confidence. The data obtained for rectangular-flat-plate surfaces having very slightly rounded chines indicated that slight differences in construction at the point of flow separation can result in decreased lift and drag coefficients obtained for a given flat-plate configuration; however, the center-of-pressure location, skin-friction coefficients, and lift-drag ratios remained approximately the same for the trims tested (8° to 18°). These data showed that slight differences in construction at the point of flow separation were probably the reason for the differences in experimental data obtained for a given configuration by various experimenters.

The proposed theory appears to predict with engineering accuracy the lift and center-of-pressure location of rectangu-

lar flat plates, triangular flat plates planing with base forward, and V-shaped surfaces having a constant angle of dead rise, horizontal chine flare, or vertical chine strips. A reasonably accurate approximation can probably be made for the crossflow drag coefficient of a given model that will result in satisfactory engineering calculations of lift and center of pressure for pure-planing surfaces similar to those considered in the present report. Also, the proposed theory (which can be applied to both the chine-immersed and the non-chine-immersed condition) together with the method for approximating the lift coefficient due to buoyancy gives a reasonably accurate method for estimating the lift characteristics of planing surfaces for a wide range of conditions.

LANGLEY AERONAUTICAL LABORATORY,
NATIONAL ADVISORY COMMITTEE FOR AERONAUTICS,
LANGLEY FIELD, VA., November 23, 1956.

REFERENCES

1. Shuford, Charles L., Jr.: A Review of Planing Theory and Experiment With a Theoretical Study of Pure-Planing Lift of Rectangular Flat Plates. NACA TN 3233, 1954.
2. Wagner, Herbert: Phenomena Associated With Impacts and Sliding on Liquid Surfaces. S-302, British A.R.C., July 14, 1936.
3. Mayo, Wilbur L.: Analysis and Modification of Theory for Impact of Seaplanes on Water. NACA Rep. 810, 1945. (Supersedes NACA TN 1008.)
4. Sokolov, N. A.: Hydrodynamic Properties of Planing Surfaces and Flying Boats. NACA TM 1246, 1950.
5. Sedov, L.: Scale Effect and Optimum Relations for Sea Surface Planing. NACA TM 1097, 1947.
6. Perelmuter, A.: On the Determination of the Take-Off Characteristics of a Seaplane. NACA TM 863, 1938.
7. Sottorf, W.: Analysis of Experimental Investigations of the Planing Process on the Surface of Water. NACA TM 1061, 1944.
8. Perring, W. G. A., and Johnston, L.: Hydrodynamic Forces and Moments on a Simple Planing Surface and on a Flying Boat Hull. R. & M. No. 1646, British A.R.C., 1935.
9. Korvin-Kroukovsky, B. V.: Lift of Planing Surfaces. Jour. Aero. Sci. (Readers' Forum), vol. 17, no. 9, Sept. 1950, pp. 597-599.
10. Siler, William: Lift and Moment of Flat Rectangular Low Aspect Ratio Lifting Surfaces. Tech. Memo. No. 96, Exp. Towing Tank, Stevens Inst. Tech., 1949.
11. Perry, Byrne: The Effect of Aspect Ratio on the Lift of Flat Planing Surfaces. Rep. No. E-24.5 (Contract N6onr-24424, Project NR 234-001), Hydrod. Lab., C.I.T., Sept. 1952.
12. Farshing, Donald David, Jr.: The Lift Coefficient of Flat Planing Surfaces. M. S. Thesis, Stevens Inst. Tech., 1955.
13. Kapryan, Walter J., and Weinstein, Irving: The Planing Characteristics of a Surface Having a Basic Angle of Dead Rise of 20° and Horizontal Chine Flare. NACA TN 2804, 1952.
14. Korvin-Kroukovsky, B. V., Savitsky, Daniel, and Lehman, William F.: Wetted Area and Center of Pressure of Planing Surfaces. Preprint No. 244, S.M.F. Fund Paper, Inst. Aero. Sci. (Rep. No. 360, Project No. NRO62-012, Office Naval Res., Exp. Towing Tank, Stevens Inst. Tech., Aug. 1949.)
15. Sottorf, W.: Experiments With Planing Surfaces. NACA TM 661, 1932.
16. Sambraus, A.: Planing-Surface Tests at Large Froude Numbers—Airfoil Comparison. NACA TM 848, 1938.
17. Locke, F. W. S., Jr.: An Empirical Study of Low Aspect Ratio Lifting Surfaces With Particular Regard to Planing Craft. Jour. Aero. Sci., vol. 16, no. 3, Mar. 1949, pp. 184-188.
18. Schnitzer, Emanuel: Theory and Procedure for Determining Loads and Motions in Chine-Immersed Hydrodynamic Impacts of Prismatic Bodies. NACA Rep. 1152, 1953. (Supersedes NACA TN 2813.)
19. Pabst, Wilhelm: Landing Impact of Seaplanes. NACA TM 624, 1931.
20. Lamb, Horace: Hydrodynamics. Sixth ed., Cambridge Univ. Press, 1932.
21. Brown, P. Ward: An Empirical Analysis of the Planing Characteristics of Rectangular Flat-Plates and Wedges. Hydrod. Note No. 47, Short Bros. & Harland Ltd. (Belfast), Sept. 1954.
22. Betz, A.: Applied Airfoil Theory. Airfoils or Wings of Finite Span. Vol. IV of Aerodynamic Theory, div. J, Ch. III, sec. 7, W. F. Durand, ed., Julius Springer (Berlin), 1935 (reprinted by Durand Reprinting Committee, 1943), pp. 69-72.
23. Weinstein, Irving, and Kapryan, Walter J.: The High-Speed Planing Characteristics of a Rectangular Flat Plate Over a Wide Range of Trim and Wetted Length. NACA TN 2981, 1953.
24. Blanchard, Ulysse J.: The Planing Characteristics of a Surface Having a Basic Angle of Dead Rise of 40° and Horizontal Chine Flare. NACA TN 2842, 1952.
25. Kapryan, Walter J., and Boyd, George M., Jr.: Hydrodynamic Pressure Distributions Obtained During a Planing Investigation of Five Related Prismatic Surfaces. NACA TN 3477, 1955.
26. Kapryan, Walter J., and Boyd, George M., Jr.: The Effect of Vertical Chine Strips on the Planing Characteristics of V-Shaped Prismatic Surfaces Having Angles of Dead Rise of 20° and 40° . NACA TN 3052, 1953.
27. Jones, Robert T.: Properties of Low-Aspect-Ratio Pointed Wings at Speeds Below and Above the Speed of Sound. NACA Rep. 835, 1946. (Supersedes NACA TN 1032.)
28. Chambliss, Derrill B., and Boyd, George M., Jr.: The Planing Characteristics of Two V-Shaped Prismatic Surfaces Having Angles of Dead Rise of 20° and 40° . NACA TN 2876, 1953.
29. Perry, Byrne: Lift Measurements on Small-Scale Flat Planing Surfaces. Rep. No. E-24.10 (Contract N6onr-24424, Project NR 234-001), Hydrod. Lab., C.I.T., Apr. 1954.
30. Davidson, Kenneth S. M.: Resistance and Powering. Detailed Considerations—Skin Friction. Vol. II of Principles of Naval Architecture, ch. II, pt. 2, sec. 7, Henry E. Rossell and Lawrence B. Chapman, eds., Soc. Naval Arch. and Marine Eng., 1939, pp. 76-83.

31. Wadlin, Kenneth L., and McGehee, John R.: Planing Characteristics of Three Surfaces Representative of Hydro-Ski Forms. NACA RM L9C03, 1949.
32. McBride, Ellis E.: An Experimental Investigation of the Scale Relations for the Impinging Water Spray Generated by a Planing Surface. NACA TN 3615, 1956.
33. Shoemaker, James M.: Tank Tests of Flat and V-Bottom Planing Surfaces. NACA TN 509, 1934.
34. Locke, F. W. S., Jr.: Tests of a Flat Bottom Planing Surface To Determine the Inception of Planing. NAVAER DR. Rep. 1096, Bur. Aero., Dec. 1948.
35. Christopher, Kenneth W.: Effect of Shallow Water on the Hydrodynamic Characteristics of a Flat-Bottom Planing Surface. NACA TN 3642, 1956.
36. Springston, George B., Jr., and Sayre, Clifford L., Jr.: The Planing Characteristics of a V-Shaped Prismatic Surface With 50 Degrees Dead Rise. Rep. 920, David W. Taylor Model Basin, Navy Dept., Feb. 1955.

TABLE I

EXPERIMENTAL PLANING DATA OBTAINED FOR A RECTANGULAR FLAT PLATE

(a) Brass model having sharp chines

Trim, τ , deg	C_V	$\frac{l_c}{b}$	$\frac{l_m}{b}$	$\frac{l_k}{b}$	$\frac{l_{cp}}{l_m}$	ν , sq ft/sec	$C_{D,b}$	$C_{L,b}$	$C_{D,s}$	$C_{L,s}$
12	18.22	1.59	1.64	1.66	0.705	1.80×10^{-5}	0.061	0.285	0.037	0.174
	18.13	2.66	2.72	2.74	.744	1.80	.087	.375	.032	.138
	18.19	3.68	3.74	3.77	.714	1.78	.108	.453	.029	.121
	18.19	4.82	4.85	4.87	.687	1.78	.126	.524	.026	.108
	18.19	5.60	5.65	5.68	.694	1.78	.141	.582	.025	.103
	18.17	6.74	6.80	6.82	.652	1.67	.156	.646	.023	.095
15	18.38	7.70	7.76	7.78	.663	1.76	.171	.698	.022	.090
	18.13	1.76	1.82	1.84	.706	1.80	.104	.389	.057	.214
	18.16	2.91	2.97	3.00	.698	1.80	.146	.517	.049	.174
	18.19	3.82	3.89	3.92	.700	1.78	.175	.615	.045	.158
	18.19	4.98	5.06	5.10	.673	1.78	.213	.739	.042	.146
	18.22	5.79	5.84	5.86	.669	1.67	.234	.806	.040	.138
18	18.10	7.00	7.05	7.07	.659	1.78	.261	.902	.037	.128
	18.32	7.74	7.80	7.84	.660	1.76	.281	.959	.036	.123
	18.13	1.82	1.88	1.92	.701	1.80	.160	.485	.085	.258
	18.16	3.01	3.05	3.07	.681	1.80	.220	.656	.072	.215
	18.16	3.88	3.93	3.95	.678	1.78	.263	.786	.067	.200
	18.19	4.45	4.49	4.51	.665	1.78	.287	.853	.064	.190
21	18.13	5.92	5.96	5.98	.655	1.78	.352	1.025	.059	.172
	18.19	6.88	6.92	6.94	.646	1.67	.388	1.135	.056	.164
	18.53	6.91	7.00	7.04	.639	1.56	.385	1.141	.055	.163
	18.53	7.93	7.99	8.02	.640	1.56	.431	1.270	.054	.159
	18.19	8.02	8.07	8.10	.641	1.67	.444	1.283	.055	.159
	18.13	1.95	2.00	2.02	.676	1.80	.226	.582	.113	.291
24	18.13	2.75	2.80	2.82	.695	1.80	.300	.764	.107	.273
	18.16	2.88	2.92	2.95	.685	1.63	.307	.780	.105	.267
	18.13	4.08	4.12	4.14	.660	1.78	.379	.964	.092	.234
	18.19	5.14	5.19	5.22	.645	1.78	.441	1.111	.085	.214
	18.04	5.98	6.04	6.07	.629	1.78	.495	1.244	.082	.206
	18.38	7.10	7.16	7.20	.632	1.56	.566	1.425	.079	.199
27	18.22	7.13	7.18	7.22	.638	1.67	.582	1.429	.081	.199
	18.44	7.99	8.03	8.05	.620	1.76	.610	1.510	.076	.188
	18.13	.79	.82	.84	.745	1.63	.171	.387	.209	.472
	18.19	1.99	2.04	2.07	.673	1.80	.304	.685	.149	.336
	18.16	3.12	3.16	3.19	.678	1.80	.427	.942	.135	.298
	18.13	4.06	4.12	4.14	.644	1.78	.511	1.121	.124	.272
30	18.19	5.16	5.22	5.24	.633	1.78	.606	1.315	.116	.252
	18.59	5.94	6.01	6.04	.642	1.56	.686	1.480	.114	.246
	18.19	6.12	6.17	6.20	.635	1.67	.697	1.512	.113	.245
	18.59	7.02	7.09	7.12	.636	1.56	.787	1.680	.111	.237
	18.50	8.10	8.15	8.18	.610	1.56	.864	1.866	.107	.229
	9.13	3.00	3.04	3.07	.660	1.63	.413	.912	.136	.300
33	9.15	4.06	4.11	4.14	.635	1.63	.514	1.122	.125	.273
	9.16	5.13	5.21	5.24	.628	1.63	.604	1.318	.116	.253
	18.25	.95	1.00	1.02	.757	1.63	.296	.520	.296	.520
	18.25	2.03	2.09	2.12	.662	1.63	.493	.851	.236	.407
	18.22	3.02	3.08	3.11	.687	1.63	.662	1.127	.215	.366
	18.33	4.24	4.57	4.36	.582	1.56	.850	1.474	.186	.323
37	18.32	5.37	5.44	5.51	.620	1.56	1.035	1.744	.190	.320
	18.47	6.21	6.31	6.36	.607	1.56	1.148	1.986	.182	.315
	18.50	7.03	7.12	7.16	-----	1.56	2.177	-----	.306	-----
	9.19	5.26	5.33	5.36	.645	1.63	1.002	1.748	.188	.328
	9.16	4.25	4.32	4.36	.649	1.63	.829	1.417	.192	.328
	9.16	3.03	3.10	3.16	.685	1.63	.639	1.111	.206	.358
41	18.25	.97	1.03	1.06	.742	1.63	.381	.582	.371	.566
	18.13	2.00	2.06	2.09	.674	1.63	.623	.914	.303	.444
	18.13	3.25	3.32	3.36	.615	1.56	.871	1.256	.262	.378
	18.32	4.25	4.37	4.42	.632	1.56	1.124	1.600	.257	.366
	18.28	5.38	5.49	5.54	.598	1.56	1.351	1.928	.246	.351
	18.65	6.47	6.57	6.62	-----	1.56	2.227	-----	.339	-----

TABLE I.—Continued

EXPERIMENTAL PLANING DATA OBTAINED FOR A RECTANGULAR FLAT PLATE

(b) Brass model having sharp chines; no wind screen

Trim, τ , deg	C_V	$\frac{l_c}{b}$	$\frac{l_m}{b}$	$\frac{l_k}{b}$	$\frac{l_{cp}}{l_m}$	ν , sq ft/sec	$C_{D,b}$	$C_{L,b}$	$C_{D,s}$	$C_{L,s}$
12	18.28	1.64	1.69	1.72	0.761	1.80×10^{-5}	0.061	0.291	0.036	0.172
	18.13	2.40	2.44	2.47	.754	1.80	.081	.361	.033	.148
	18.16	3.54	3.59	3.62	.716	1.80	.101	.445	.028	.124
	18.12	4.67	4.72	4.75	.689	1.80	.118	.519	.025	.110
	18.13	5.66	5.72	5.74	.676	1.80	.132	.578	.023	.101
	18.19	6.87	6.92	6.95	.663	1.80	.165	.692	.021	.088
18	18.13	1.87	1.92	1.94	.719	1.80	.151	.493	.078	.257
	18.19	2.88	2.94	2.96	.705	1.80	.206	.653	.070	.222
	18.13	4.00	4.05	4.07	.666	1.80	.259	.798	.064	.197
	18.15	5.92	5.97	6.00	.651	1.80	.346	1.027	.058	.172
	18.13	7.10	7.25	7.18	.641	1.80	.399	1.189	.055	.164
	18.18	7.97	8.03	8.06	.628	1.80	.426	1.253	.053	.156

(c) Brass model having sharp chines; no wind screen or spray shield

Trim, τ , deg	C_V	$\frac{l_c}{b}$	$\frac{l_m}{b}$	$\frac{l_k}{b}$	$\frac{l_{cp}}{l_m}$	ν , sq ft/sec	$C_{D,b}$	$C_{L,b}$	$C_{D,s}$	$C_{L,s}$
12	18.28	1.54	1.59	1.62	0.744	1.64×10^{-5}	0.060	0.286	0.038	0.180
	18.19	2.70	2.75	2.78	.709	1.64	.089	.388	.032	.141
	18.13	3.83	3.88	3.91	.688	1.64	.105	.462	.027	.119
	18.22	4.74	4.80	4.82	.671	1.64	.120	.528	.025	.110
	18.19	5.84	5.89	5.92	.664	1.64	.135	.595	.023	.101
	18.00	7.53	7.57	7.59	.701	1.78	.0749	.3740	.0099	.0494
18	17.93	1.58	1.62	1.65	.709	1.78	.0611	.2885	.0377	.1781
	17.93	4.01	4.06	4.08	.686	1.78	.1092	.4669	.0269	.1150
	17.93	5.70	5.75	5.77	.675	1.78	.1374	.5773	.0239	.1004
	18.10	7.77	7.82	7.85	.666	1.80	.1713	.6889	.0219	.0881
	17.86	1.								

TABLE I.—Concluded
EXPERIMENTAL PLANING DATA OBTAINED FOR A RECTANGULAR FLAT PLATE

(e) Plastic model having $\frac{1}{64}$ -inch-radius chines

Trim, τ , deg	C_V	$\frac{l_e}{b}$	$\frac{l_m}{b}$	$\frac{l_k}{b}$	$\frac{l_{cp}}{l_m}$	ν , sq ft/sec	$C_{D,b}$	$C_{L,b}$	$C_{D,s}$	$C_{L,s}$
12	18.35	1.79	1.84	1.86	.711	1.67×10^{-5}	0.0638	0.2950	0.0347	0.1603
	18.13	2.54	2.59	2.62	.705	1.67	.0761	.3445	.0294	.1330
	18.19	3.59	3.64	3.66	.708	1.67	.0972	.4222	.0267	.1160
	18.19	4.79	4.84	4.87	.685	1.67	.1181	.4995	.0244	.1032
	18.16	5.52	5.56	5.59	.663	1.67	.1290	.5399	.0232	.0971
	18.07	6.87	6.92	6.95	.663	1.67	.1550	.6297	.0224	.0910
	18.07	7.60	7.66	7.69	.651	1.67	.1662	.6764	.0217	.0883
18	18.28	2.00	2.05	2.08	.708	1.67	.1615	.4869	.0788	.2375
	18.19	2.84	2.90	2.93	.684	1.67	.2068	.6200	.0713	.2138
	18.19	3.79	3.84	3.86	.672	1.67	.2508	.7438	.0653	.1937
	18.19	4.92	4.94	4.98	.500	1.67	.2948	.8620	.0592	.1731
	18.13	5.89	5.94	5.97	.646	1.67	.3380	.9789	.0569	.1648
	18.19	7.02	7.06	7.08	.644	1.67	.3911	1.1261	.0554	.1595
	18.22	7.76	7.82	7.84	.637	1.67	.4197	1.2055	.0537	.1542

(f) Plastic model having $\frac{1}{16}$ -inch-radius chines

Trim, τ , deg	C_V	$\frac{l_e}{b}$	$\frac{l_m}{b}$	$\frac{l_k}{b}$	$\frac{l_{cp}}{l_m}$	ν , sq ft/sec	$C_{D,b}$	$C_{L,b}$	$C_{D,s}$	$C_{L,s}$
8	18.13	1.64	1.68	1.58	.712	1.78×10^{-5}	0.0272	0.1605	0.0162	0.0957
	18.13	2.13	2.18	2.20	.751	1.78	.0320	.1820	.0147	0.0835
	18.00	3.50	3.55	3.58	.730	1.78	.0437	.2318	.0123	0.0653
	17.86	5.38	5.43	5.45	.720	1.78	.0504	.2624	.0111	0.0578
	17.93	6.49	6.54	6.56	.706	1.78	.0654	.3257	.0100	0.0498
	18.00	7.53	7.58	7.61	.694	1.78	.0713	.3487	.0094	0.0460
	18.27	1.64	1.69	1.71	.707	1.80	.0558	.2630	.0330	.1556
12	18.27	2.62	2.68	2.70	.704	1.80	.0748	.3371	.0279	.1258
	18.27	3.75	3.80	3.83	.692	1.80	.0931	.4081	.0245	.1074
	18.33	4.64	4.69	4.71	.689	1.78	.1116	.4728	.0238	.1008
	18.20	5.71	5.75	5.78	.678	1.78	.1288	.5365	.0224	.0933
	18.13	6.76	6.82	6.84	.674	1.78	.1453	.5981	.0213	.0877
	18.13	7.81	7.86	7.89	.665	1.78	.1651	.6626	.0210	.0843
	18.13	1.75	1.80	1.83	.686	1.78	.1463	.4466	.0813	.2481
18	18.13	2.74	2.79	2.81	.683	1.63	.1987	.5903	.0713	.2118
	18.13	4.01	4.06	4.08	.660	1.78	.2498	.7429	.0616	.1832
	18.13	5.02	5.09	5.09	.649	1.78	.2917	.8566	.0573	.1683
	18.26	6.22	6.26	6.29	.641	1.78	.3389	.9786	.0541	.1562
	18.13	6.90	6.95	6.99	.642	1.78	.3670	1.0627	.0528	.1529
	18.13	7.91	7.96	7.99	.641	1.78	.4068	1.1677	.0511	.1467

TABLE II
EXPERIMENTAL DATA OBTAINED FOR A PLANING SURFACE HAVING A 20° ANGLE OF DEAD RISE

Trim, τ , deg	C_V	$\frac{l_e}{b}$	$\frac{l_m}{b}$	$\frac{l_k}{b}$	$\frac{l_{cp}}{l_m}$	ν , sq ft/sec	$C_{D,b}$	$C_{L,b}$	$C_{D,s}$	$C_{L,s}$
12	18.31	1.68	1.90	2.12	.708	1.76×10^{-5}	0.051	0.236	0.027	0.124
	18.13	2.16	2.39	2.62	.721	1.73	.065	.275	.027	.115
	18.19	2.29	2.52	2.74	.725	1.73	.068	.277	.027	.110
	18.19	3.45	3.68	3.91	.696	1.73	.085	.353	.023	.096
	18.19	4.27	4.48	4.68	.680	1.71	.099	.403	.022	.090
	18.19	5.49	5.70	5.91	.665	1.71	.114	.467	.020	.082
	18.13	6.29	6.38	6.73	.684	1.71	.128	.485	.020	.076
18	18.47	1.80	1.93	2.06	.709	1.76	.129	.396	.067	.205
	18.31	2.78	2.90	3.03	.681	1.73	.174	.513	.060	.177
	18.28	3.80	3.93	4.06	.663	1.73	.212	.629	.054	.160
	18.13	4.72	4.85	4.98	.665	1.71	.252	.742	.052	.153
	18.13	5.70	5.83	5.95	.643	1.71	.286	.840	.049	.144
	18.22	6.66	6.79	6.92	.634	1.71	.326	.944	.048	.139
	18.16	7.81	7.94	8.06	.620	1.71	.373	1.064	.047	.134
24	18.31	2.02	2.12	2.21	.680	1.76	.257	.568	.121	.268
	18.25	3.04	3.14	3.20	.665	1.67	.349	.772	.111	.246
	18.16	3.94	4.03	4.12	.649	1.72	.423	.931	.105	.231
	18.13	4.90	4.99	5.08	.625	1.72	.509	1.103	.102	.221
	18.13	6.26	6.35	6.44	.620	1.67	.610	1.314	.096	.207
	18.19	7.06	7.14	7.24	.628	1.70	.671	1.442	.094	.202
	18.31	7.86	7.93	8.00	.616	1.54	.730	1.586	.092	.200
30	9.10	3.11	3.19	3.28	.655	1.67	.348	.778	.109	.244
	9.11	4.12	4.19	4.27	.635	1.67	.436	.968	.104	.231
	9.07	5.17	5.24	5.33	.614	1.67	.529	1.148	.101	.219
	18.28	1.40	1.45	1.51	.660	1.63	.302	.523	.208	.361
	18.19	2.32	2.38	2.43	.624	1.63	.445	.771	.187	.324
	18.19	3.38	3.44	3.50	.630	1.63	.605	1.020	.176	.297
	18.37	3.26	3.32	3.39	.637	1.56	.588	.993	.177	.299
34	18.31	4.27	4.32	4.38	.620	1.56	.721	1.205	.167	.279
	18.31	5.38	5.43	5.49	.614	1.54	.885	1.472	.163	.271
	18.25	6.51	6.55	6.62	.604	1.54	1.035	1.703	.158	.260
	18.25	7.21	7.27	7.32	.609	1.54	1.156	1.876	.159	.258
	18.13	1.54	1.61	1.68	.622	1.63	.406	.610	.252	.379
	18.16	2.42	2.46	2.49	.632	1.63	.590	.868	.240	.353
	18.31	3.66	3.70	3.75	.616	1.56	.821	1.184	.222	.320
34	18.25	4.68	4.71	4.74	.605	1.56	.994	1.432	.211	.304
	18.31	5.61	5.66	5.69	.600	1.56	1.194	1.692	.211	.299
	18.41	6.42	6.46	6.50	.602	1.54	1.337	1.867	.207	.289
	18.32	7.52	7.56	7.60	-----	1.54	2.192	-----	.290	-----

TABLE III
EXPERIMENTAL DATA OBTAINED FOR A PLANING SURFACE HAVING 40° ANGLE OF DEAD RISE

Trim, τ , deg	C_V	$\frac{l_e}{b}$	$\frac{l_m}{b}$	$\frac{l_k}{b}$	$\frac{l_{cp}}{l_m}$	ν , sq ft/sec	$C_{D,b}$	$C_{L,b}$	$C_{D,s}$	$C_{L,s}$
12	18.07	0.58	1.14	1.69	0.756	1.72×10^{-5}	0.025	0.100	0.022	0.088
	18.07	1.60	2.14	2.68	.688	1.72	.041	.167	.019	.078
	18.13	2.82	3.36	3.91	.655	1.72	.060	.228	.018	.068
	18.13	3.85	4.40	4.95	.639	1.72	.072	.273	.016	.062
	18.16	4.96	5.51	6.06	.634	1.72	.094	.331	.017	.060
	18.22	6.99	7.52	8.06	.622	1.69	.120	.414	.016	.055</td

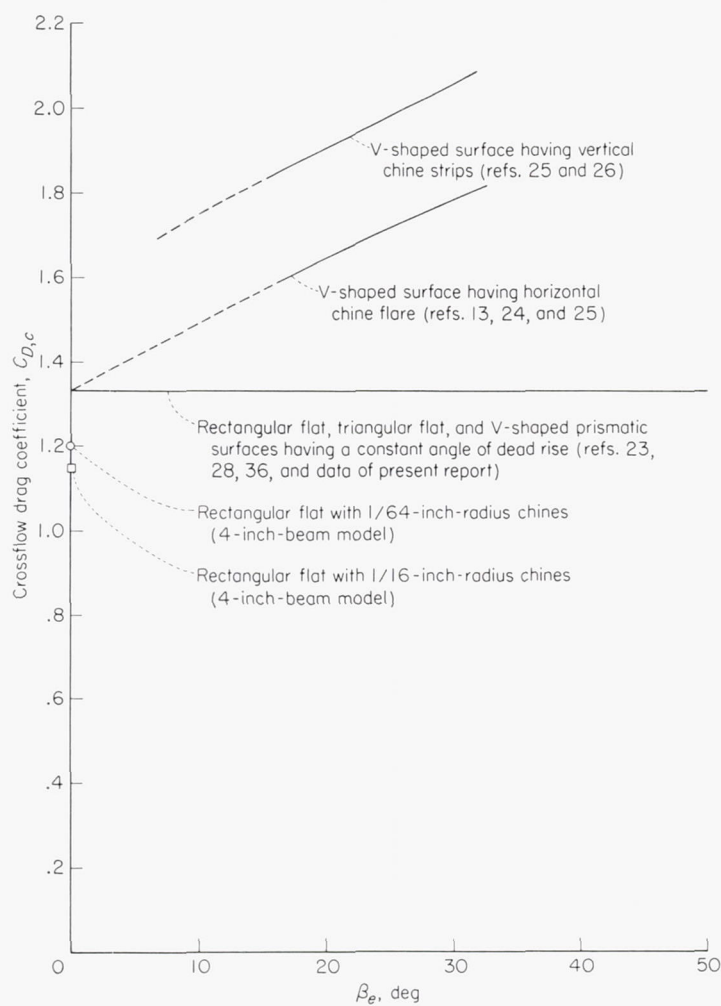
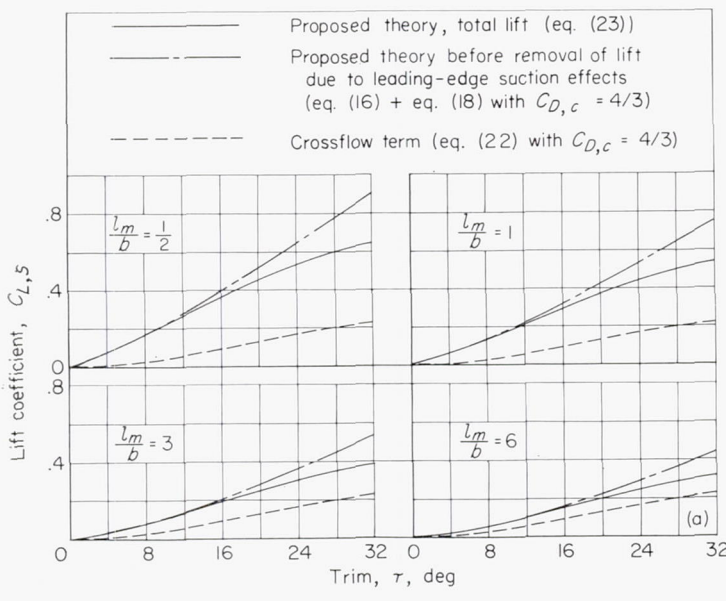
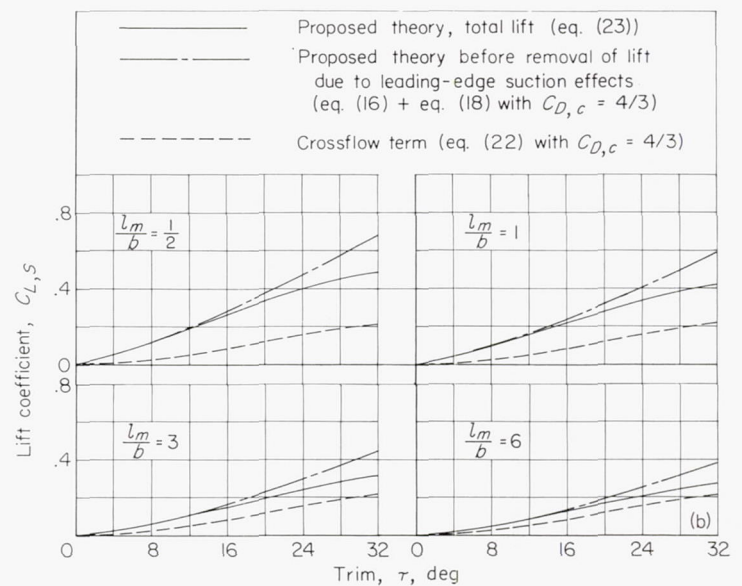


FIGURE 3.—Variation of crossflow drag coefficient for various types of planing surfaces.

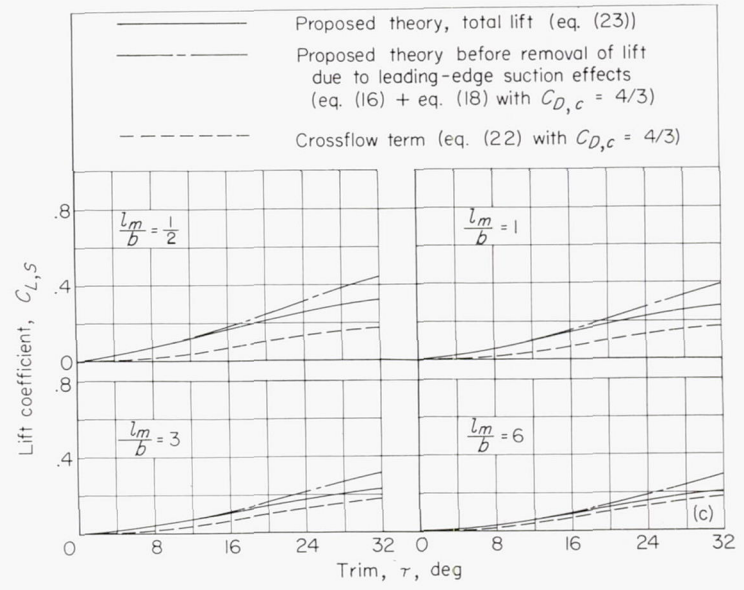


(a) Flat plate.

FIGURE 4.—Relative magnitude of components of proposed theory.



(b) Dead rise, 20°.
FIGURE 4.—Continued.



(c) Dead rise, 40°.
FIGURE 4.—Concluded.

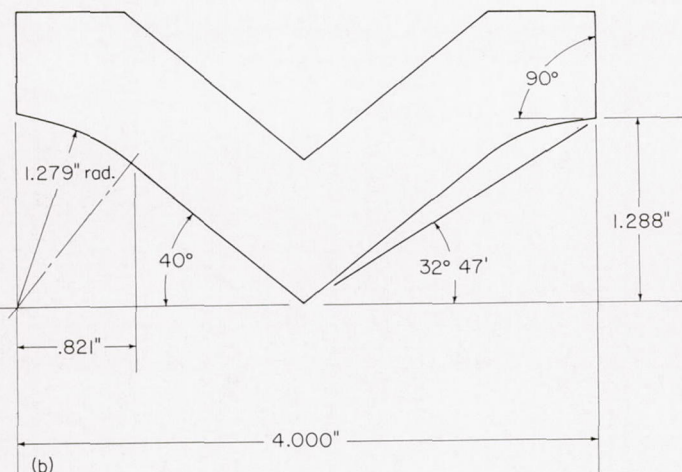
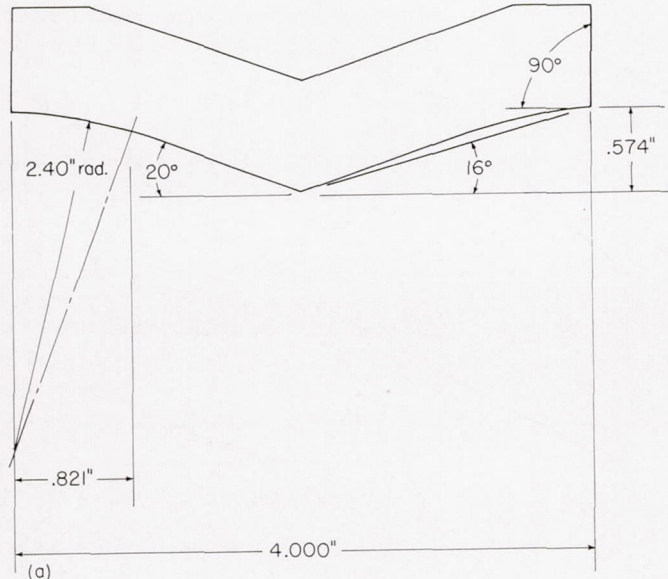


FIGURE 5.—Cross section of surfaces having horizontal chine flare.

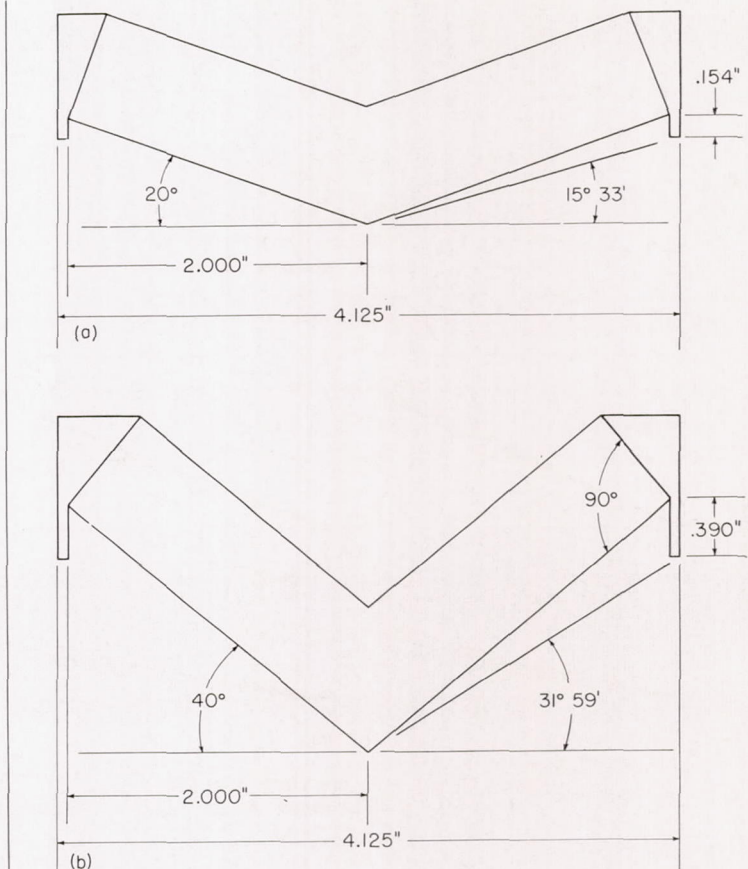
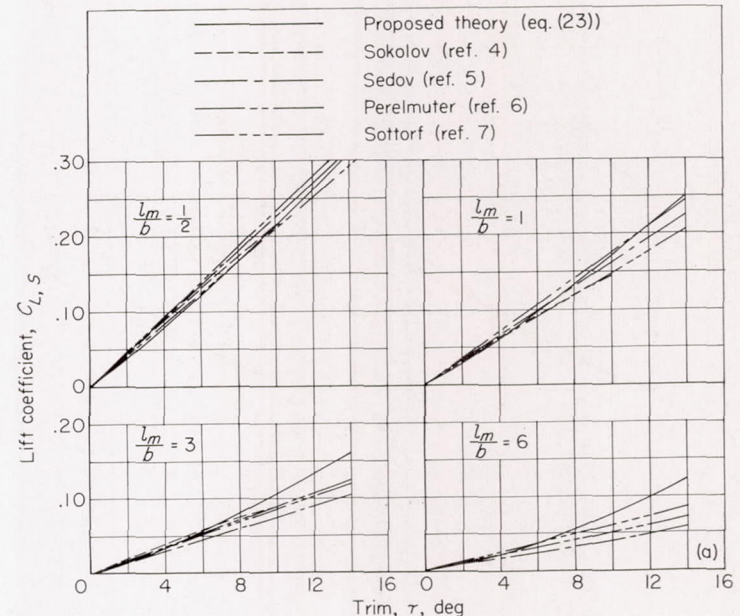
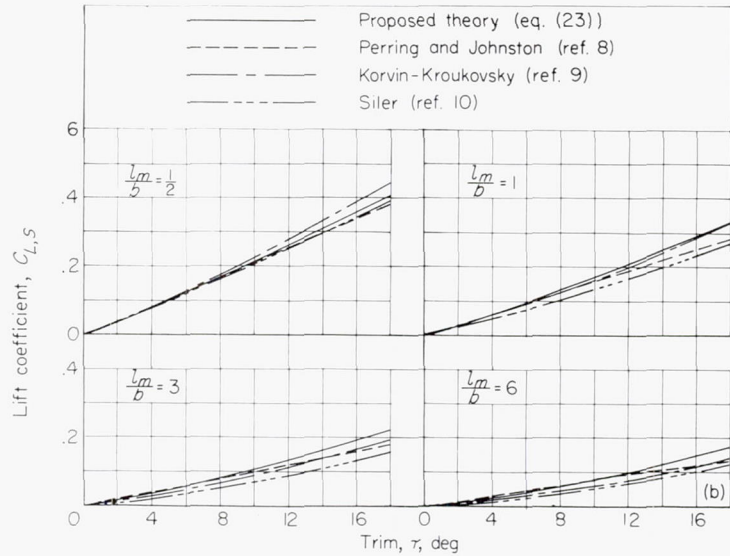


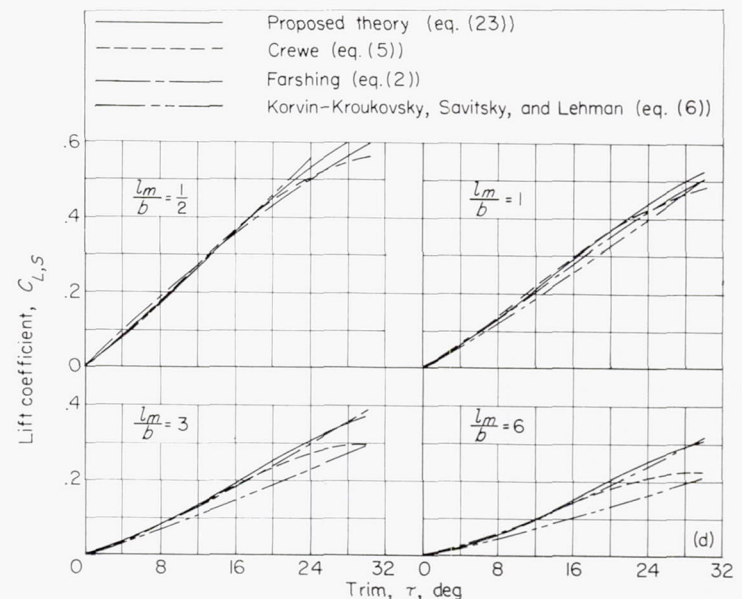
FIGURE 6.—Cross section of surfaces having vertical chine strips.

(a) Proposed theory and references 4 to 7.
FIGURE 7.—Variation of lift coefficient with trim for rectangular flat-plate lift formulas.



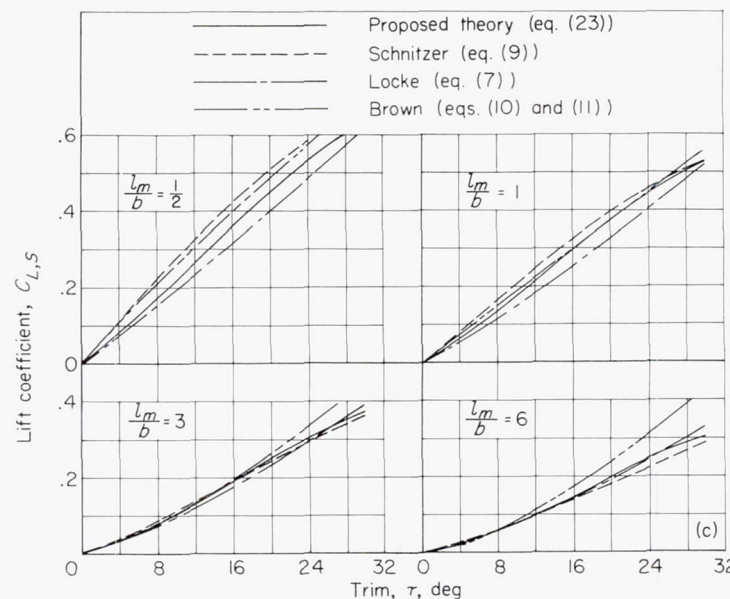
(b) Proposed theory and references 8 to 10.

FIGURE 7.—Continued.



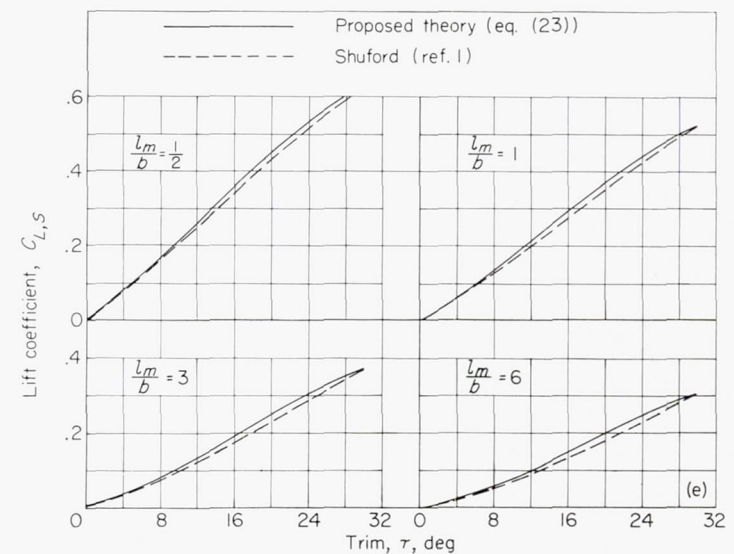
(d) Proposed theory and references 12, 14, and Crewe's equation (eq. (5)).

FIGURE 7.—Continued.



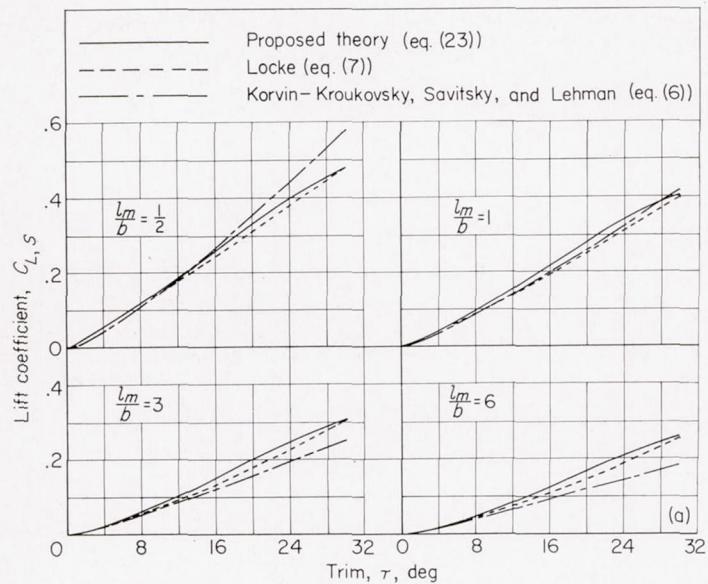
(c) Proposed theory and references 17, 18, and 21.

FIGURE 7.—Continued.



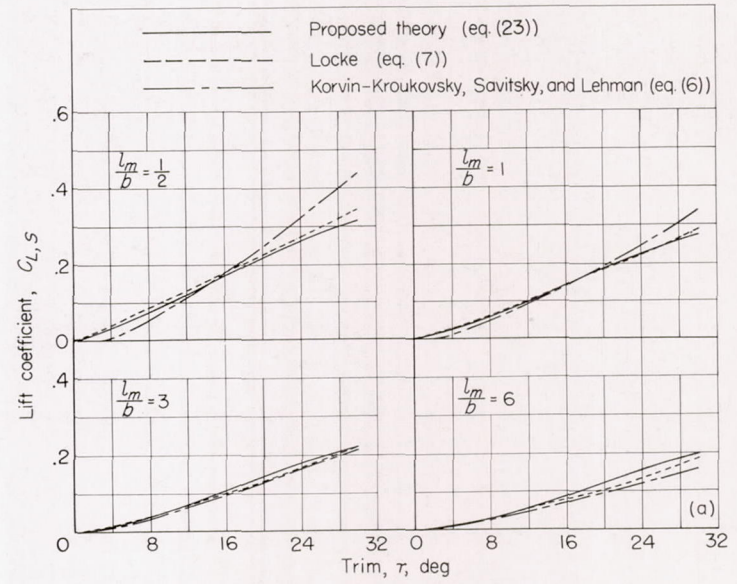
(e) Proposed theory and reference 1.

FIGURE 7.—Concluded.



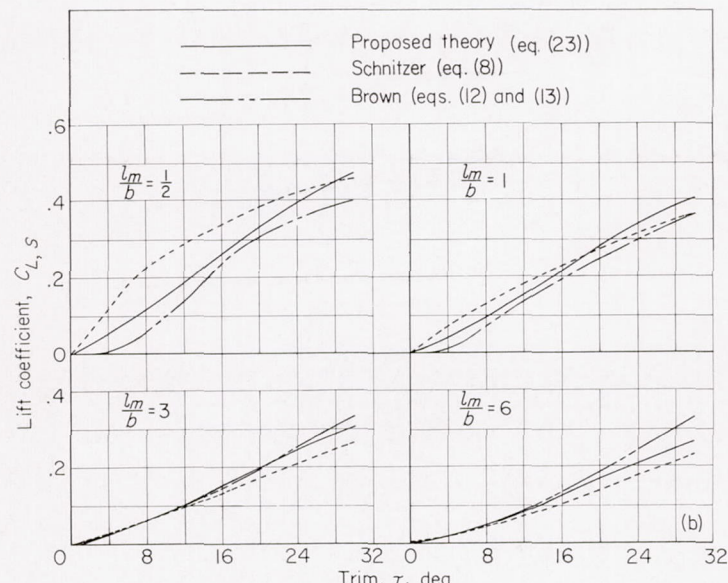
(a) Proposed theory and references 14 and 17.

FIGURE 8.—Variation of lift coefficient with trim for a surface having an angle of dead rise of 20° .



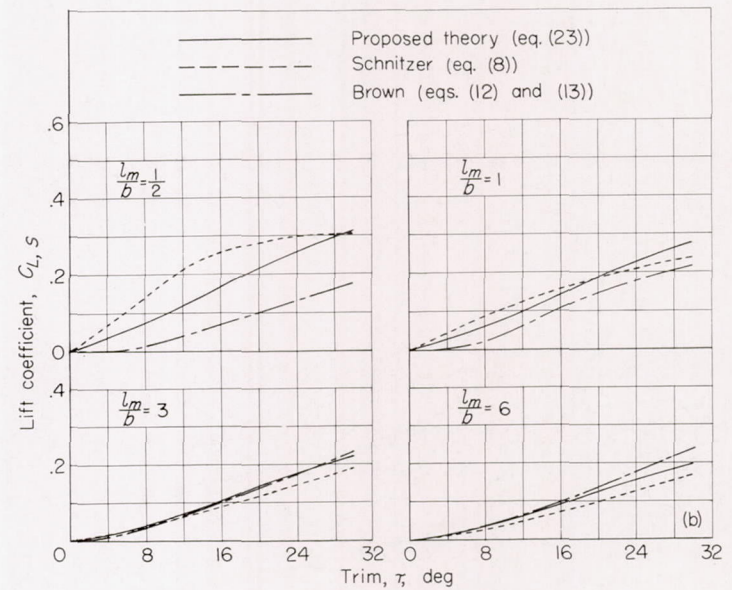
(a) Proposed theory and references 14 and 17.

FIGURE 9.—Variation of lift coefficient with trim for a surface having an angle of dead rise of 40° .



(b) Proposed theory and references 18 and 21.

FIGURE 8.—Concluded.



(b) Proposed theory and references 18 and 21.

FIGURE 9.—Concluded.

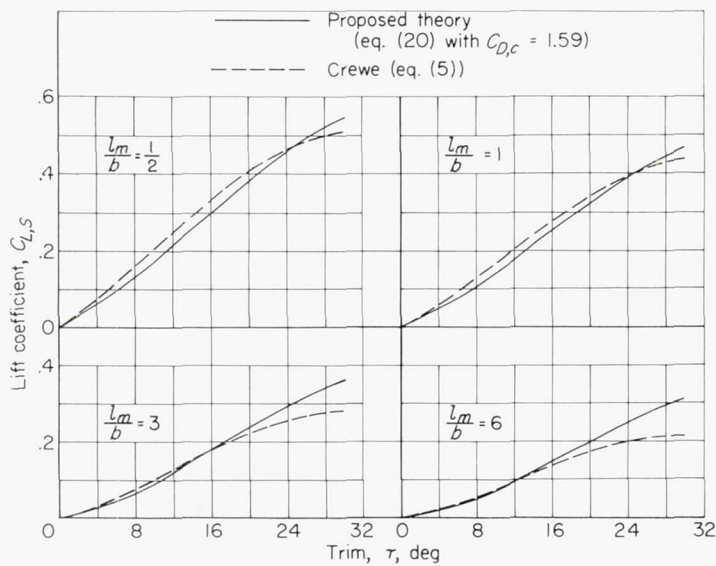
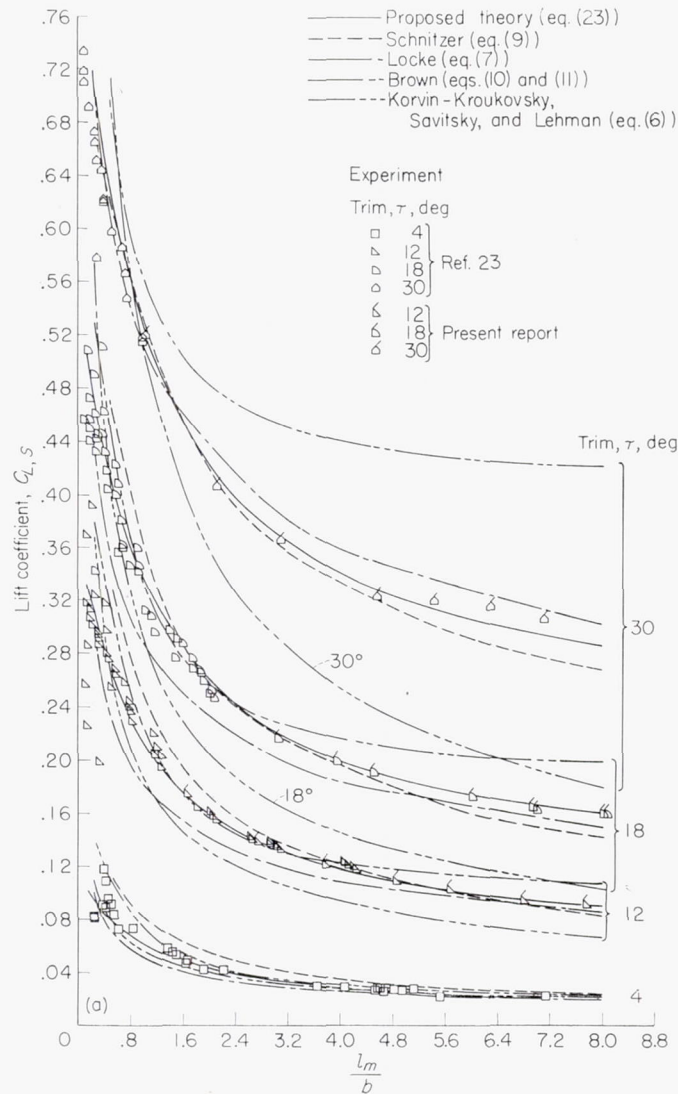
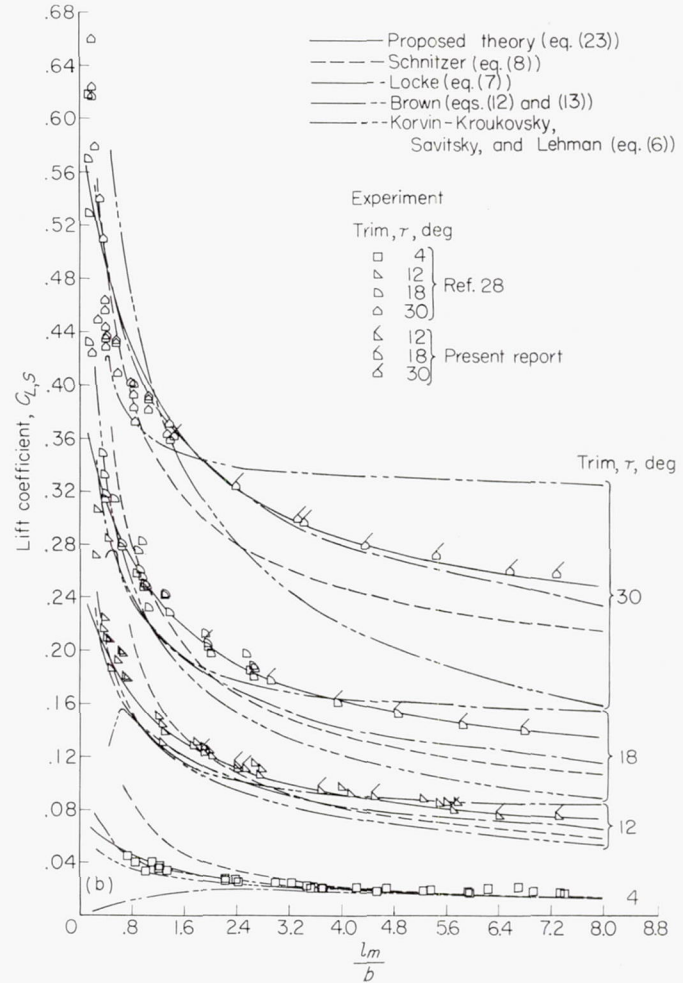


FIGURE 10.—Variation of lift coefficient with trim for a surface having a basic angle of dead rise of 20° and horizontal chine flare.

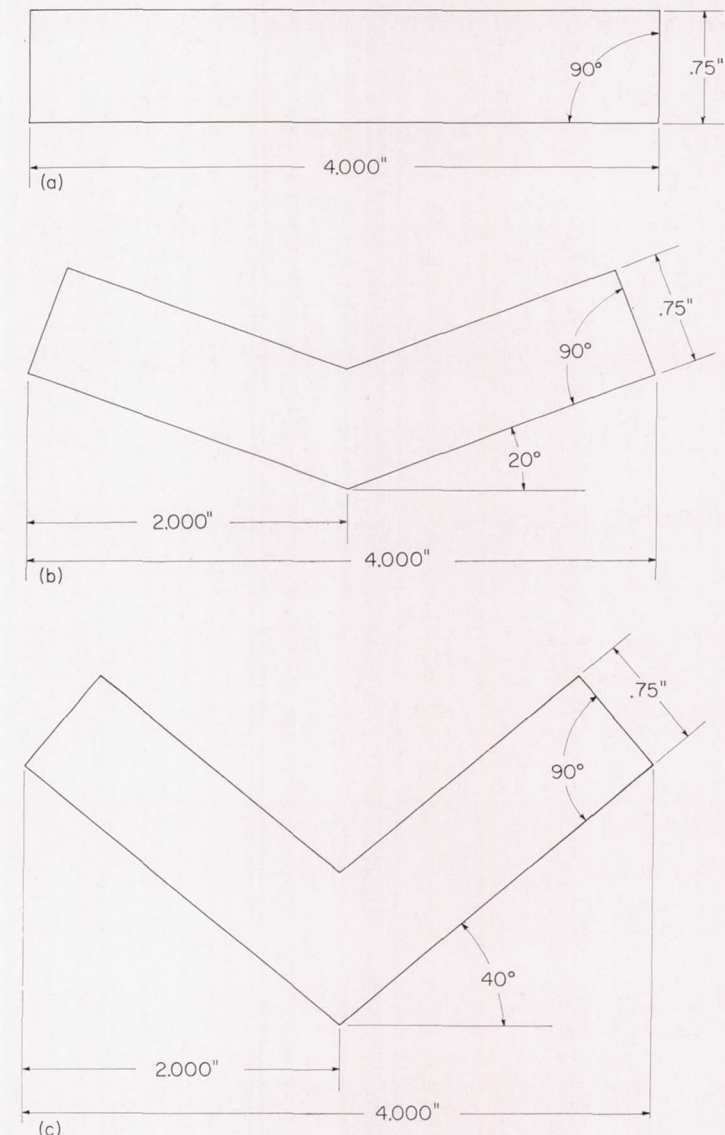
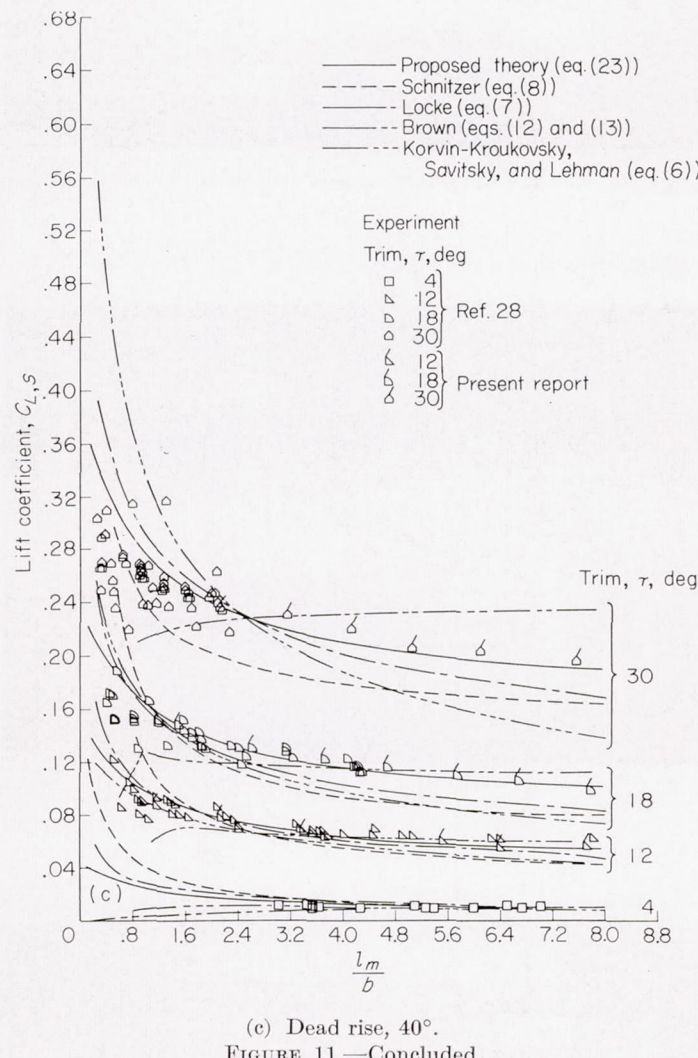


(a) Flat plate.

FIGURE 11.—Comparison of the results calculated from the proposed theory and references 14, 17, 18, and 21 with experiment.



(b) Dead rise, 20° .
FIGURE 11.—Continued.



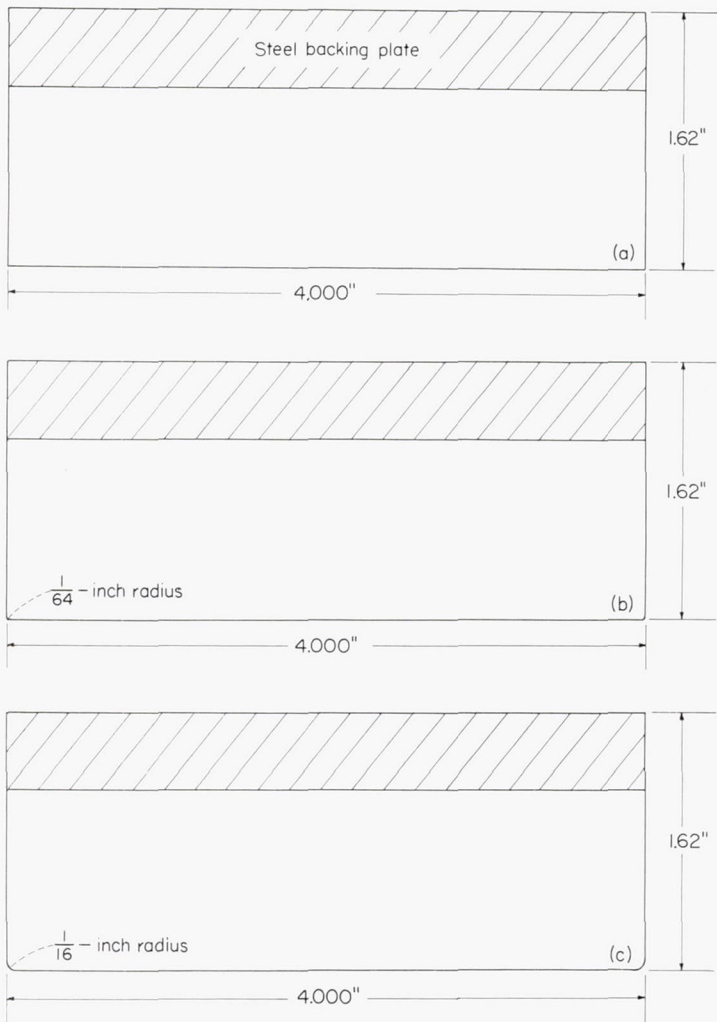


FIGURE 13.—Cross sections of plastic models.

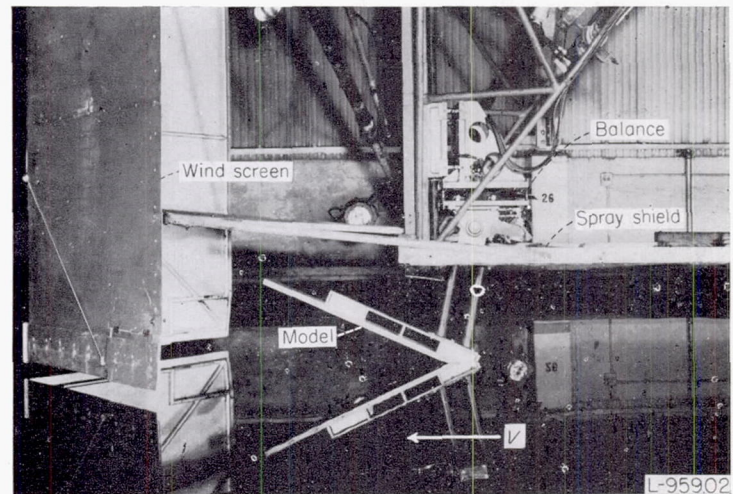
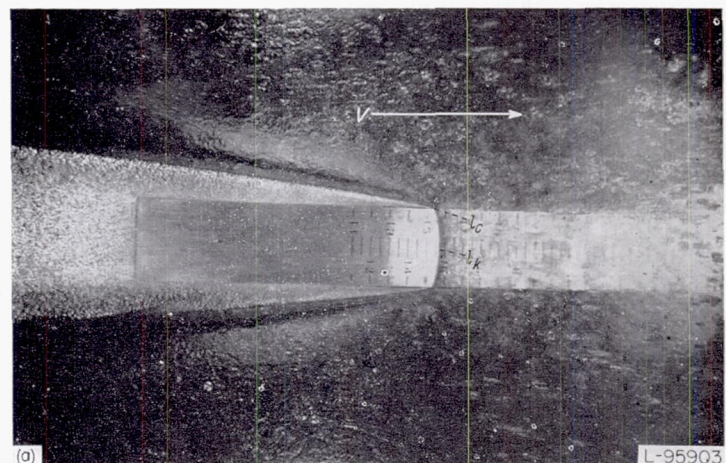
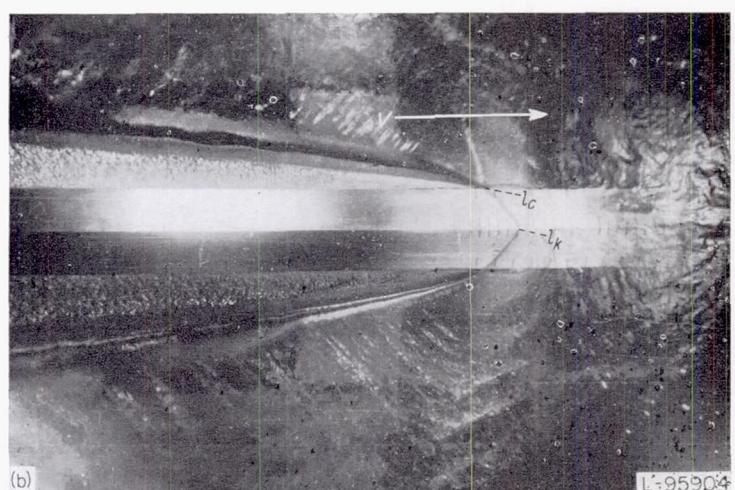
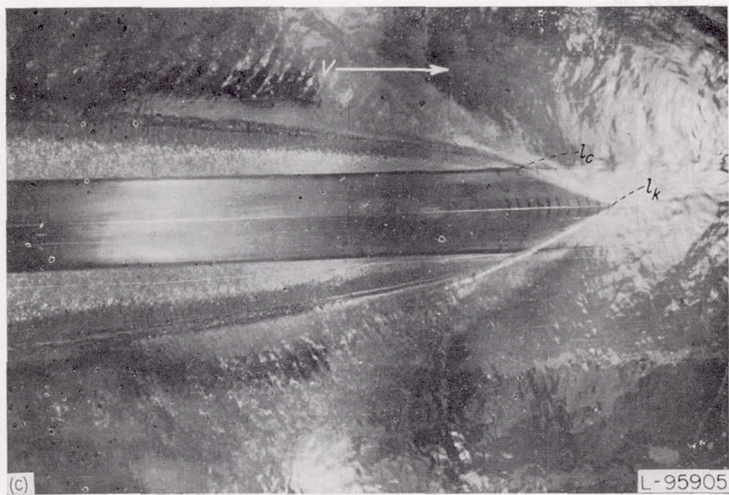
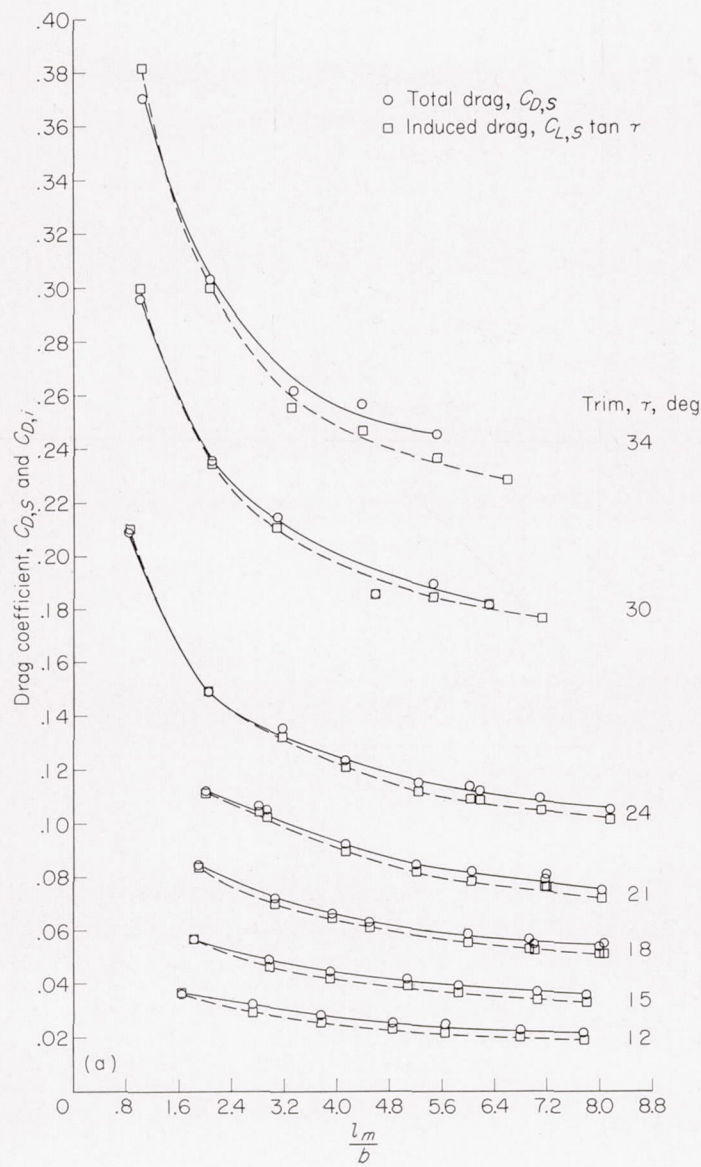


FIGURE 14.—Photograph of flat-plate model attached to towing carriage.

(a) Flat plate.
FIGURE 15.—Underwater photographs.(b) Dead rise, 20°.
FIGURE 15.—Continued

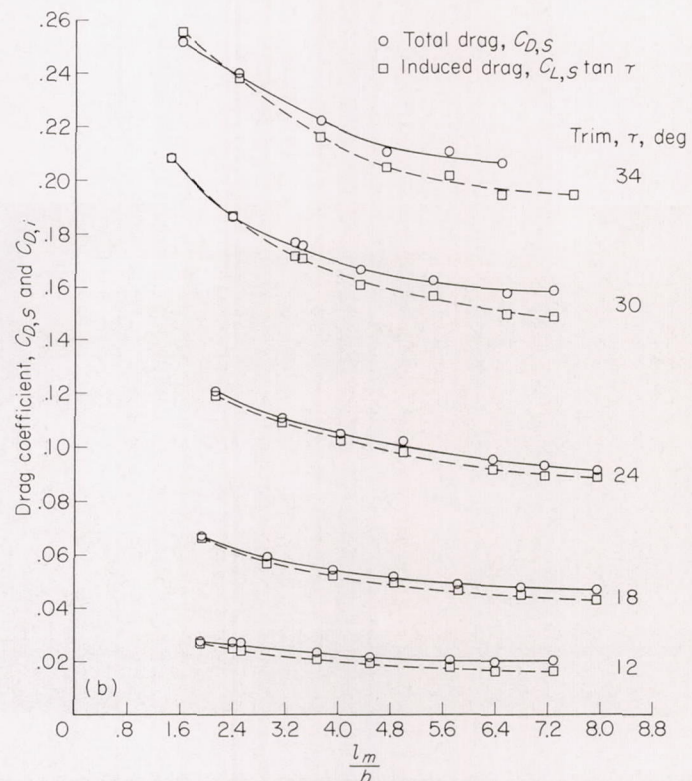


(c) Dead rise, 40°.
FIGURE 15.—Concluded.

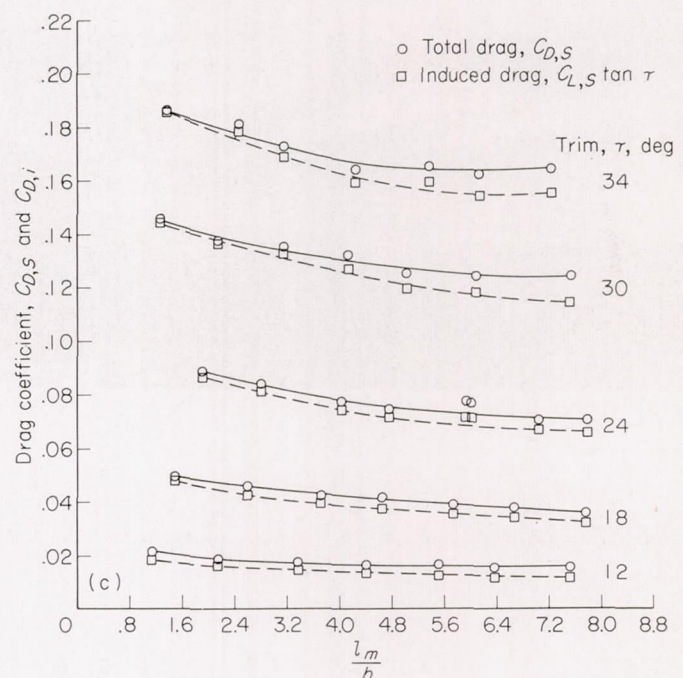


(a) Flat plate.

FIGURE 16.—Comparison of total drag with induced drag.



(b) Dead rise, 20°.
FIGURE 16.—Continued.



(c) Dead rise, 40°.
FIGURE 16.—Concluded.

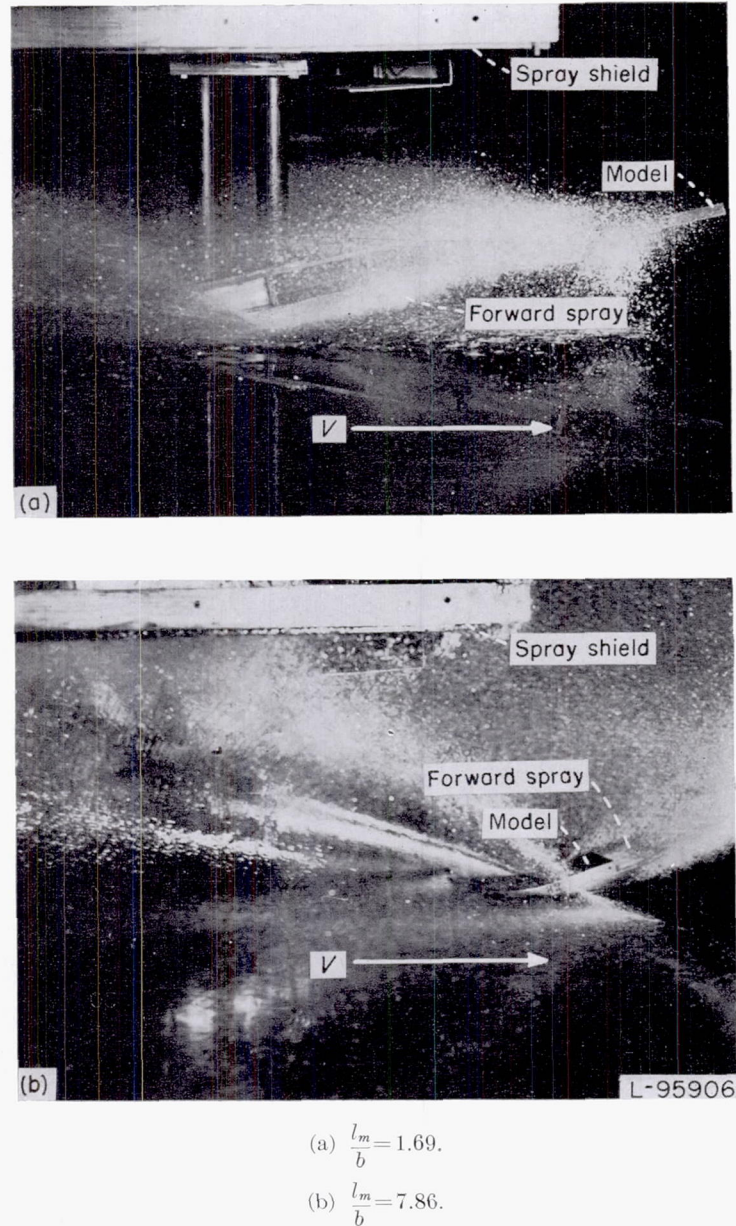


FIGURE 17.—Spray photographs of flat-plate model with wind screen removed. Trim, 12°.

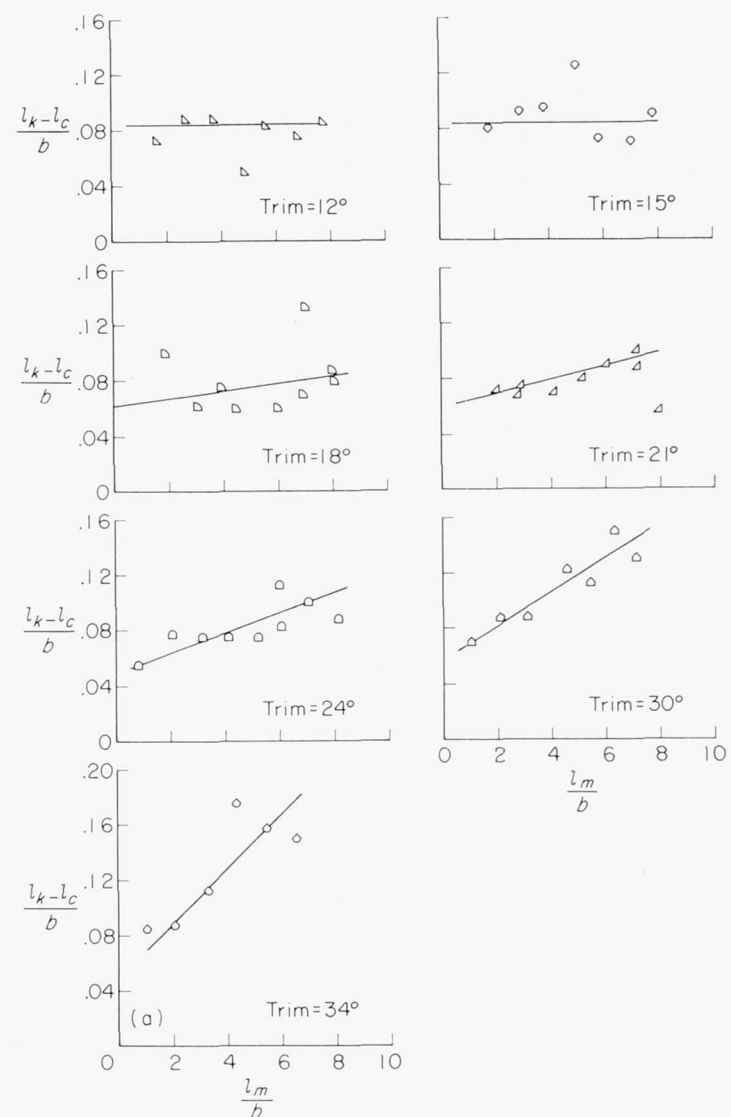


FIGURE 18.—Variation of $\frac{l_k - l_c}{b}$ with trim.

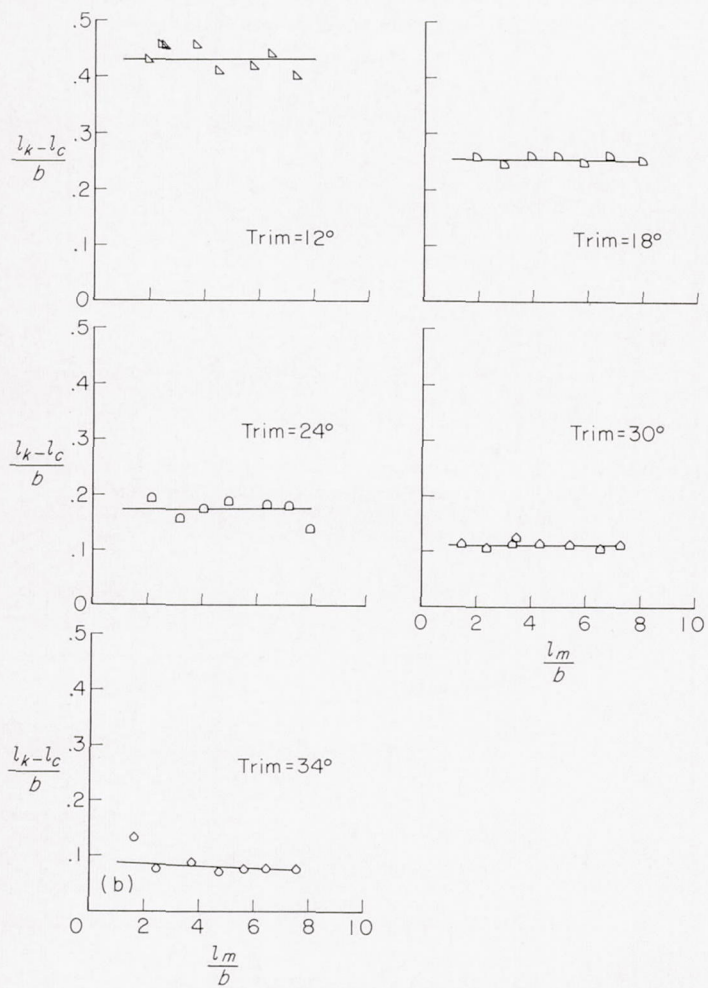


FIGURE 18.—Continued.

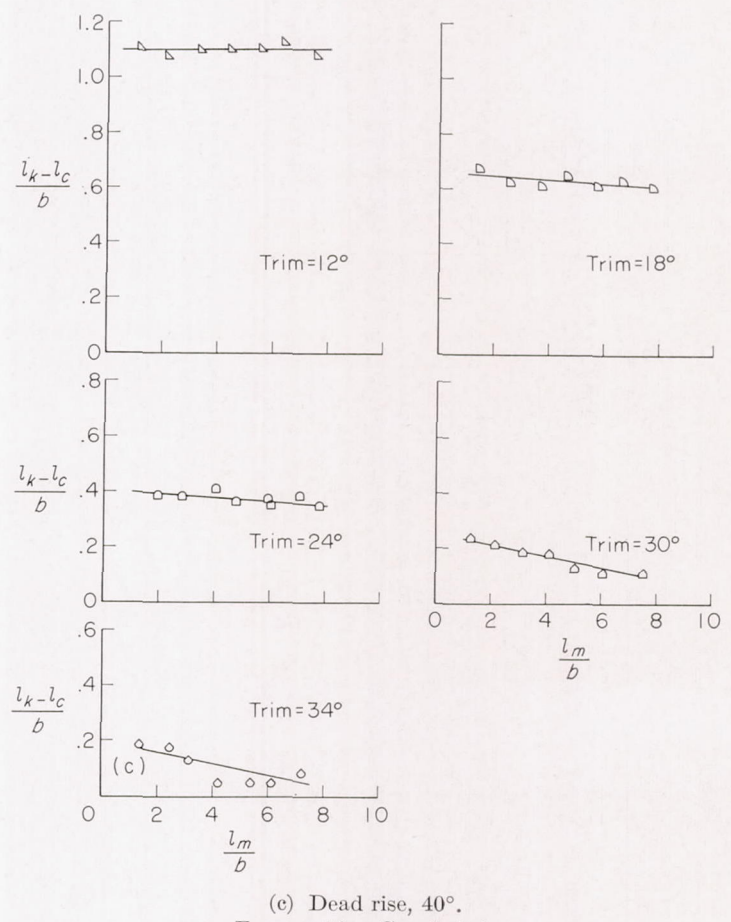


FIGURE 18.—Concluded.

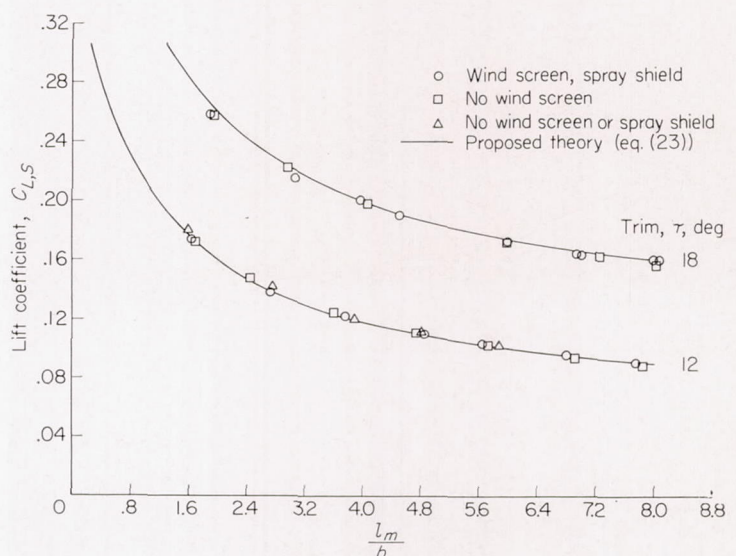


FIGURE 19.—Effect of wind screen and spray shield on the lift of a rectangular flat plate.

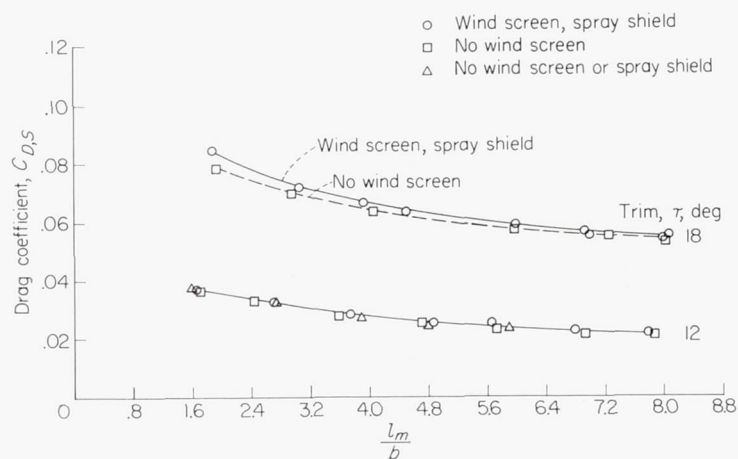


FIGURE 20.—Effect of wind screen and spray shield on the drag of a rectangular flat plate.

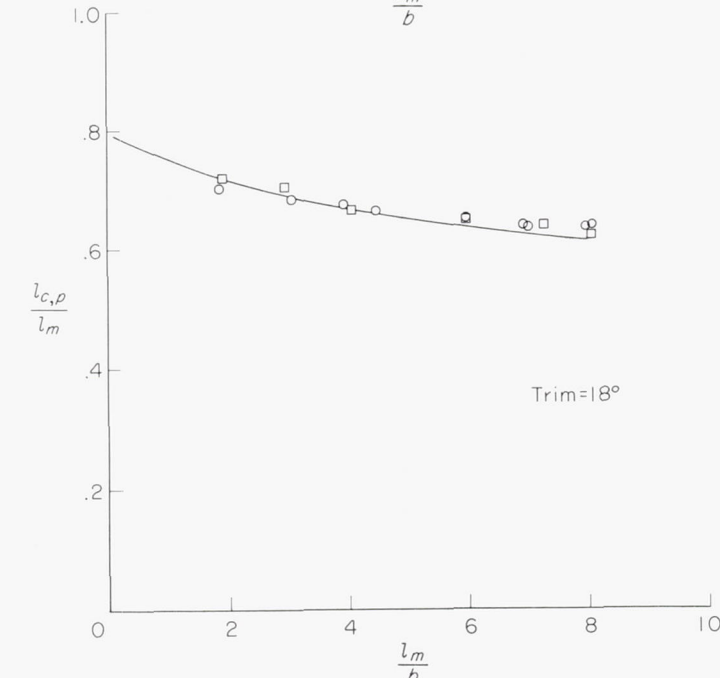
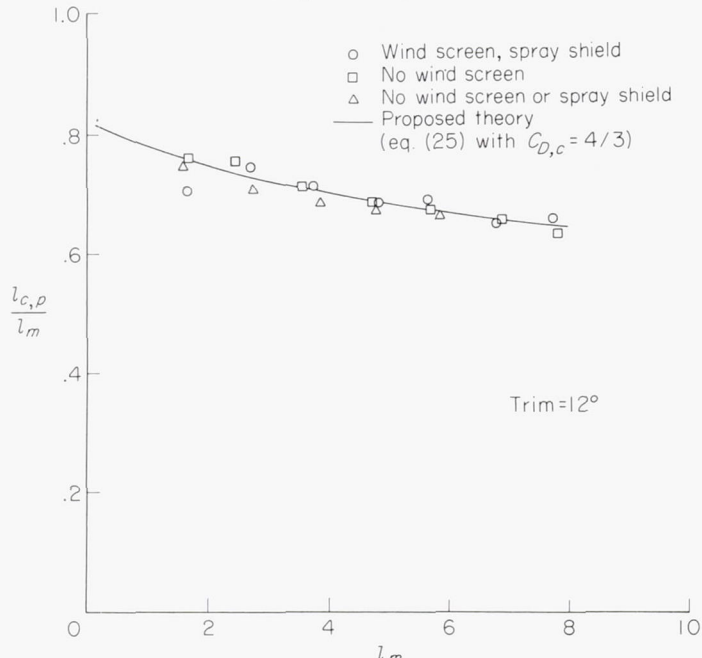
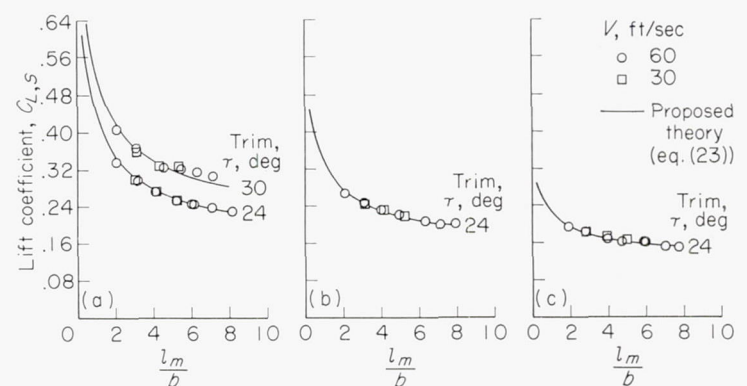
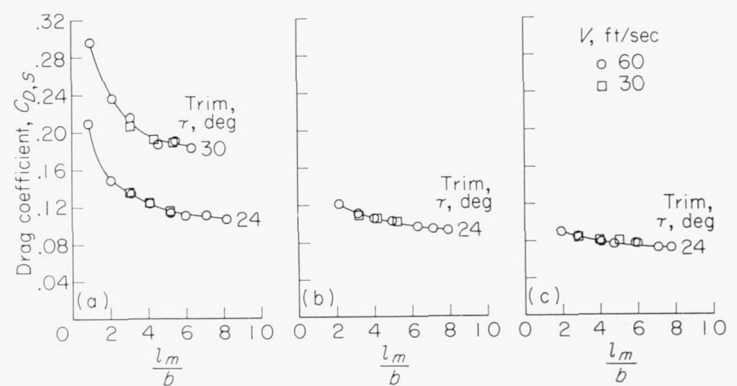


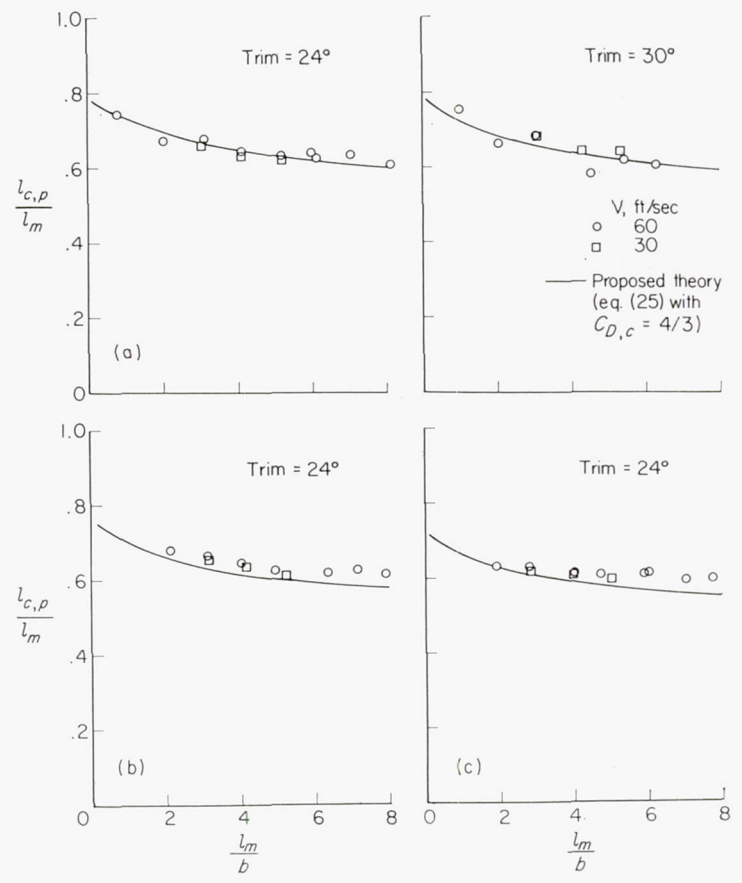
FIGURE 21.—Effect of wind screen and spray shield on the center of pressure of a rectangular flat plate.



(a) Flat plate. (b) Dead rise, 20°. (c) Dead rise, 40°.
FIGURE 22.—The effect of speed on lift coefficient.



(a) Flat plate. (b) Dead rise, 20°. (c) Dead rise, 40°.
FIGURE 23.—The effect of speed on drag coefficient.



(a) Flat plate. (b) Dead rise, 20°. (c) Dead rise, 40°.
FIGURE 24.—The effect of speed on center of pressure.

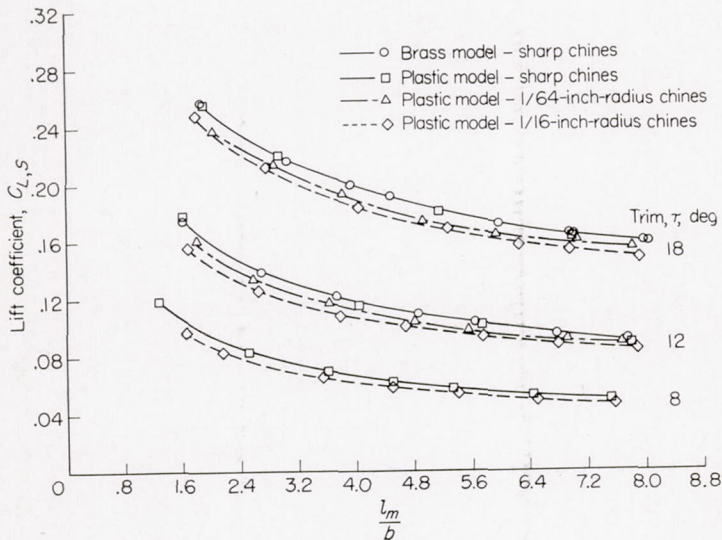


FIGURE 25.—The effect of rounded chines on the lift of a 4-inch-beam rectangular-flat-plate planing surface.

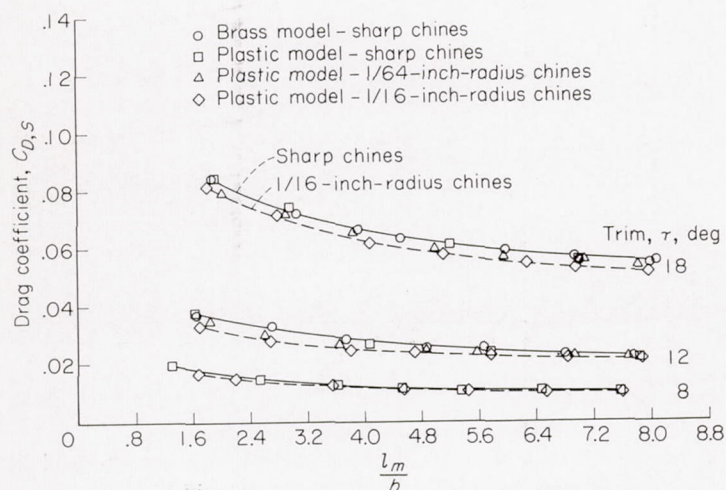


FIGURE 26.—The effect of rounded chines on the drag of a 4-inch-beam rectangular flat plate.

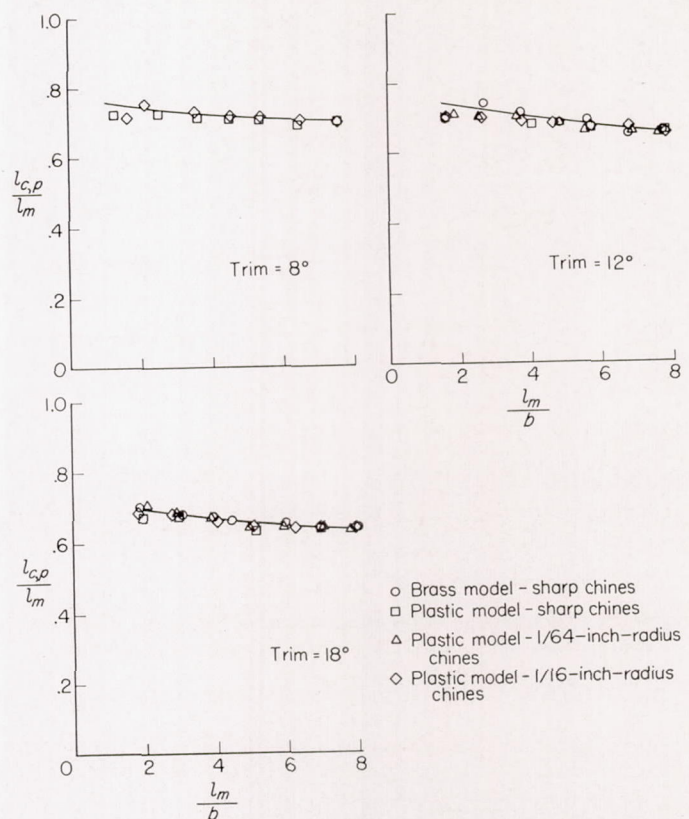


FIGURE 27.—The effect of rounded chines on the center of pressure of a 4-inch-beam rectangular flat plate.

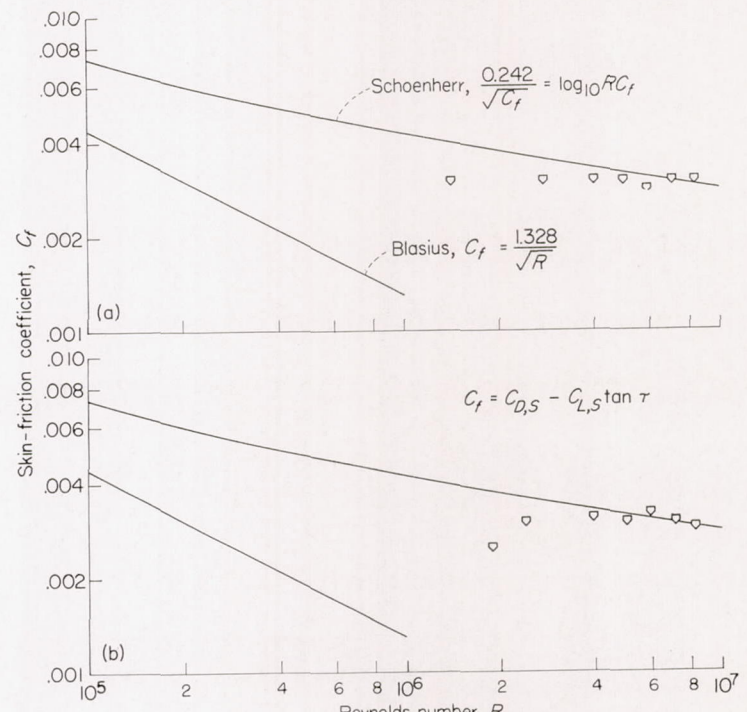


FIGURE 28.—Variation of skin-friction coefficient with Reynolds number. Trim, 8°.
 (a) Sharp chines.
 (b) $\frac{1}{16}$ -inch-radius chines.

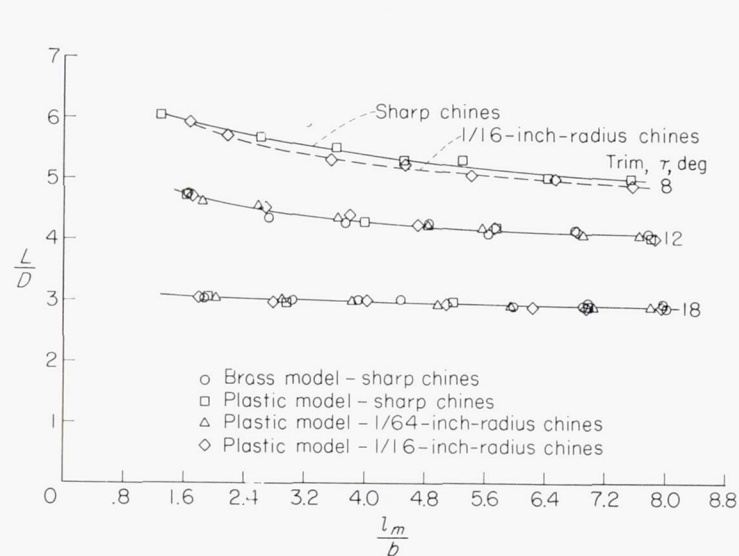


FIGURE 29.—Comparison of lift-drag ratios for flat-plate models having sharp chines with flat-plate models having rounded chines.

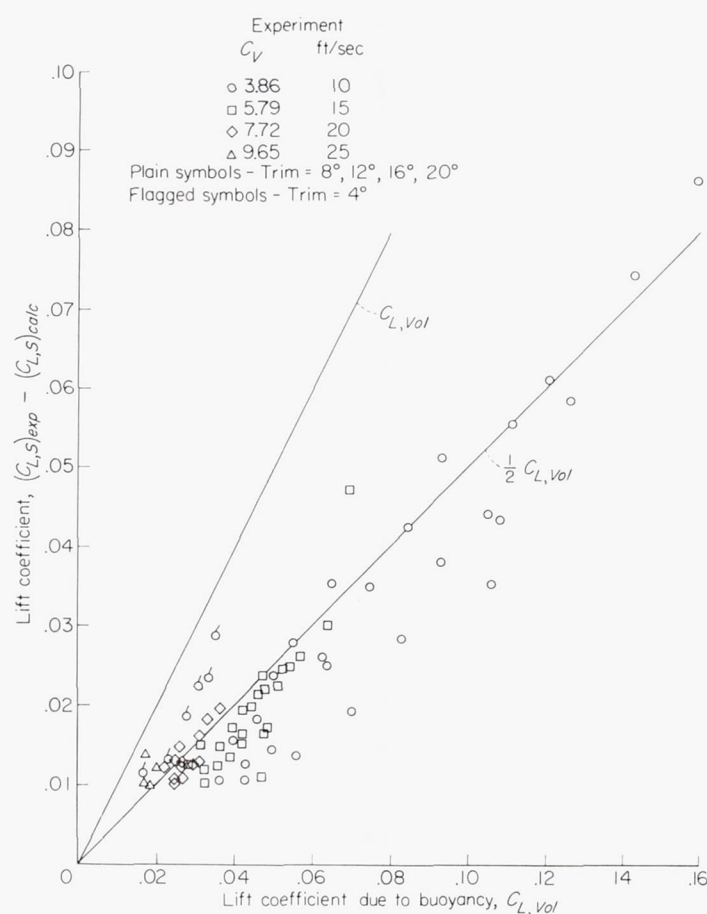
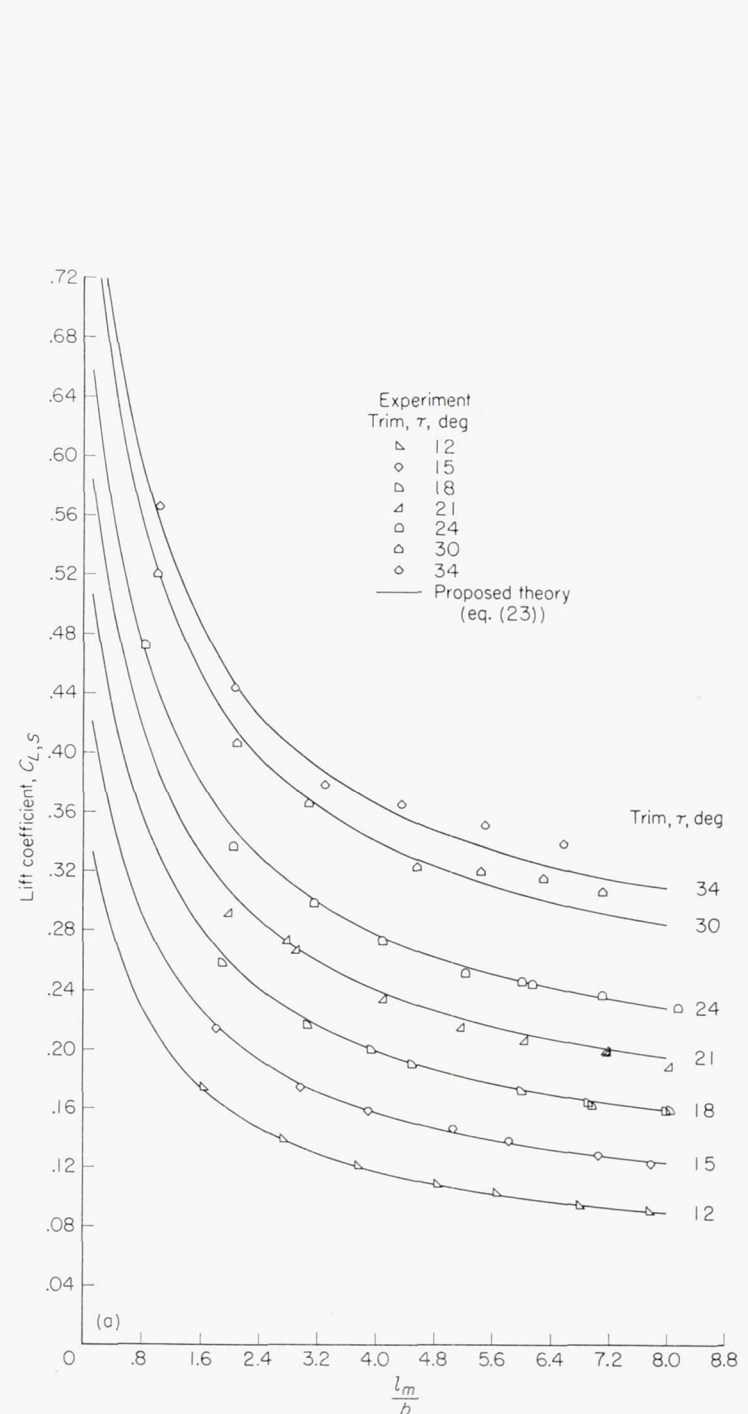
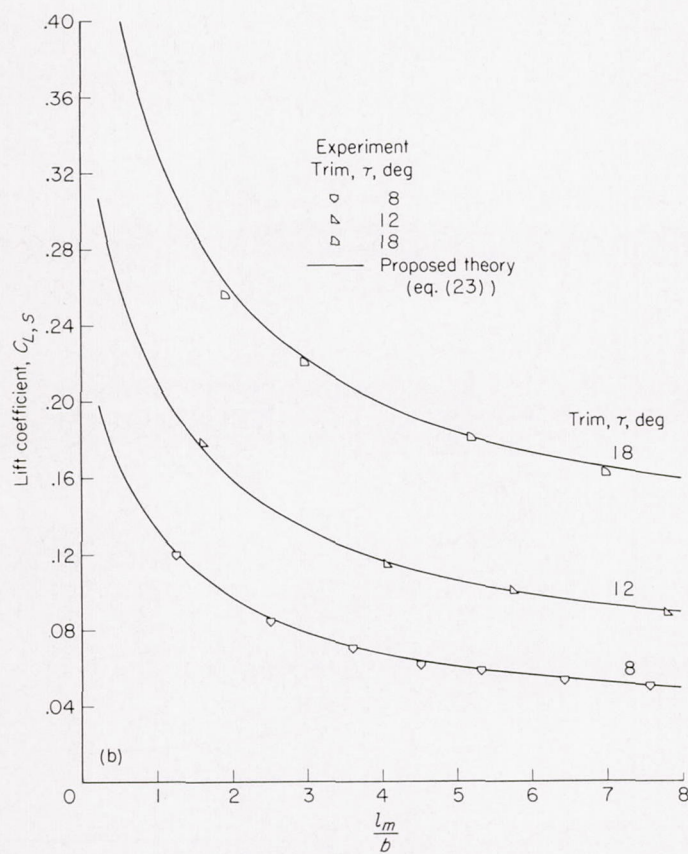


FIGURE 30.—Lift coefficient due to buoyancy for various speed coefficients. (Data of ref. 31.) Calculated value of $C_{L,S}$ was determined from equation (20) with $C_{D,e}=1.15$ (see fig. 32 (c)).

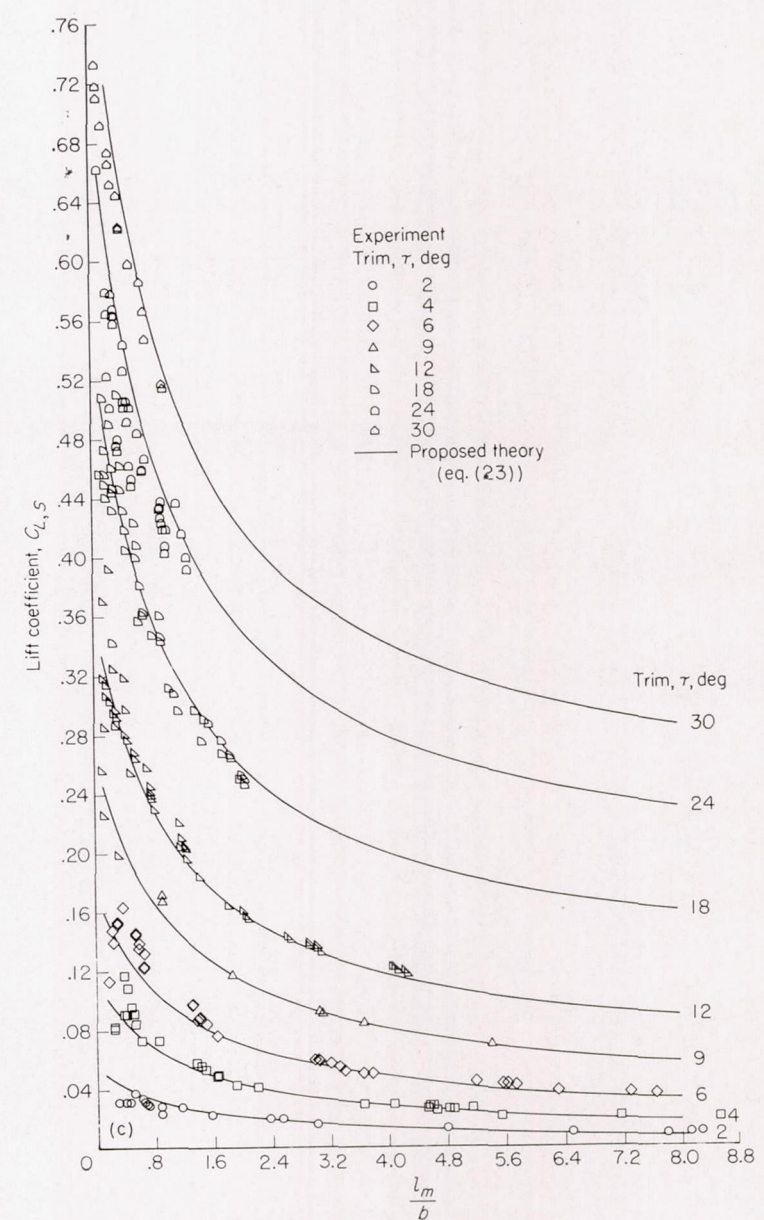


(a) Data of present report (brass model).
FIGURE 31.—Comparison of proposed theory with experimental lift coefficients for rectangular-flat-plate planing surfaces.



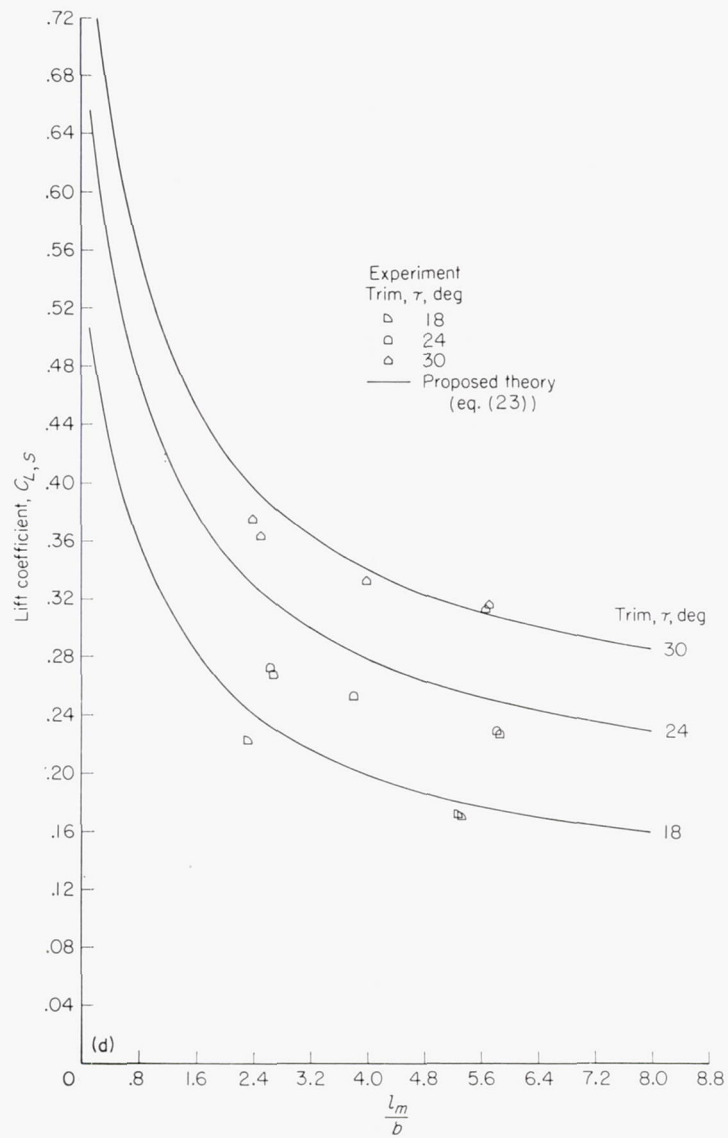
(b) Data of present report (sharp-chine plastic model).

FIGURE 31.—Continued.

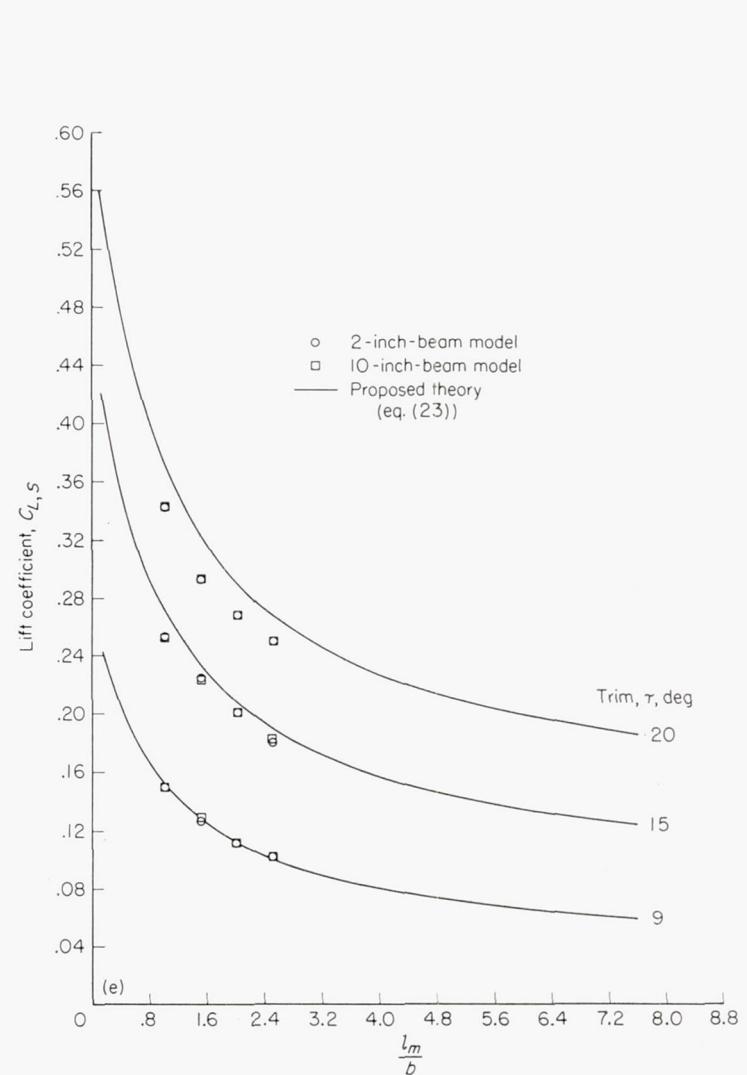


(c) Data of Weinstein and Kapryan (ref. 23).

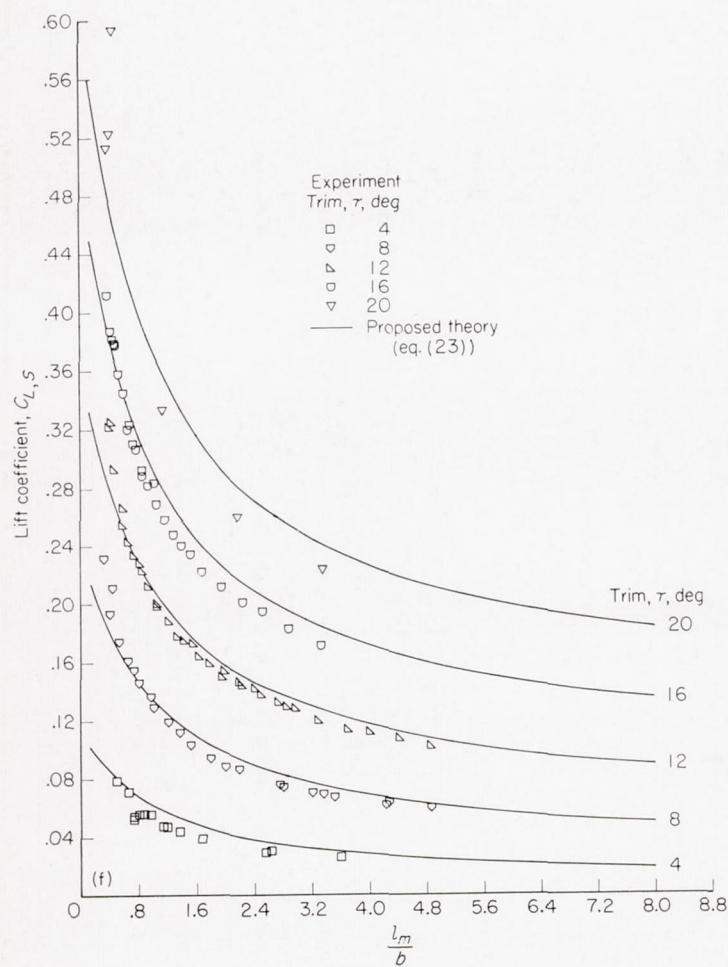
FIGURE 31.—Continued.



(d) Data of Farshing (ref. 12).
FIGURE 31.—Continued.

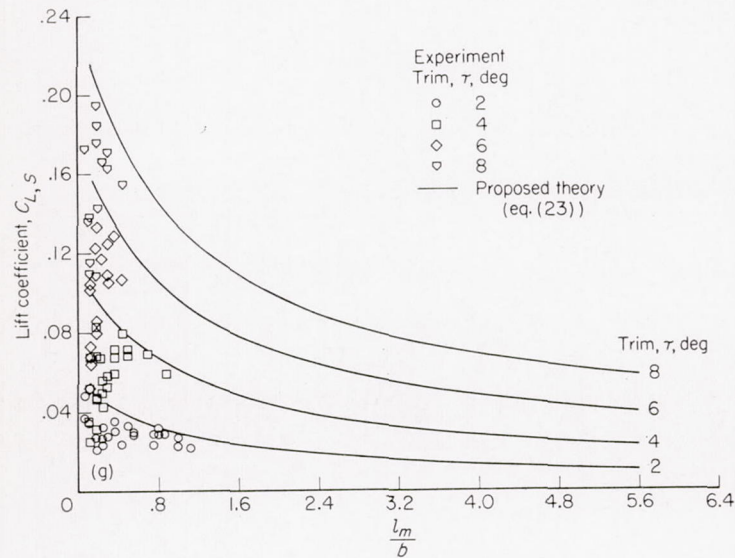


(e) Data of McBride (ref. 32).
FIGURE 31.—Continued.



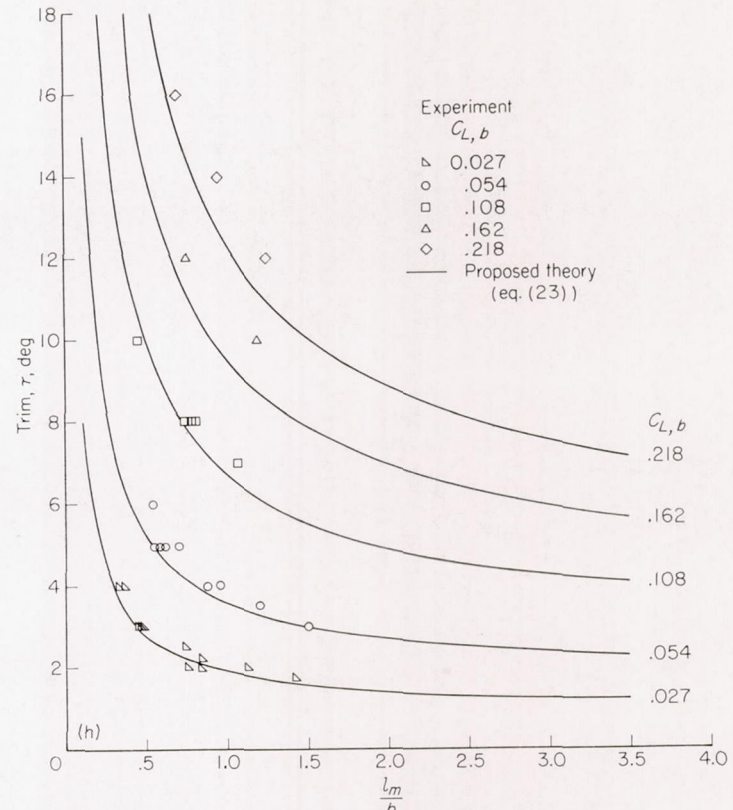
(f) Data of Wadlin and McGehee (ref. 31).

FIGURE 31.—Continued.



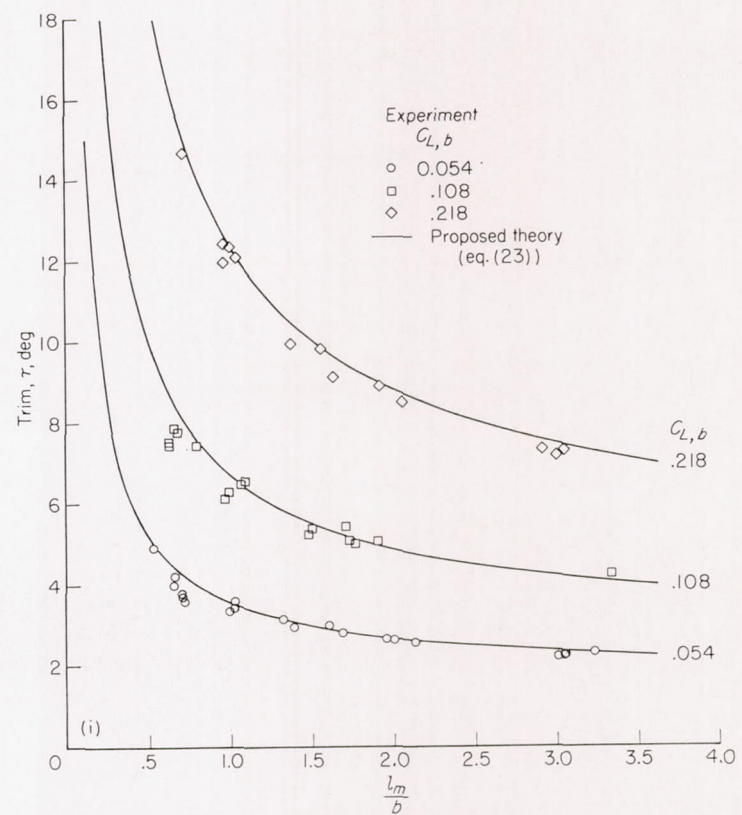
(g) Data of Shoemaker (ref. 33).

FIGURE 31.—Continued.



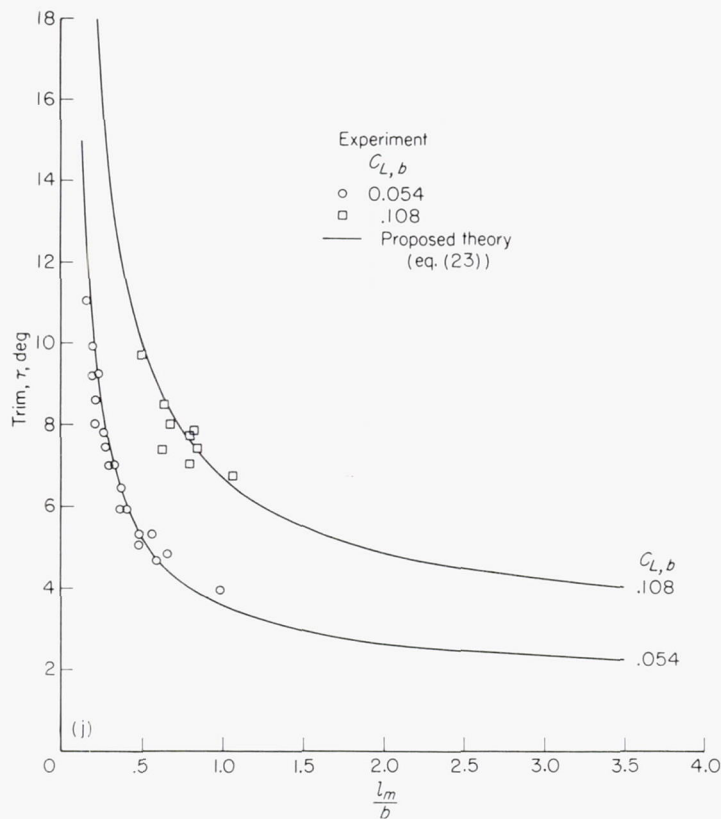
(h) Data of Locke (ref. 34).

FIGURE 31.—Continued.

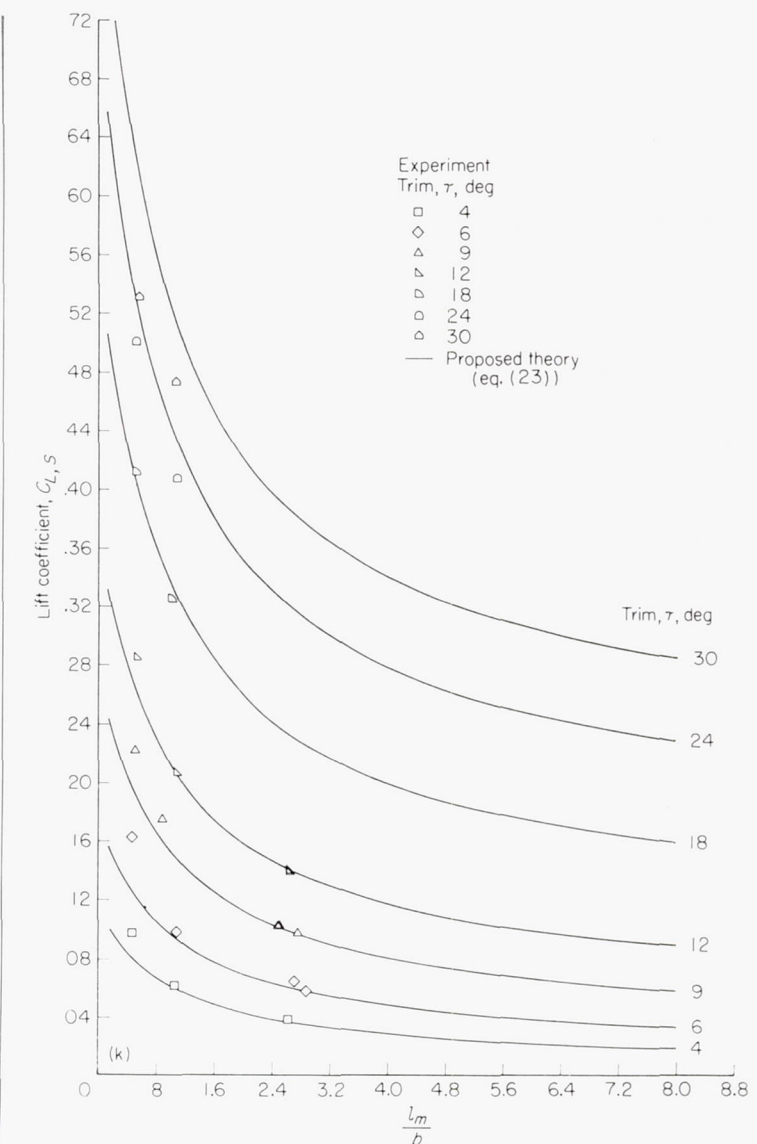


(i) Data of Sambraus (ref. 16).

FIGURE 31.—Continued.



(j) Data of Sottorf (ref. 15).
FIGURE 31.—Continued.



(k) Data of Kapryan and Boyd (ref. 25).
FIGURE 31.—Concluded.

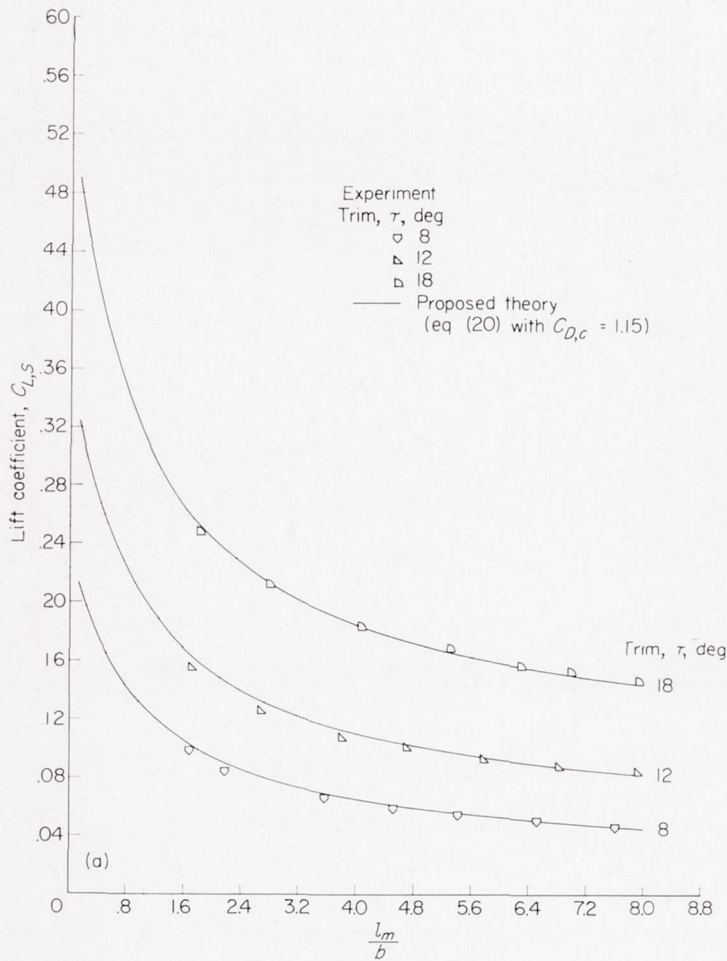
(a) Data of present report ($\frac{1}{16}$ -inch-radius chines).

FIGURE 32.—Comparison of proposed theory with experimental lift coefficients for rectangular-flat-plate planing surfaces having rounded chines.

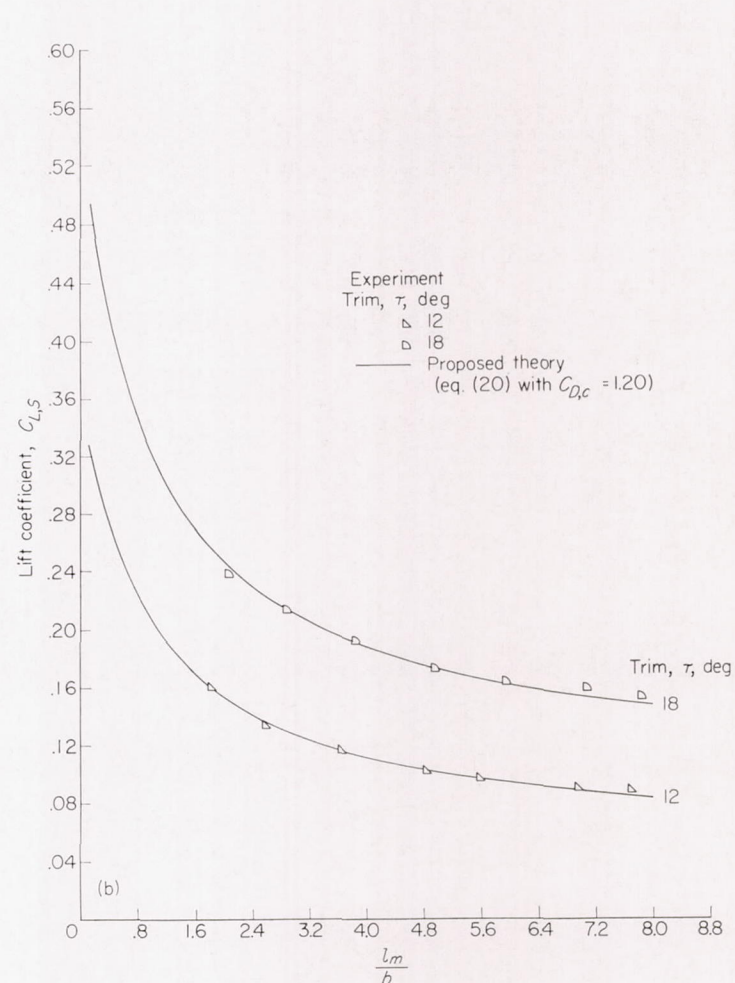
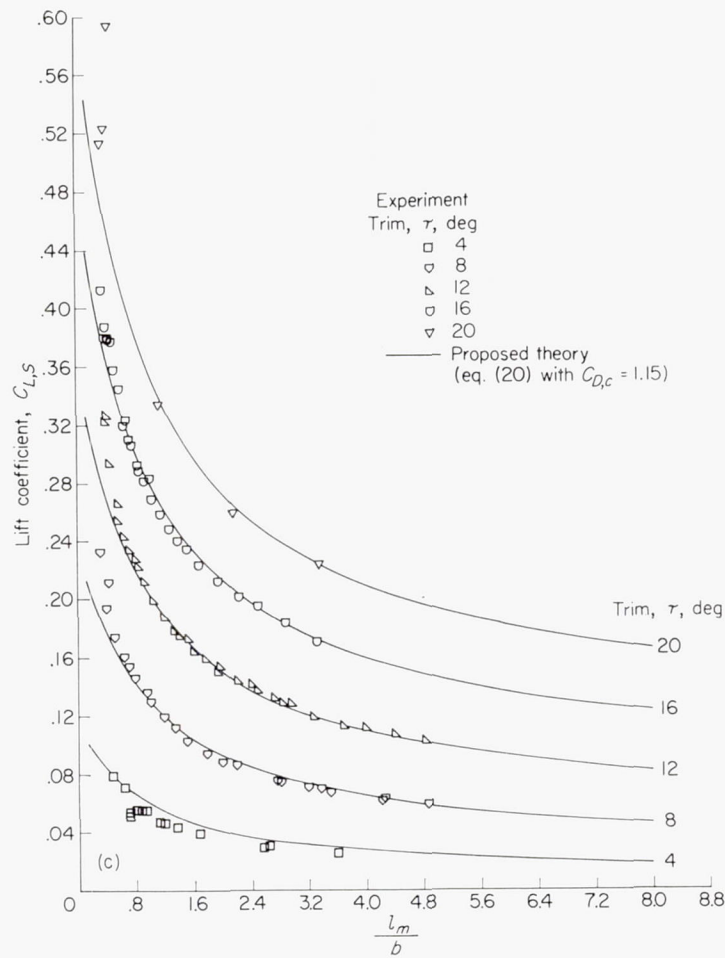
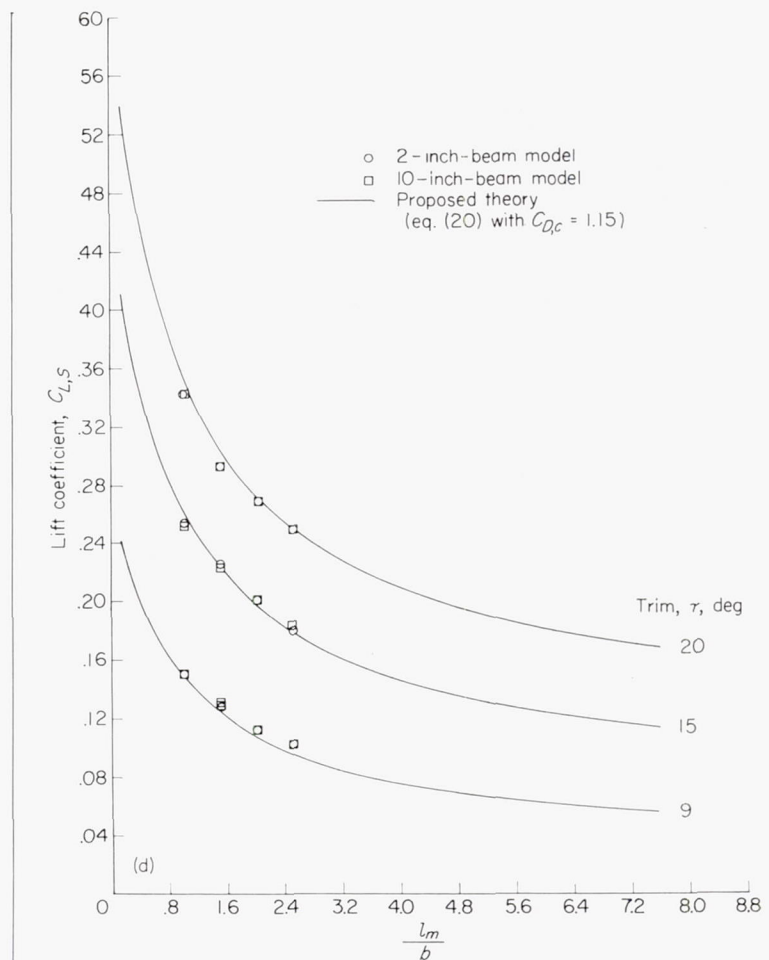
(b) Data of present report ($\frac{1}{64}$ -inch-radius chines).

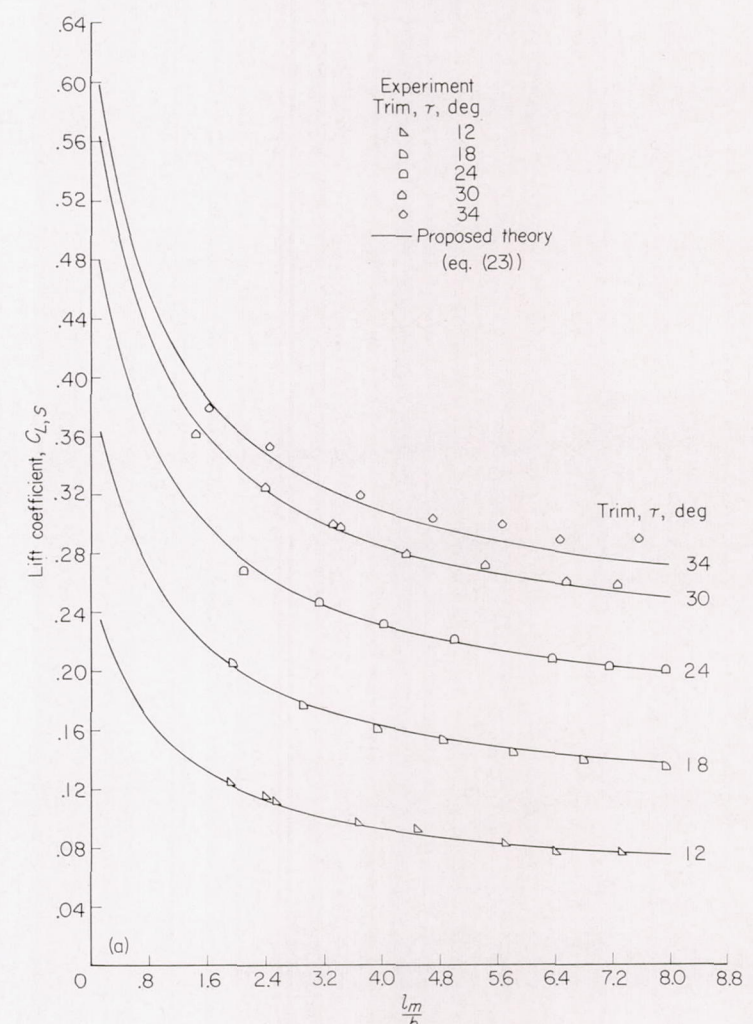
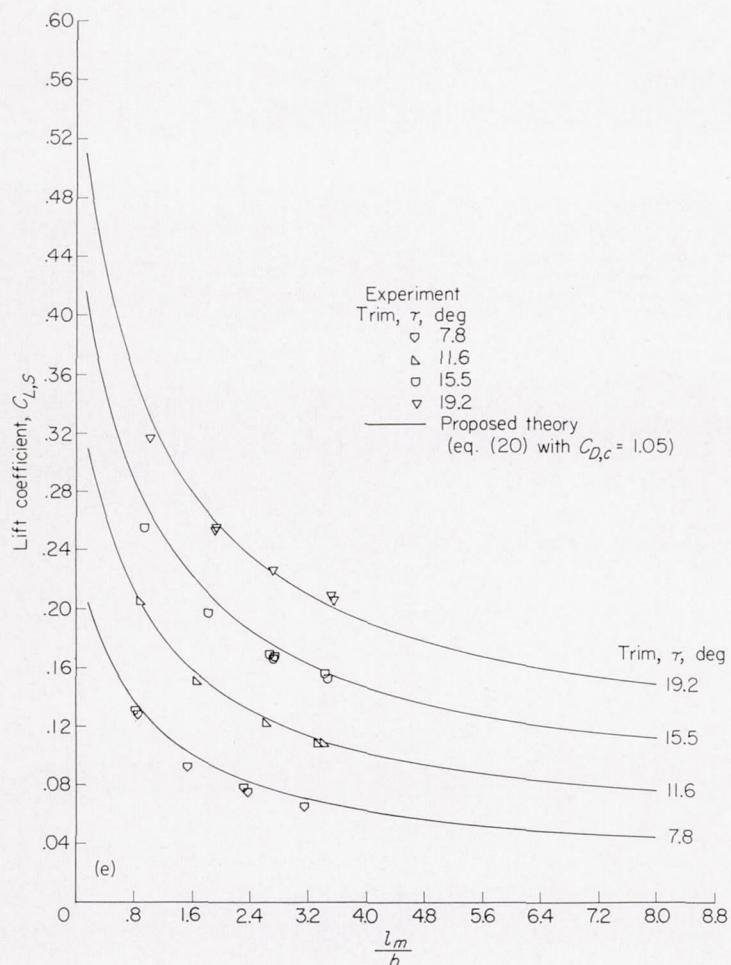
FIGURE 32.—Continued.

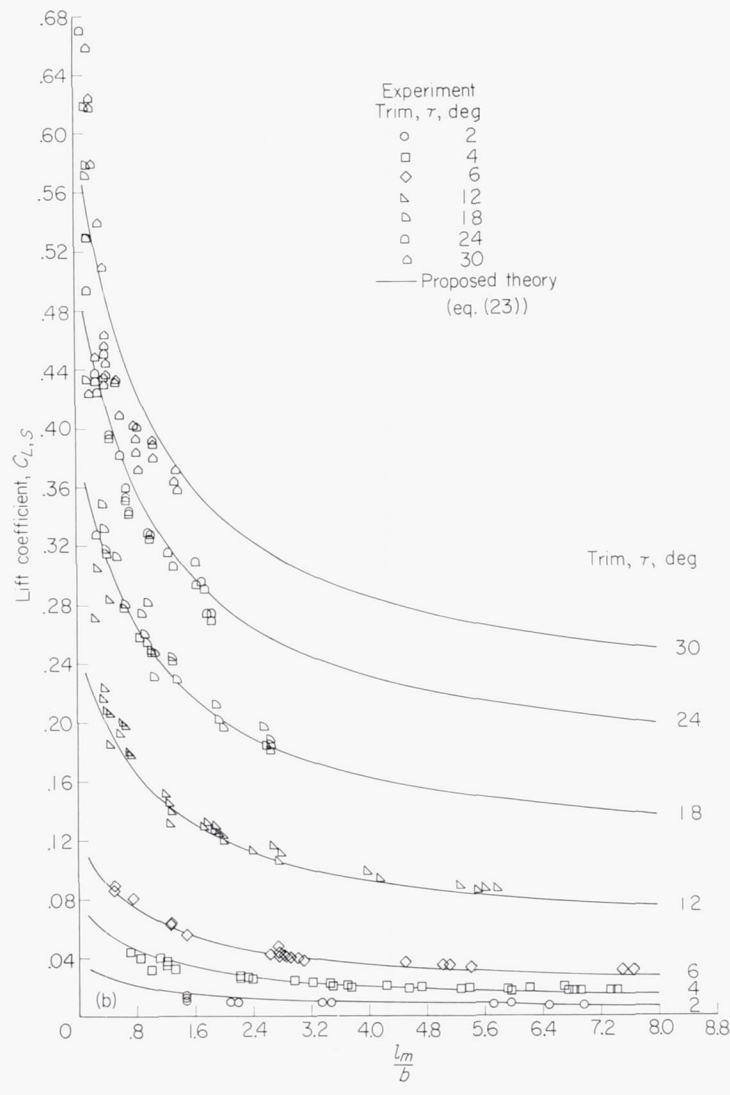


(c) Data of Wadlin and McGehee (ref. 31).
FIGURE 32.—Continued.

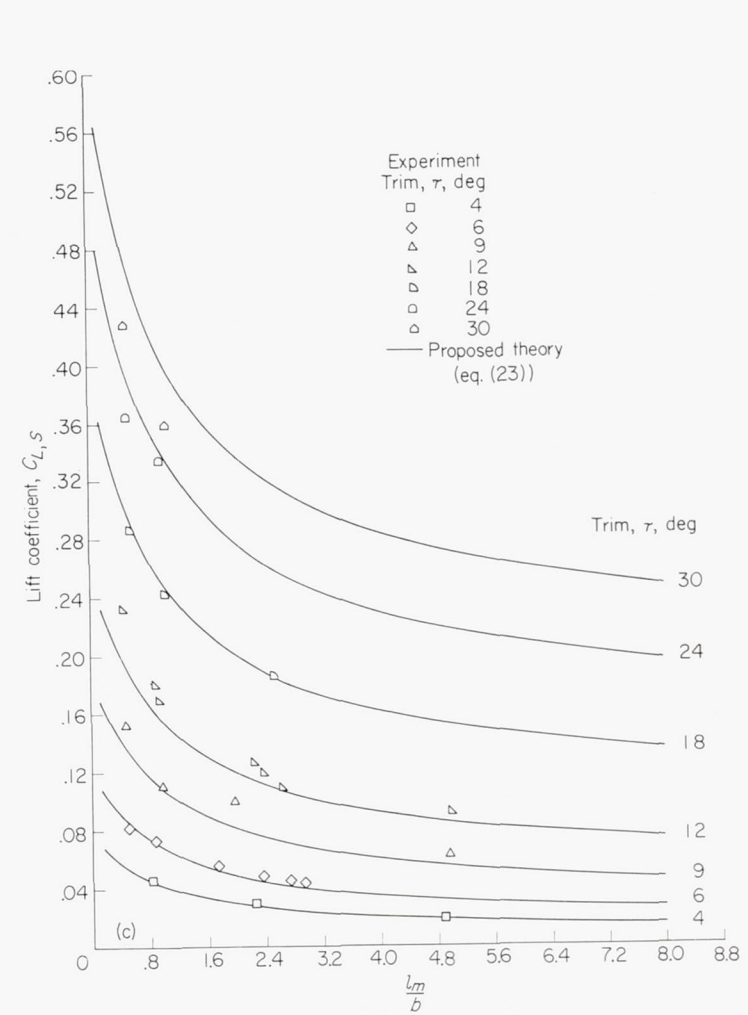


(d) Data of McBride (ref. 32).
FIGURE 32.—Continued.





(b) Data of Chambliss and Boyd (ref. 28).
 FIGURE 33.—Continued.



(c) Data of Kapryan and Boyd (ref. 25).
 FIGURE 33.—Concluded.

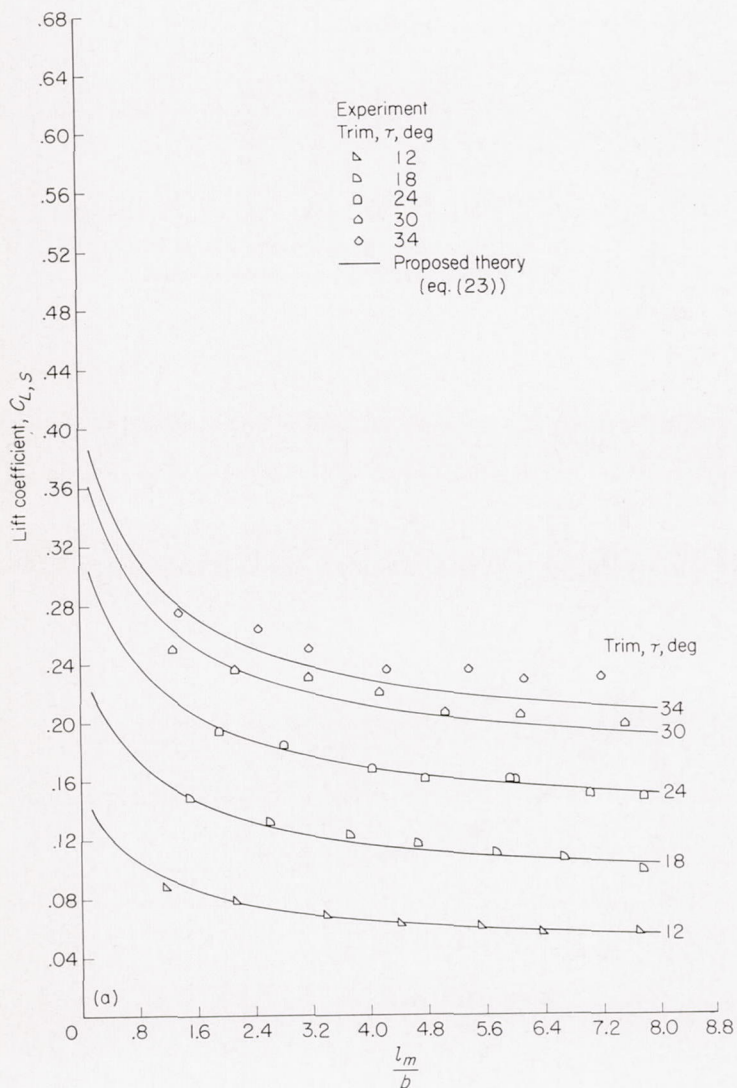


FIGURE 34.—Comparison of proposed theory with experimental lift coefficients for a surface having a 40° angle of dead rise.

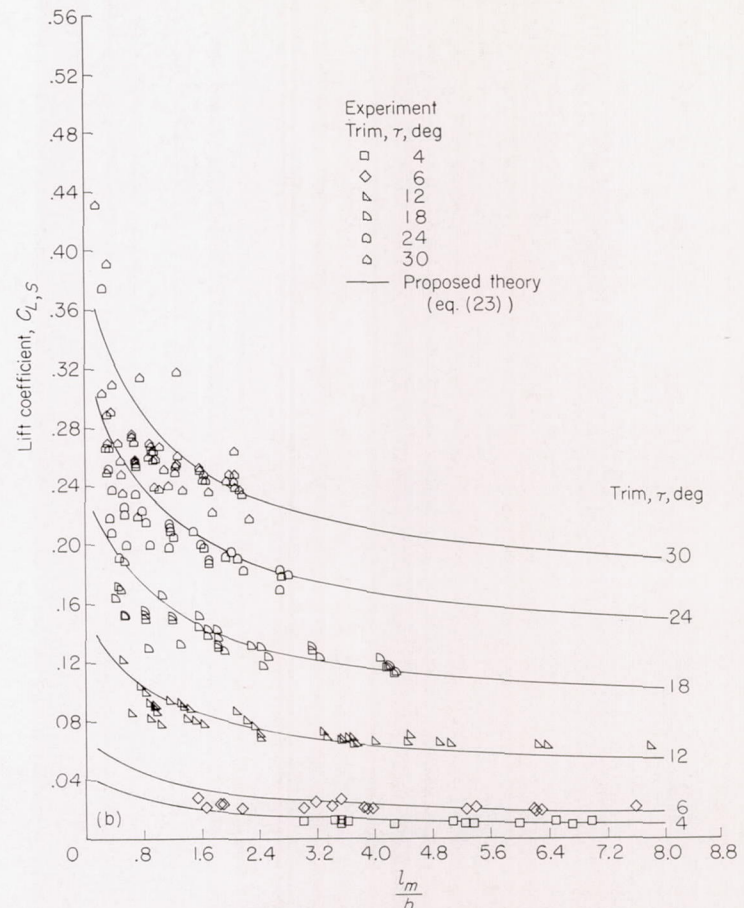


FIGURE 34.—Continued.

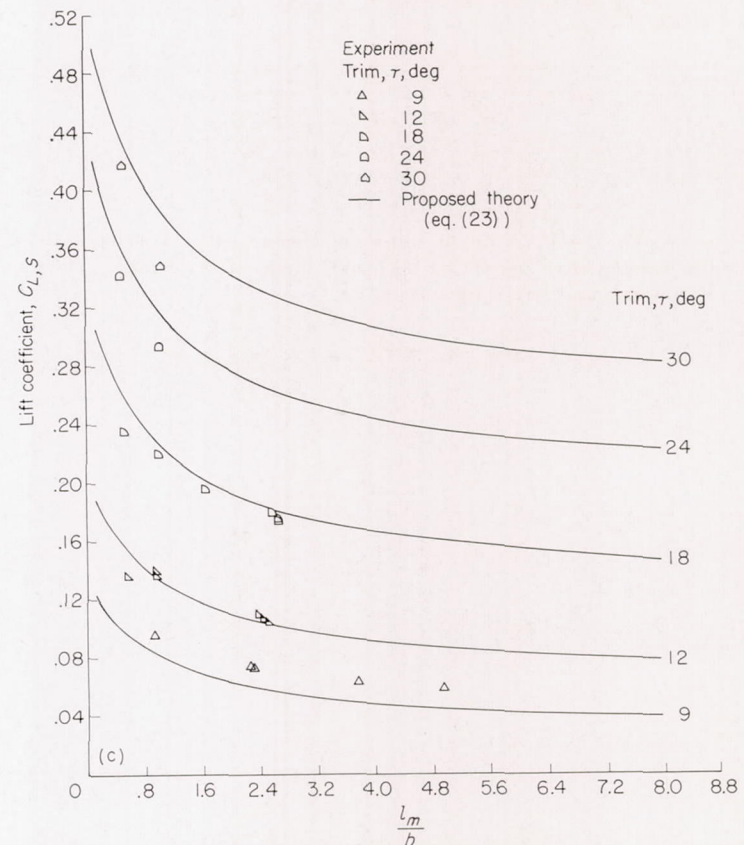


FIGURE 34.—Concluded.

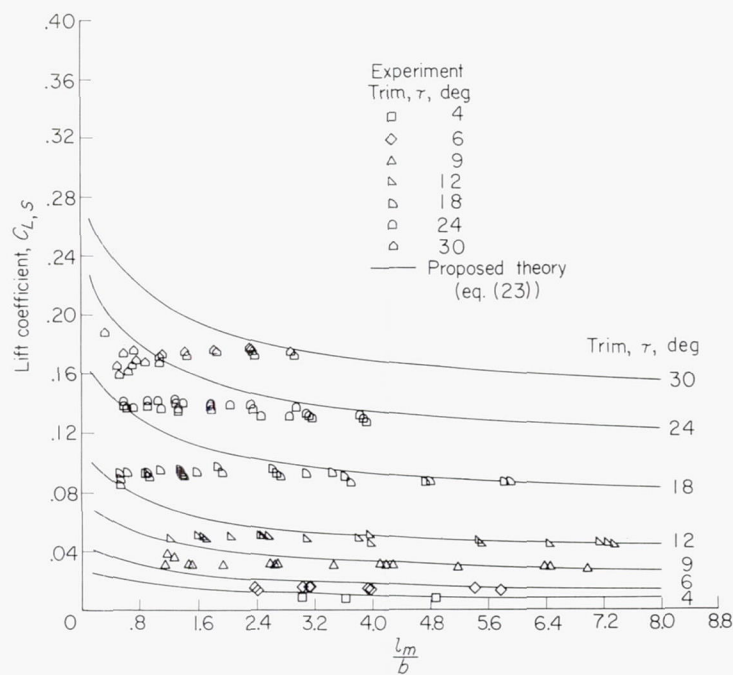
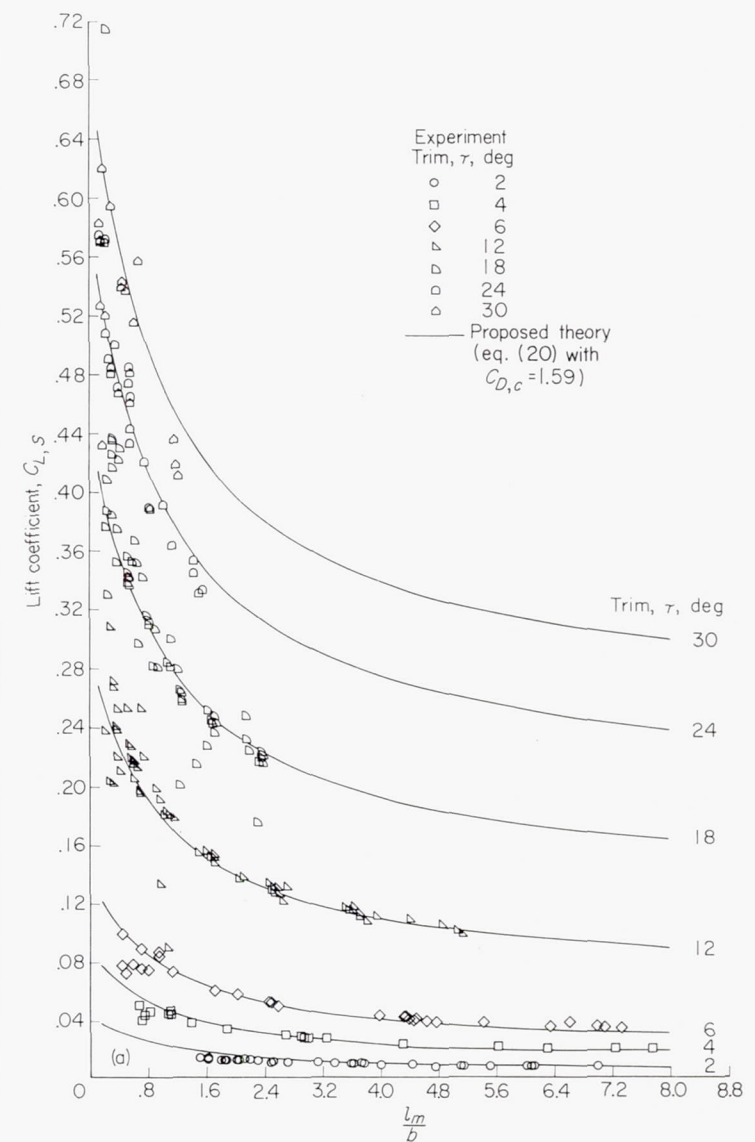
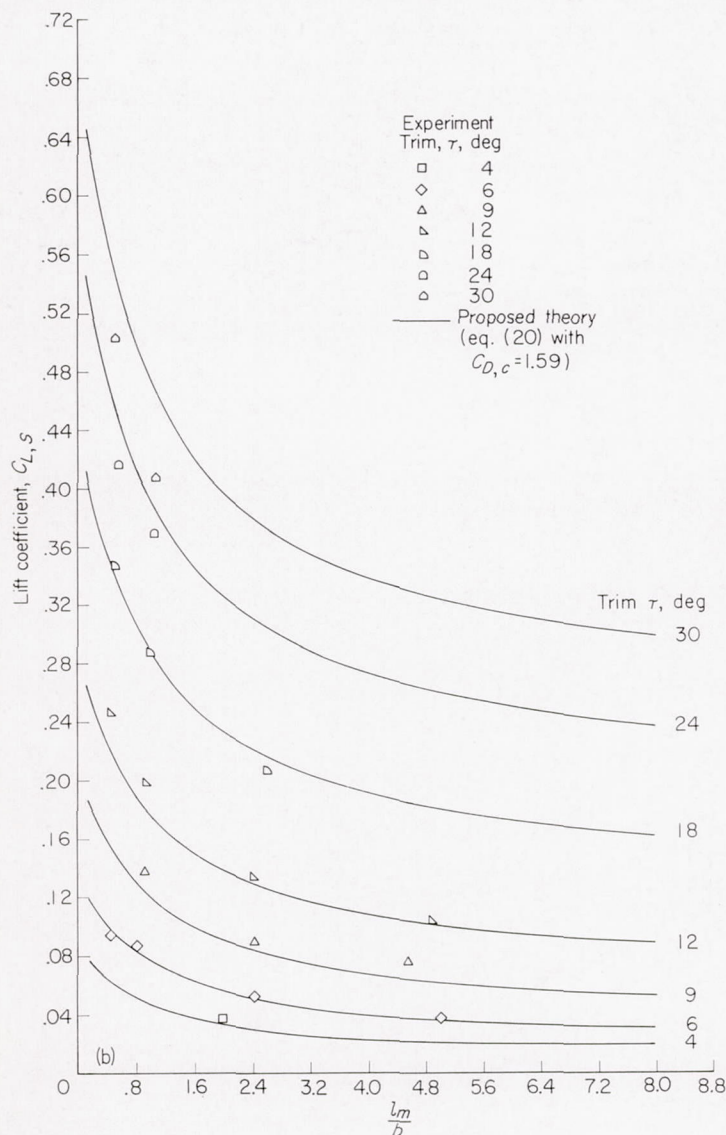


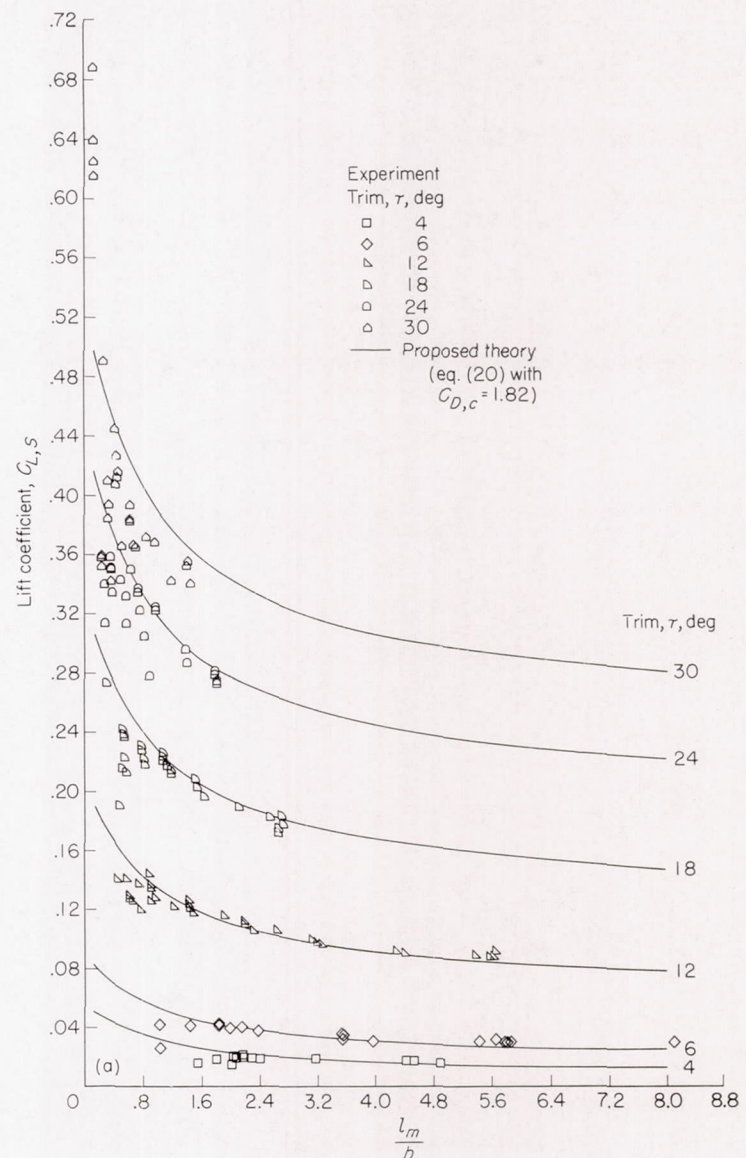
FIGURE 35.—Comparison of proposed theory with experimental lift coefficients for a model having a 50° angle of dead rise. (Data of Springston and Sayre (ref. 36).)



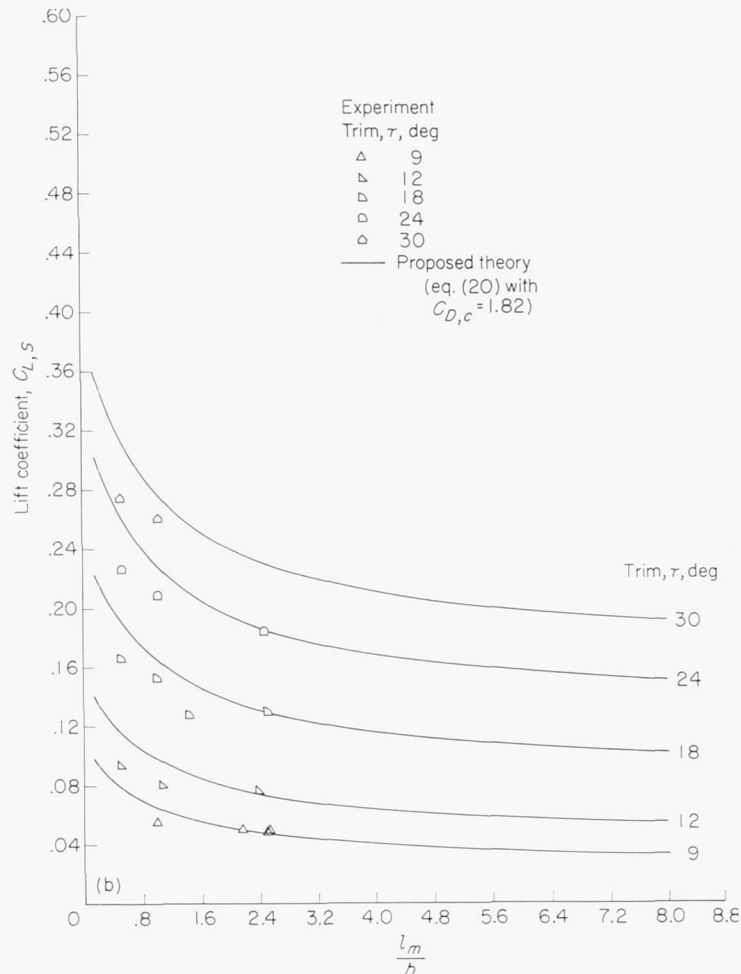
(a) Data of Kapryan and Weinstein (ref. 13).
FIGURE 36.—Comparison of proposed theory with experimental lift coefficients for a surface having a basic angle of dead rise of 20° and horizontal chine flare. (Effective angle of dead rise, 16°.)



(b) Data of Kapryan and Boyd (ref. 25).
FIGURE 36.—Concluded.



(a) Data of Blanchard (ref. 24).
FIGURE 37.—Comparison of proposed theory with experimental lift coefficients for a surface having a basic angle of dead rise of 40° and horizontal chine flare. (Effective angle of dead rise, 32°47'.)



(b) Data of Kapryan and Boyd (ref. 25).
FIGURE 37.—Concluded.

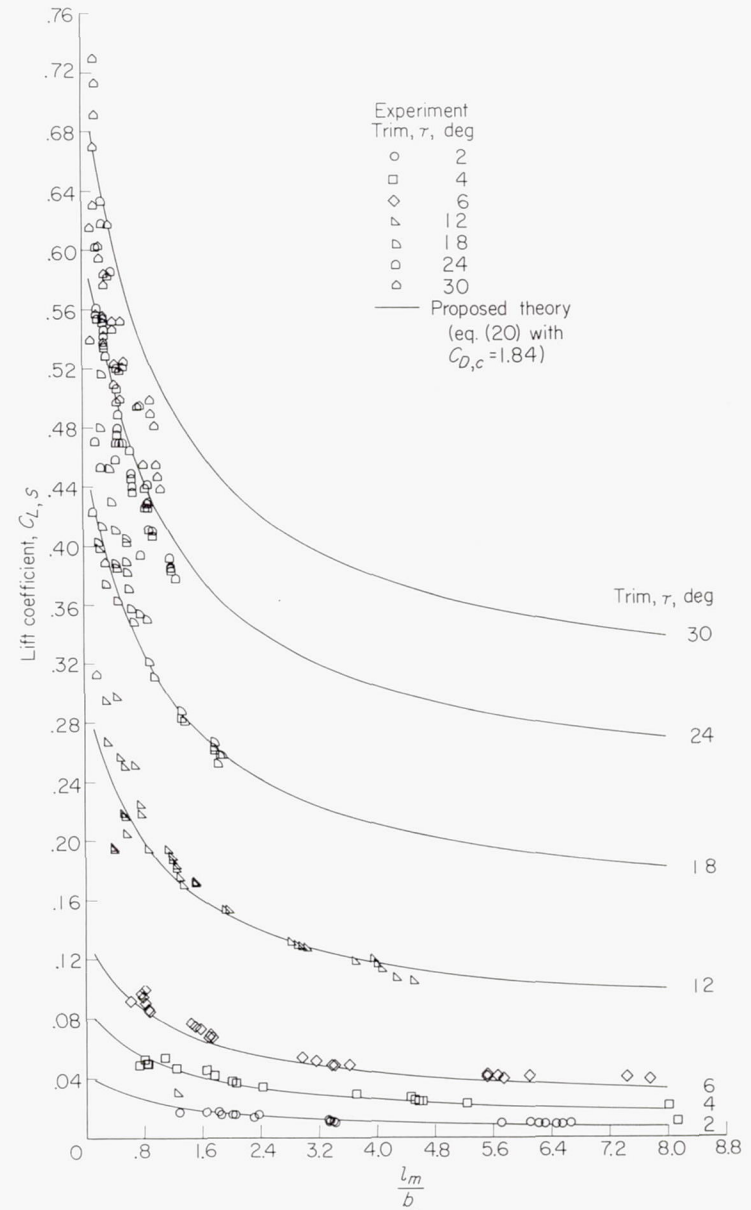


FIGURE 38.—Comparison of proposed theory with experimental lift coefficients for a surface having a basic angle of dead rise of 20° and vertical chine strips. (Effective angle of dead rise, $15^\circ 33'$.) (Data of Kapryan and Boyd (ref. 26).)

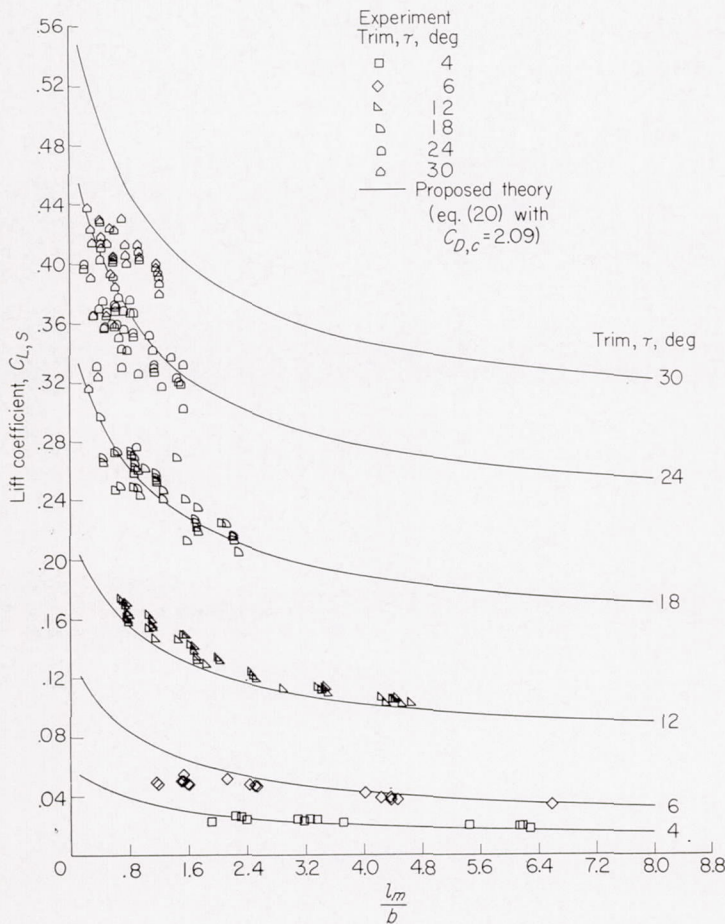
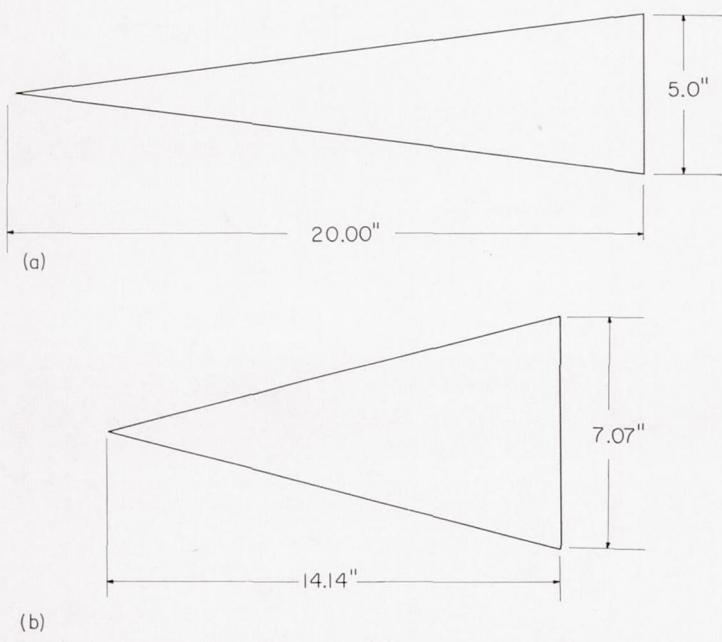


FIGURE 39.—Comparison of proposed theory with experimental lift coefficients for a surface having a basic angle of dead rise of 40° and vertical chine strips. (Effective angle of dead rise, $31^\circ 59'$.) (Data of Kapryan and Boyd (ref. 26).)



(a) Triangular flat plate; $\frac{l}{b} = 4$; $A_t = \frac{1}{4}$.

(b) Triangular flat plate; $\frac{l}{b} = 2$; $A_t = \frac{1}{2}$.

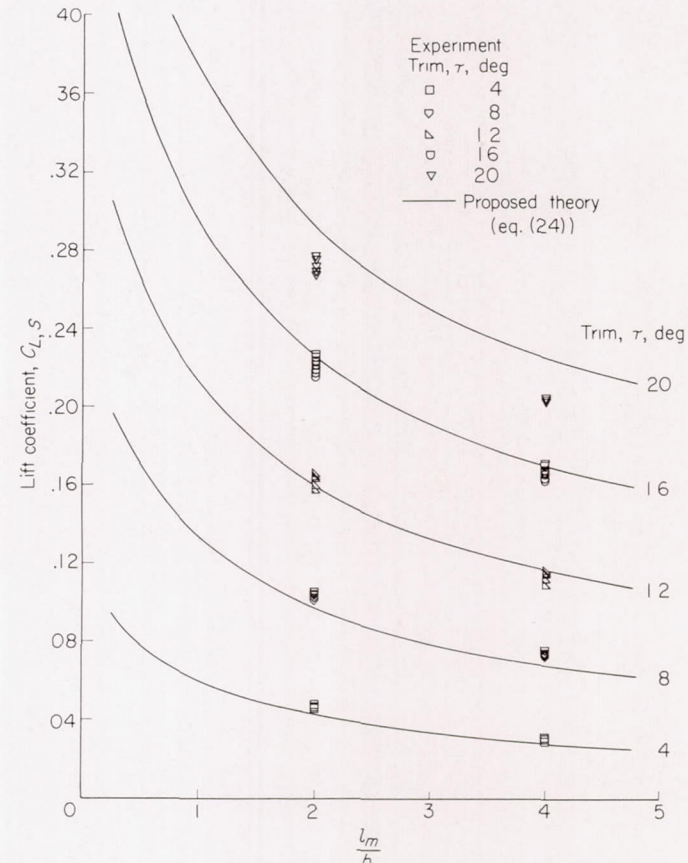
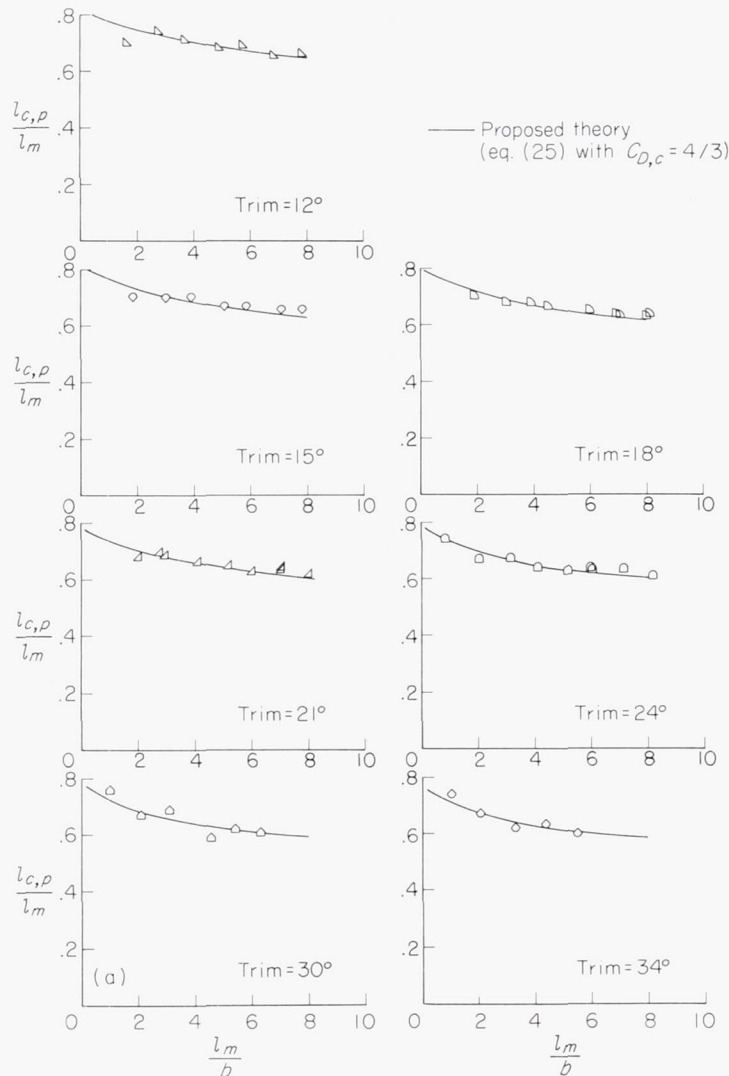


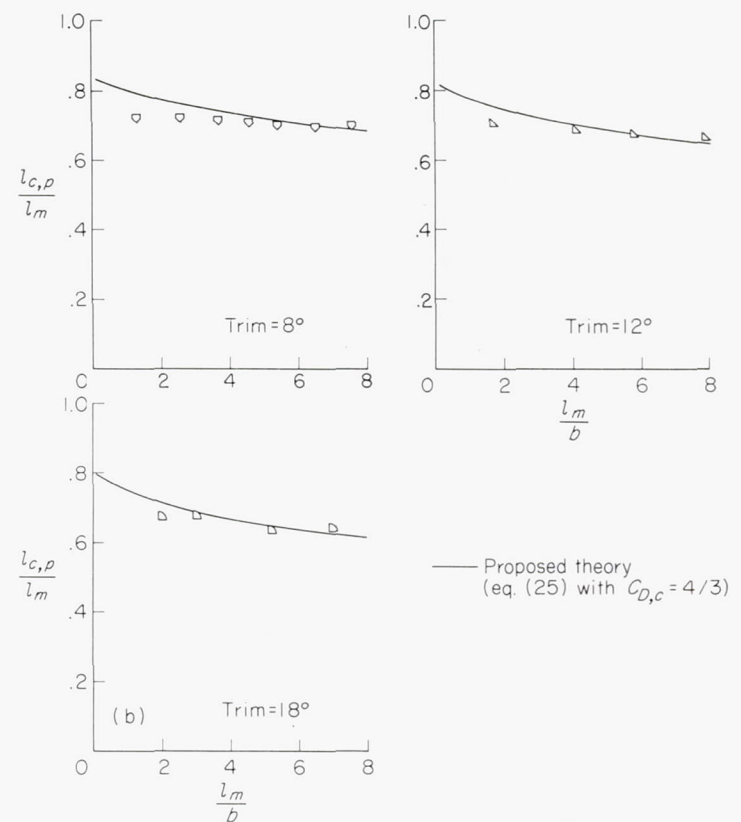
FIGURE 41.—Comparison of proposed theory with experimental lift coefficients for triangular-flat-plate surfaces planing with base forward. (Data of Wadlin and McGehee (ref. 31) and unpublished tank no. 2 data.)

FIGURE 40.—Plan forms of triangular-flat-plate models (wooden) planing with base forward.



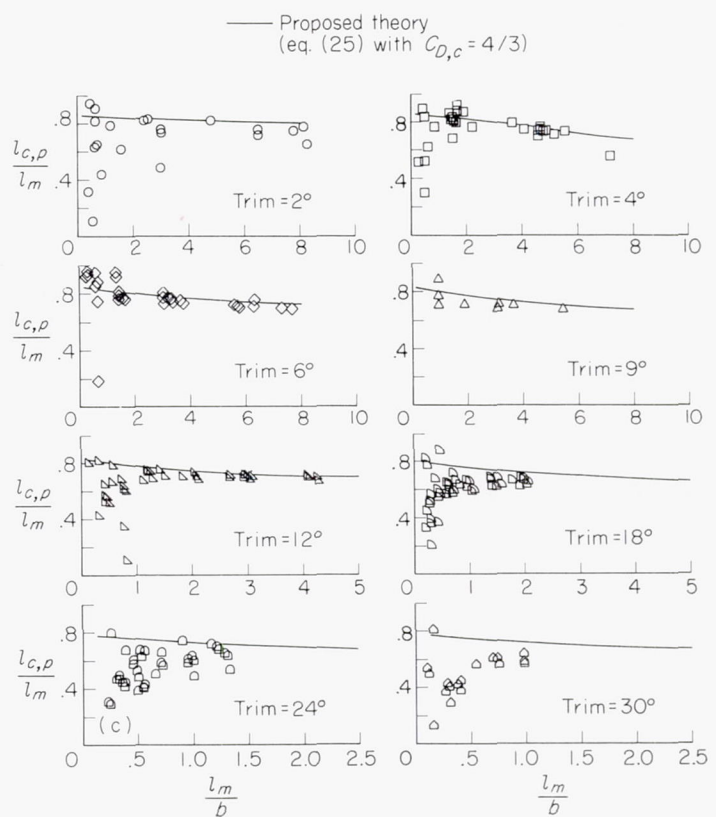
(a) Data of present report (brass model).

FIGURE 42.—Variation of center-of-pressure location with mean wetted-length-beam ratio for rectangular-flat-plate planing surfaces.



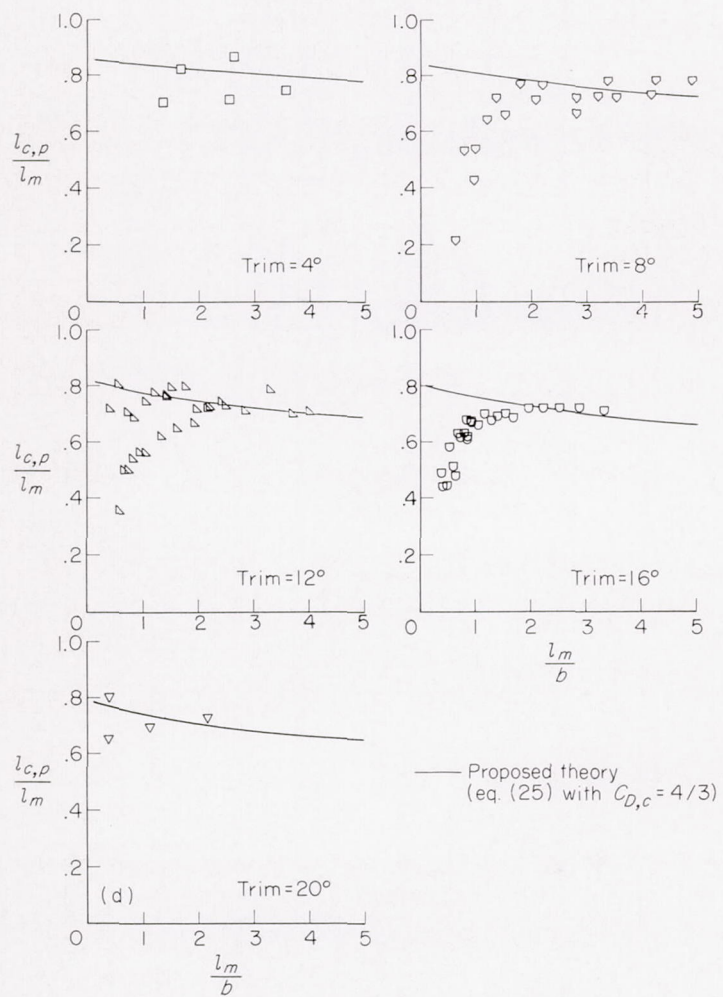
(b) Data of present report (sharp-chine plastic model).

FIGURE 42.—Continued.

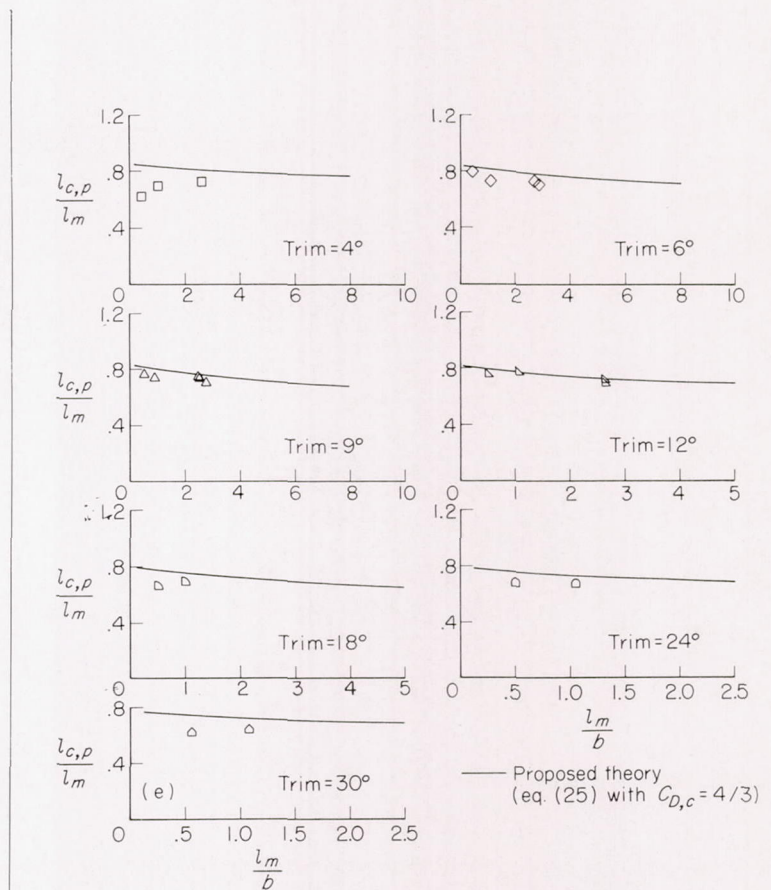


(c) Data of Weinstein and Kapryan (ref. 23).

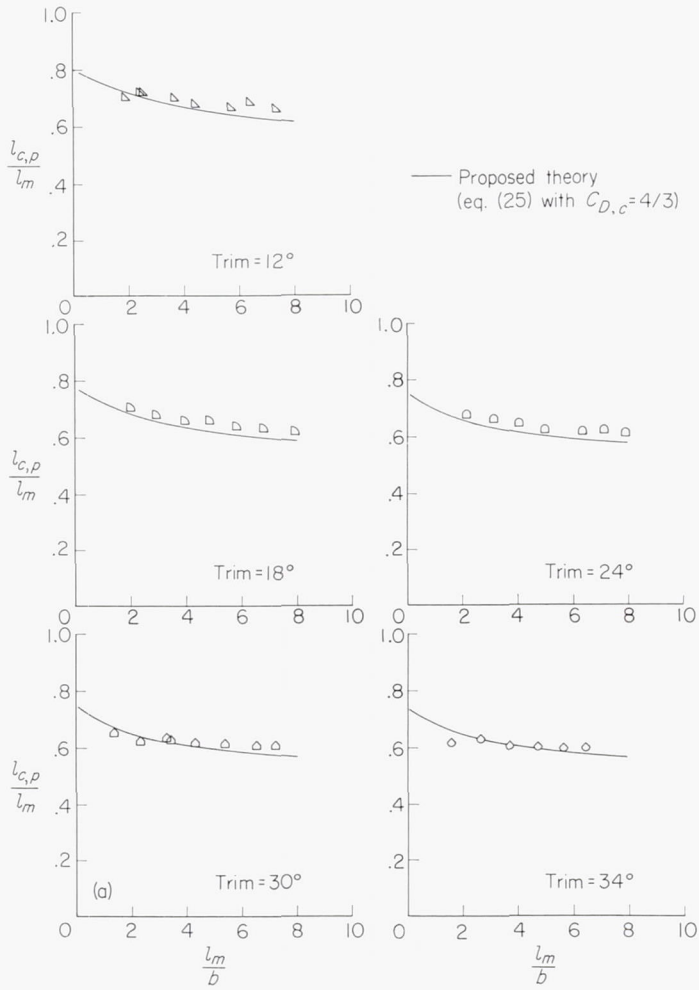
FIGURE 42.—Continued.



(d) Data of Wadlin and McGehee (ref. 31).
FIGURE 42.—Continued.

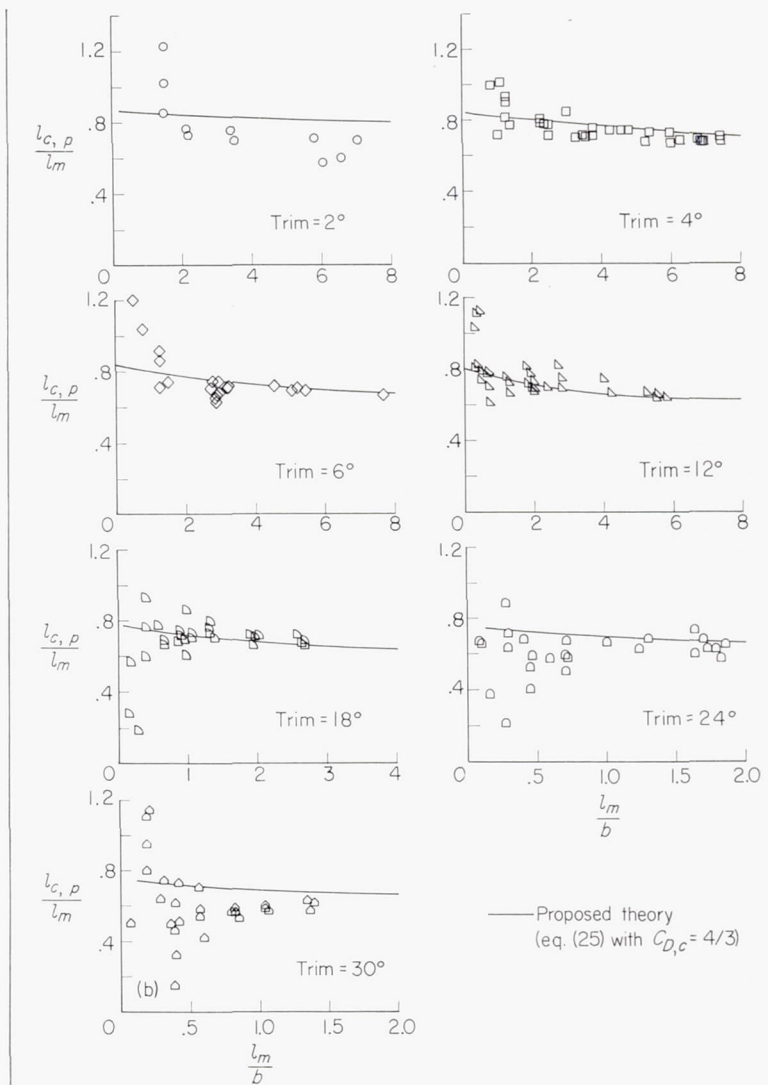


(e) Data of Kapryan and Boyd (ref. 25).
FIGURE 42.—Concluded.



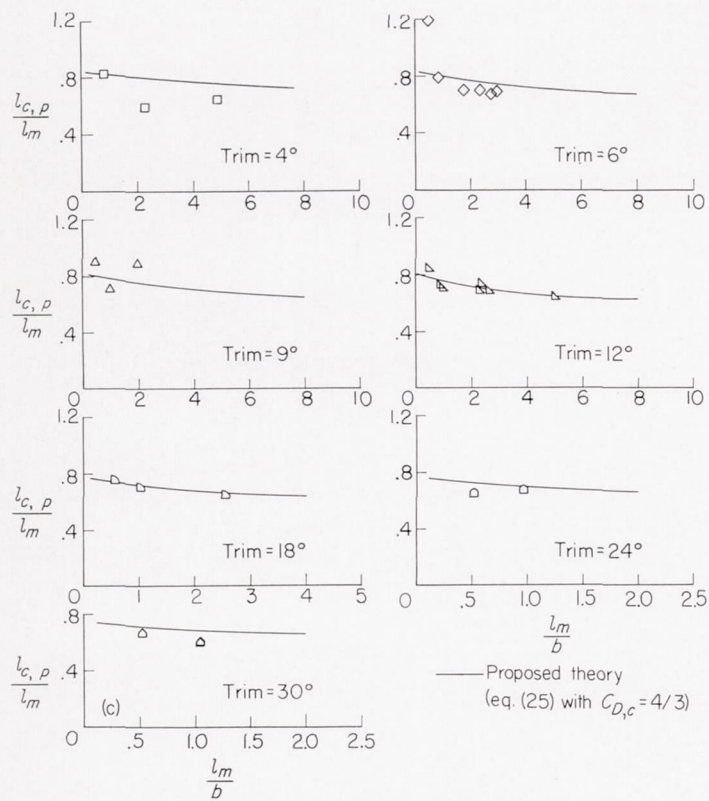
(a) Data of present report.

FIGURE 43.—Variation of center-of-pressure location with mean wetted-length-beam ratio for a surface having a 20° angle of dead rise.

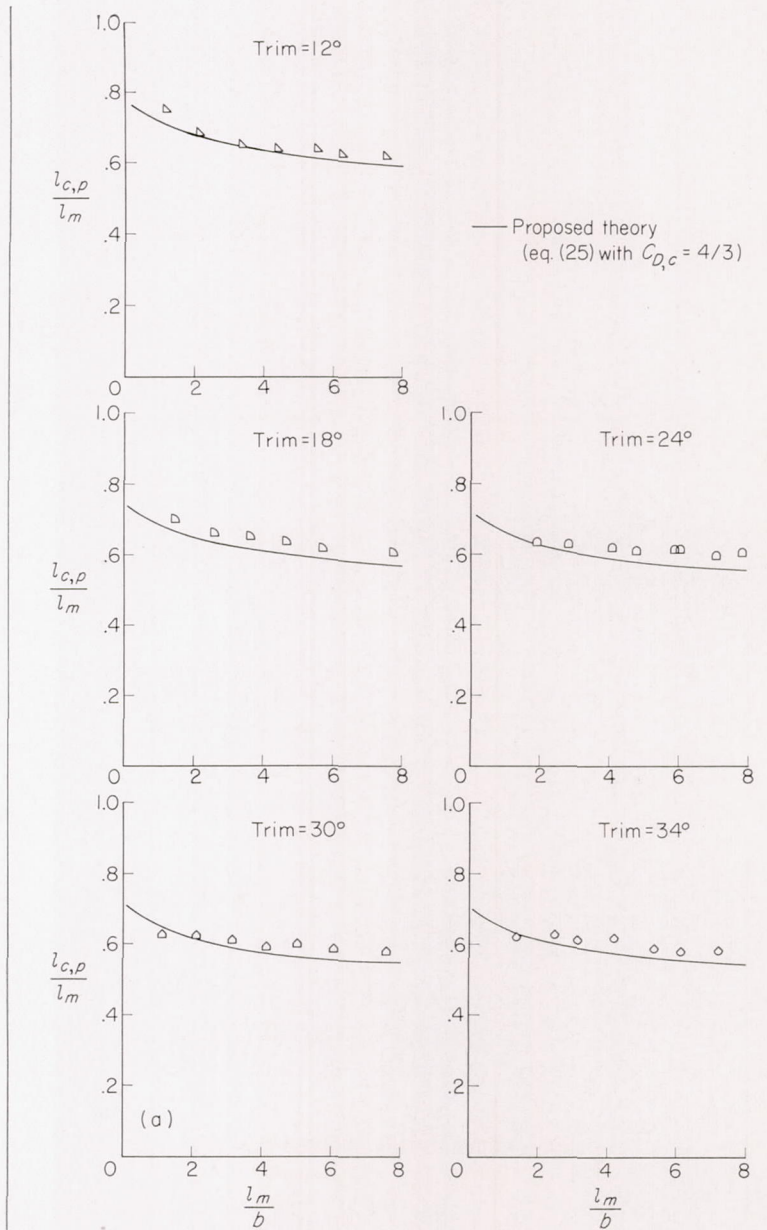


(b) Data of Chambliss and Boyd (ref. 28).

FIGURE 43.—Continued.

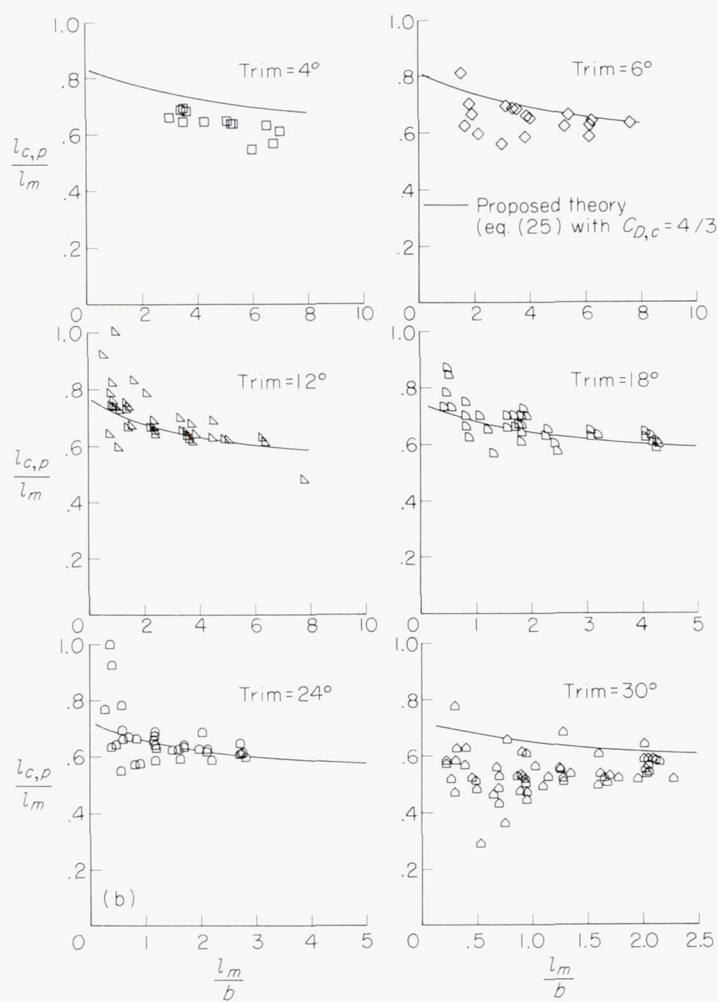


(c) Data of Kapryan and Boyd (ref. 25).
FIGURE 43.—Concluded.

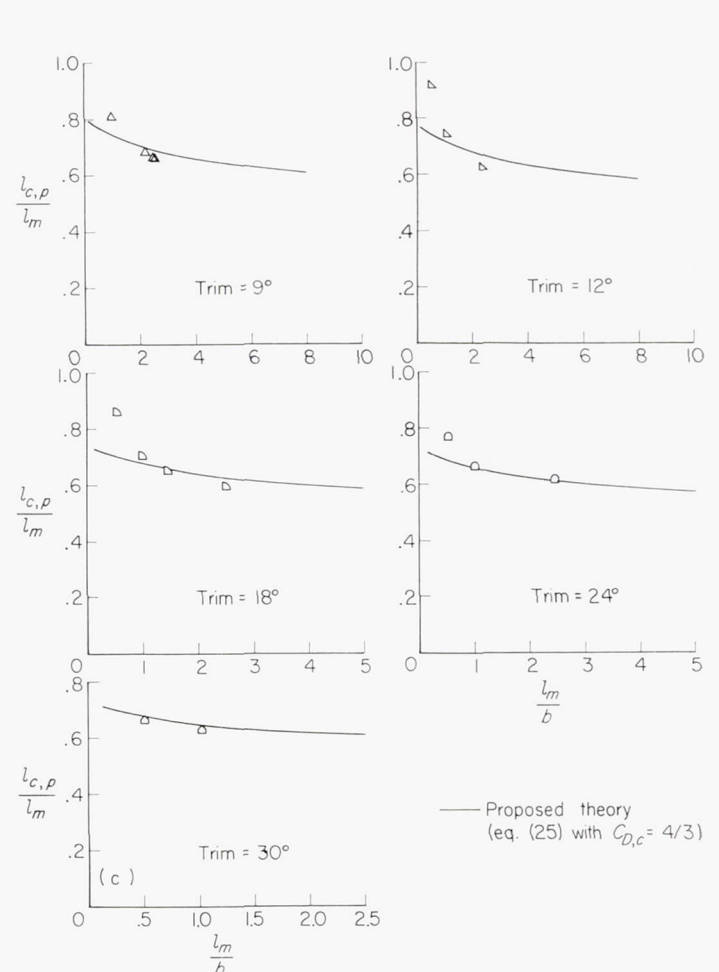


(a) Data of present report.

FIGURE 44.—Variation of center-of-pressure location with mean wetted-length-beam ratio for a surface having a 40° angle of dead rise.



(b) Data of Chambliss and Boyd (ref. 28).
FIGURE 44.—Continued.



(c) Data of Kapryan and Boyd (ref. 25).
FIGURE 44.—Concluded.

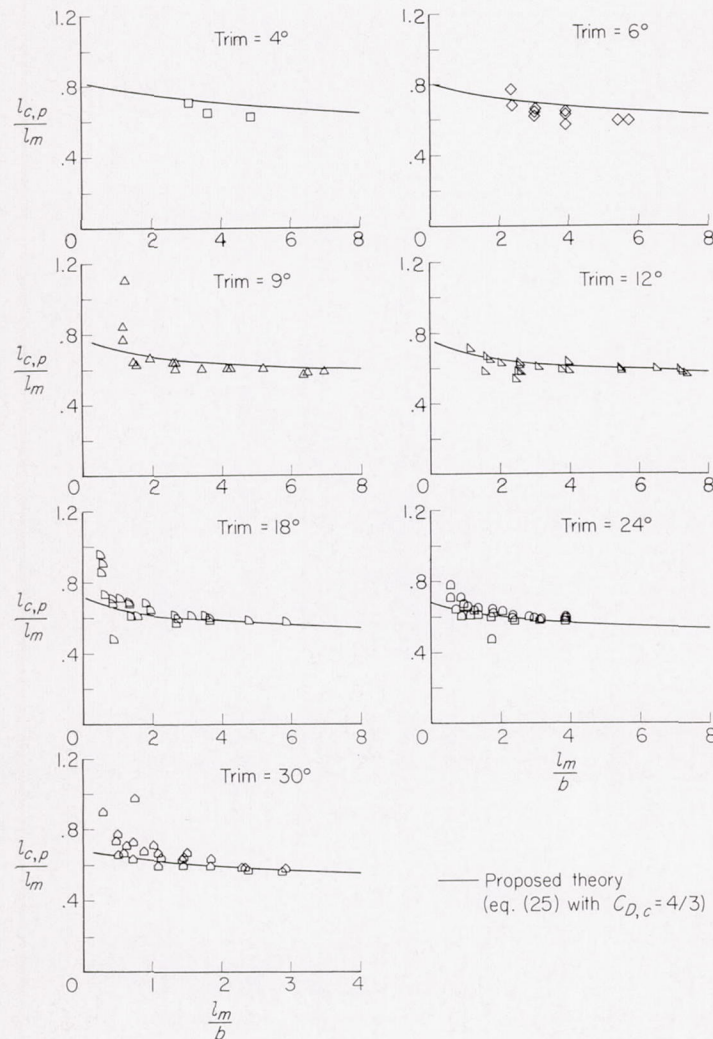
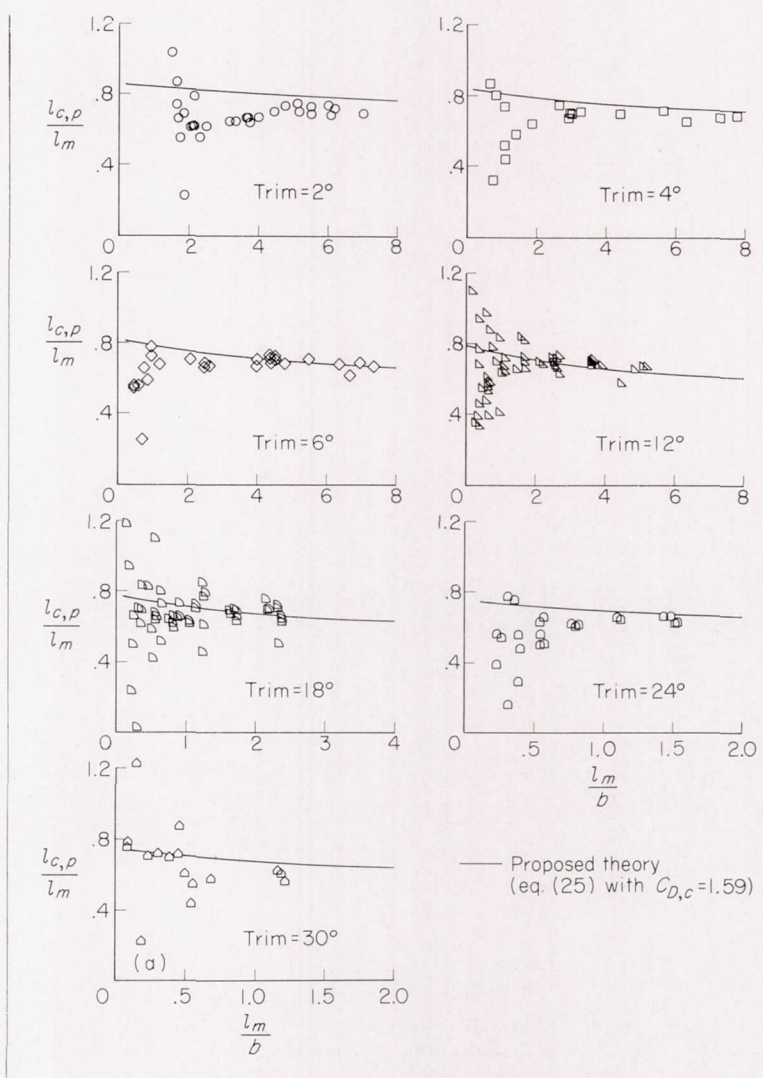
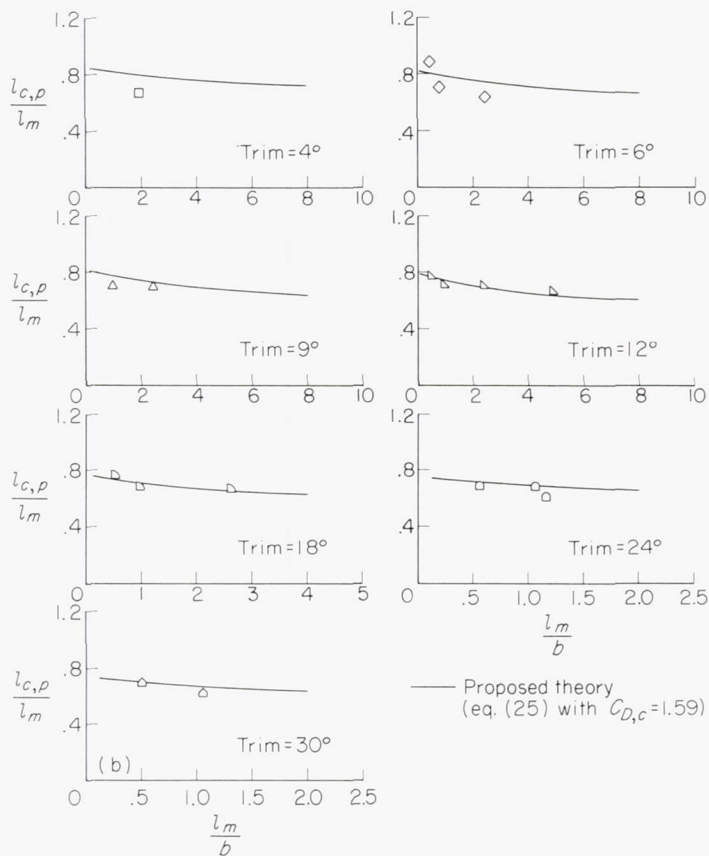


FIGURE 45.—Variation of center-of-pressure location with mean wetted-length-beam ratio for a model having a 50° angle of dead rise. (Data of Springston and Sayre (ref. 36).)

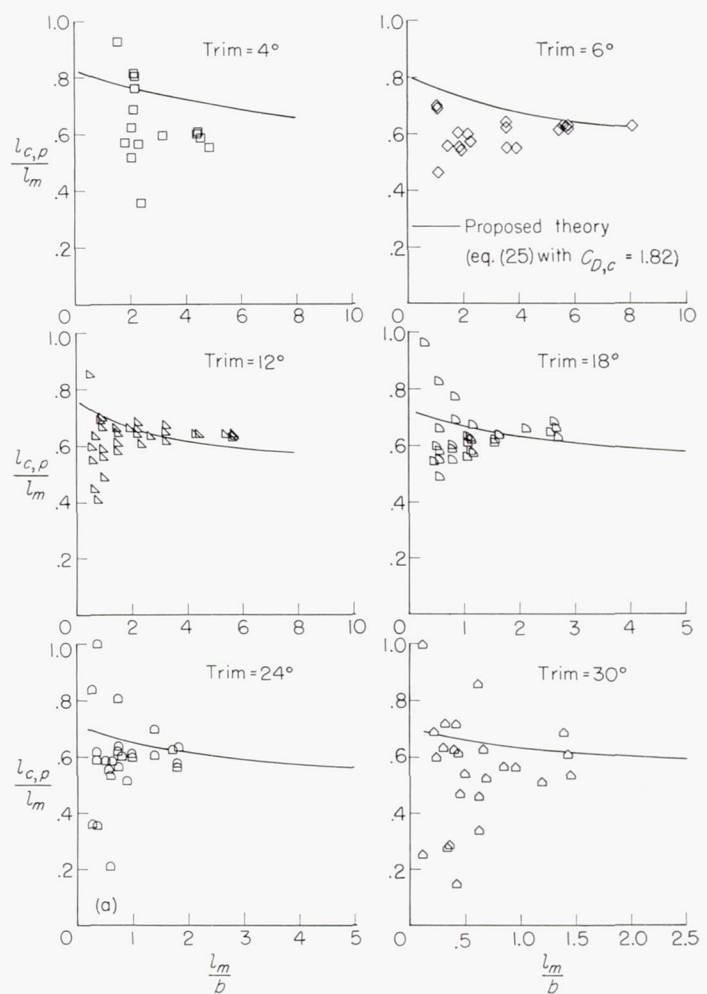


(a) Data of Kapryan and Weinstein (ref. 13).
 FIGURE 46.—Variation of center-of-pressure location with mean wetted-length-beam ratio for a surface having a basic angle of dead rise of 20° and horizontal chine flare. (Effective angle of dead rise, 16°.)



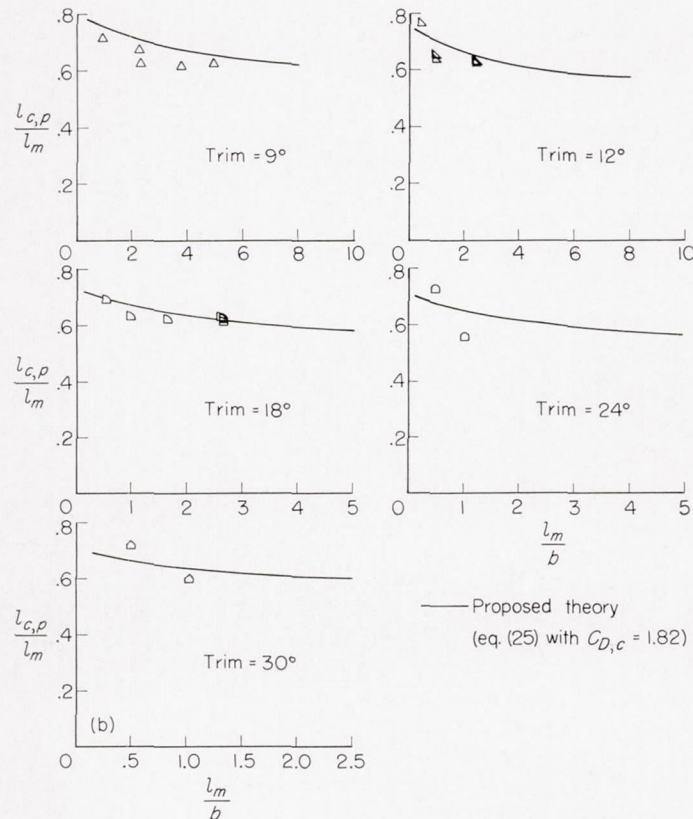
(b) Data of Kapryan and Boyd (ref. 25).

FIGURE 46.—Concluded.



(a) Data of Blanchard (ref. 24).

FIGURE 47.—Variation of center-of-pressure location with mean wetted-length-beam ratio for a surface having a basic angle of dead rise of 40° and horizontal chine flare. (Effective angle of dead rise, 32°47'.)



(b) Data of Kapryan and Boyd (ref. 25).
FIGURE 47.—Concluded.

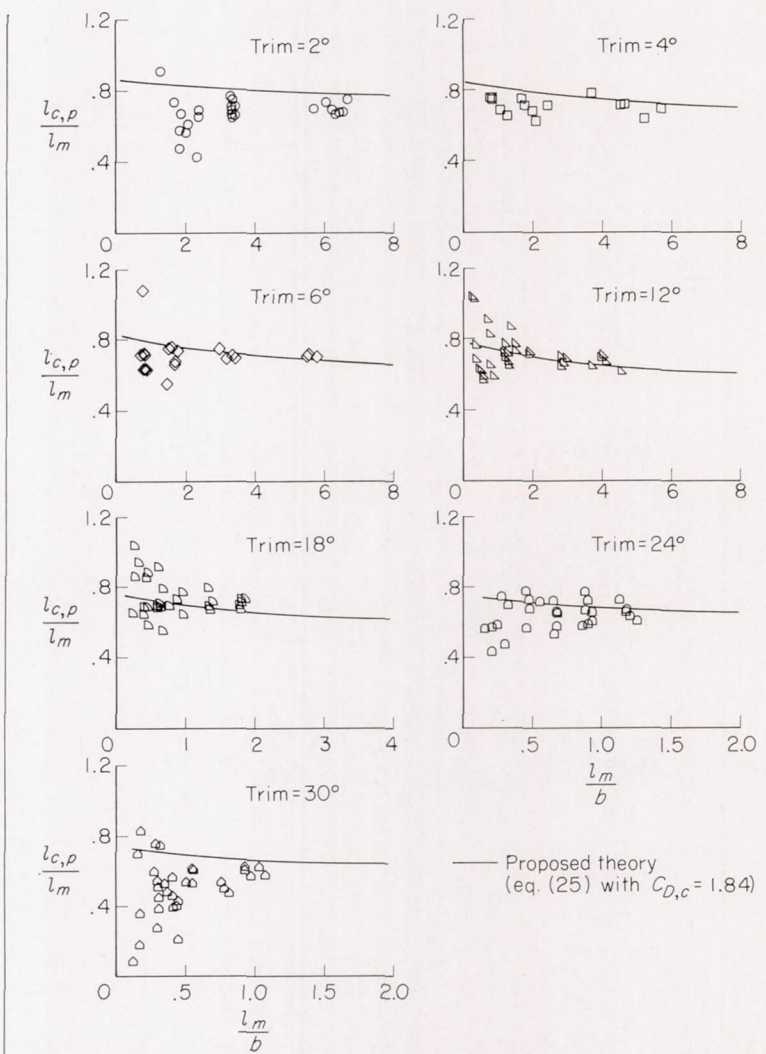


FIGURE 48.—Variation of center-of-pressure location with mean wetted-length-beam ratio for a surface having a basic angle of dead rise of 20° and vertical chine strips. (Effective angle of dead rise, 15°33'.) (Data of Kapryan and Boyd (ref. 26).)

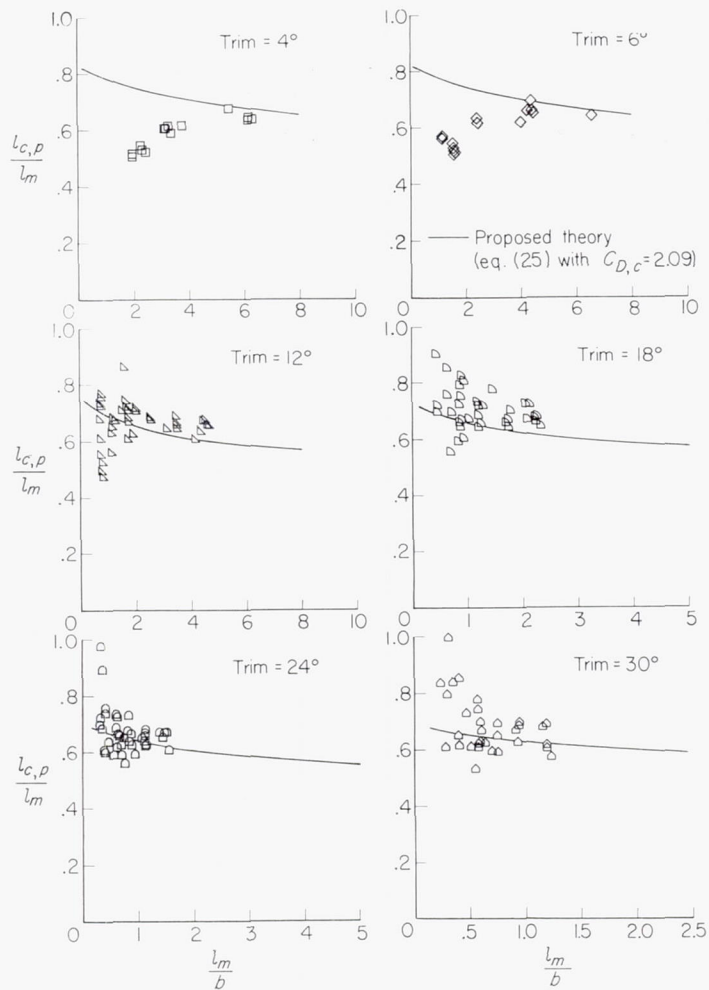


FIGURE 49.—Variation of center-of-pressure location with mean wetted-length-beam ratio for a surface having a basic angle of dead rise of 40° and vertical chine strips. (Effective angle of dead rise, $31^\circ 59'$.) (Data of Kapryan and Boyd (ref. 26).)

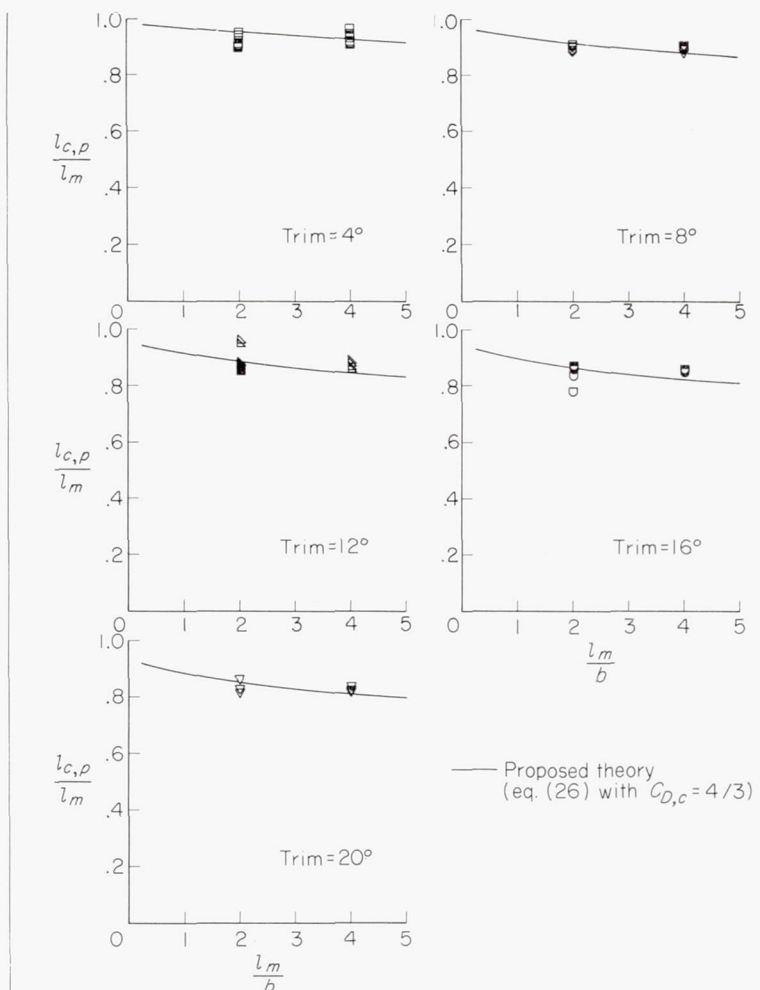


FIGURE 50.—Variation of center-of-pressure location with length-beam ratio for triangular-flat-plate surfaces planing with base forward. (Data of Wadlin and McGehee (ref. 31) and unpublished tank no. 2 data.)